Politecnico di Torino

Politecnico di Torino

Corso di Laurea Magistrale in Ingegneria Energetica e Nucleare

A.a. 2021/2022

Sessione di Laurea Dicembre 2021

Experimental assessment of the thermophysical properties of Choline Proline and its performance as a post-combustion carbon capture solvent

Relatori:
Massimo Santarelli
Salvatore Cannone

Candidata:
Irina Popescu

Acknowledgements

My sincere thanks go to Professor Massimo Santarelli for giving me the opportunity to work on this project and to Salvatore Cannone for his guidance throughout these months and for providing helpful feedbacks to my work. I would also like to thank Sergio Bocchini, Michel Tawil, Silvia Mazzotta, and all the people I had the pleasure to work with in the few months I've been in IIT.

My endless gratitude goes then to my parents, for their loving support and for the sacrifices they made to ensure me the privilege of the many opportunities I've been given so far.

Deserved thanks to my sister, who has probably carried the heaviest burden of the stressful periods of my university career. Thanks for your continuous efforts to keep me 'young' and for all the moments we shared together, with all the deep talks and sudden nonsense.

Special thanks to who supported me in these last months, cheering me up whenever I was in need despite being many kilometres away.

Last, but absolutely not least, thanks to all the friends that accompanied me during these years. To the ones that have been by my side for a very long time and to the ones that have become part of my life recently, though creating meaningful and lasting bonds. To the ones that encouraged me in some tough moments and to the ones that helped me to change perspective and overcome my limits.

Abstract

Carbon capture technologies are expected to play a significant role in the energy transition, as a powerful tool for the decarbonisation of the already existing power stations and the hard-to-abate industrial sectors, and as part of biogas upgrading systems and blue hydrogen production processes. Nowadays, amine scrubbing stands among the most solid technologies in the carbon sequestration field, though being renowned for the high energy requirements, the toxicity, the corrosiveness and the fast degradation they undergo.

Ionic liquids (ILs) are emerging as a viable alternative to the aqueous amine solutions for post-combustion carbon capture processes. In this regard, recent studies show that choline proline ([Cho][Pro]) has a very good potential, thanks to its ring structure and to the presence of amine functionalities in the amino acid moiety – which promote the physical and the chemical CO_2 absorption, respectively. On the downside, the high viscosity values constitute a serious drawback in practical applications, which can be overcome through the use of solutions of [Cho][Pro] in solvents such as DMSO.

The present work aims at providing insights into the thermophysical properties and performance of [Cho][Pro]. Firstly, the IL was synthesised according to an innovative procedure which replaces the expensive and corrosive choline hydroxide with choline chloride as a mean of cation source. Next, density and viscosity were measured for solutions of [Cho][Pro] in DMSO at varying concentrations (12.5%wt, 25%wt and 50%wt) in a temperature interval ranging from 25°C to 70°C. The data obtained were correlated with empirical equations to allow subsequent calculations. The absorption process of the same solutions was later investigated through a gravimetric method in a ~5ml vol reactor.

At last, the 50%wt solution was employed in a set of tests performed on a bench-scale test plant. The cyclability of the solution was assessed by calculating the capacity loading and the regeneration efficiency for three consecutive absorption/desorption cycles carried out for 90 minutes at 30°C and 80°C, respectively. Then the effect of temperature (from 30°C to 60°C for the absorption step and from 70°C to 110°C for the desorption one) was investigated and discussed. The results were compared to the ones obtained in a former study carried out on the same test bench with a 12.5%wt [Cho][Pro] in DMSO solution – showing the very poor performances of the current solution with respect to the latter.

Table of Contents

List of figures

List of tables

List of abbreviations

AA	Amino Acid
AC	Absorption Capacity
ASTM	American Society for Testing and Materials
ATR-IR	Attenuated Total Reflection Infrared
BECCS	Bioenergy with Carbon Capture and Storage
CC	Carbon Capture
CCL	CO2 Circle Lab
CCS	Carbon Capture and Storage
CCUS	Carbon Capture, Utilisation and Storage
CFC	Chlorofluorocarbon
DAC	Direct Air Capture
DCA	Dicyanamide
DMSO	Dimethyl Sulfoxide
FT-IR	Fourier-Transform Infrared
GHG	Greenhouse Gases
IL	Ionic Liquid
IPCC	Intergovernmental Panel on Climate Change
IR	Infrared
MEA	Monoethanolamine
PEG	Polyethylene Glycol
RES	Renewable Energy Sources
RETM	Reaction Equilibrium Thermodynamic Model
RPC	Representative Concentration Pathways
RTIL	Room Temperature Ionic Liquid
TRL	Technology Readiness Level
TSIL	Task Specific Ionic Liquid
UV	Ultraviolet

List of chemical symbols

Ala	alanine
BF_4	tetrafluoro borate
BF_6	hexafluoro borate
bmim	butyl methyl imidazolium
CH_3COO^-	acetate
CH_4	methane
Cho	choline
CO	carbon monoxide
CO_2	carbon dioxide
COOH	carboxyl group
Gly	glycine
H_2	hydrogen
H_2S	hydrogen sulphide
H_2O	water
Lys	lysine
N_2	nitrogen
N_2O	nitrous oxide
NH_2	amine
O_2	oxygen
O_3	ozone
OH	hydroxyl group
PF_6	hexafluorophosphate
Pro	proline
SO_x	sulphur oxides

1. Introduction

Earth is the only planet in the solar system with an atmosphere able to harbour life by absorbing ultraviolet (UV) radiation, reducing excessive variations in temperature between day and night and retaining the heat coming from the Sun [1]. The mechanism which stands behind the latters is known as the greenhouse effect and is due to the presence of the infrared (IR) active gases – or greenhouse gases (GHG) – in the Earth's atmosphere, principally water vapour (H_2O), carbon dioxide (CO_2), and ozone (O_3) [2].

CO_2 and the other GHGs are therefore essential to life on Earth. The problem derives from the significant increases in concentration of some of them (CO_2, CH_4, N_2O and CFC) over the industrial period – as it can be seen in *Table 1.1*.

The main contribution to anthropogenic GHG emissions is attributed to carbon dioxide, which has been proved to be strongly connected to the global surface temperature rise [3]. The Fifth Assessment Report of the Intergovernmental Panel on Climate Change (IPCC) shows that the warming of the climate system is undeniable and, since the middle of the 19th century, unprecedented phenomena were observed over millennia.

To this regard, some of the evidence they brought is that the global average land and ocean temperature rose of $0.85°C$ between 1880 and 2012, with the ocean warming dominating the increase in energy stored; global water cycle over oceans has significantly changed, as proved by the differences in ocean surface salinity; the oceanic uptake of CO_2 led to its acidification, resulting in a 26% increase; Greenland and Antarctic ice caps have been losing mass at a large rate from the beginning of the millennium and glaciers have kept decreasing in extent; global sea level rose by 0.19 m, with a rate of increase larger than the mean rate during the previous two millennia [3].

Table 1.1. GHG concentration values from the pre-industrial era to nowadays. Sources [4]–[7].

	pre-industrial era	**1994**	**2021**
CO_2	280 [ppm]	359 [ppm]	415 [ppm]
CH_4	700 [ppb]	1721 [ppb]	1886 [ppb]
N_2O	275 [ppb]	312 [ppb]	334 [ppb]
CFC	-	265 [ppt]	226 [ppt]

Once established the correlation between the GHG concentrations in the atmosphere and the rise in temperature on Earth's surface, the Fifth Report of the IPCC, presents the so-called Representative Concentration Pathways (RPCs).

RPCs are projections of land use and GHG and air pollutant emissions over the 21st century that result from the combination of multiple factors, like population size, economic activity, energy use, lifestyle, land use patterns, technology and climate policies. Four different pathways are outlined: RCP2.6, RCP4.5, RCP6.0, and RCP8.5, where in the RCP2.6 scenario the temperature rise with respect to pre-industrial levels is kept below $2°C$, while in the RCP8.5 projection large amounts GHG emissions are involved.

According to this analysis, the business-as-usual scenario would result in pathways between RCP6.0 and RCP8.5, causing further warming and long-lasting changes with irreversible impacts on people and ecosystems.

It is of utmost importance, therefore, to undertake stringent measures able to curb the human activities that contribute to climate change, by mobilising international political response and by developing reliable and efficient technologies capable of curtailing the emissions.

In order to choose the direction to be followed, it is necessary to analyse which sectors are the main contributors to the global emissions and to find solutions for their abatement. *Figure 1.1* shows the global GHG emissions for the year 2016 broken down by consumption sectors and represented in percentage terms calculated on a total of $49.4\ billion\ tons$ of equivalent CO_2. It can be seen that 73.2% of CO_2 emissions come from the energy sector, where the main responsible are the emissions deriving from the energy usages of industry (24.2%), transport (16.2%) and buildings (17.5%).

The energy transition from a high to a low carbon economy demands thus the decarbonisation of the power, transport, and industrial systems, according to the characteristics and the energy-mix of the country under analysis. Until the TRLs will be high enough to guarantee an efficient and secure power supply from RES and the installed fleet of thermal power plants will be dismissed, carbon capture and storage (CCS) technologies will have an important role in the achievement of the net-zero emissions.

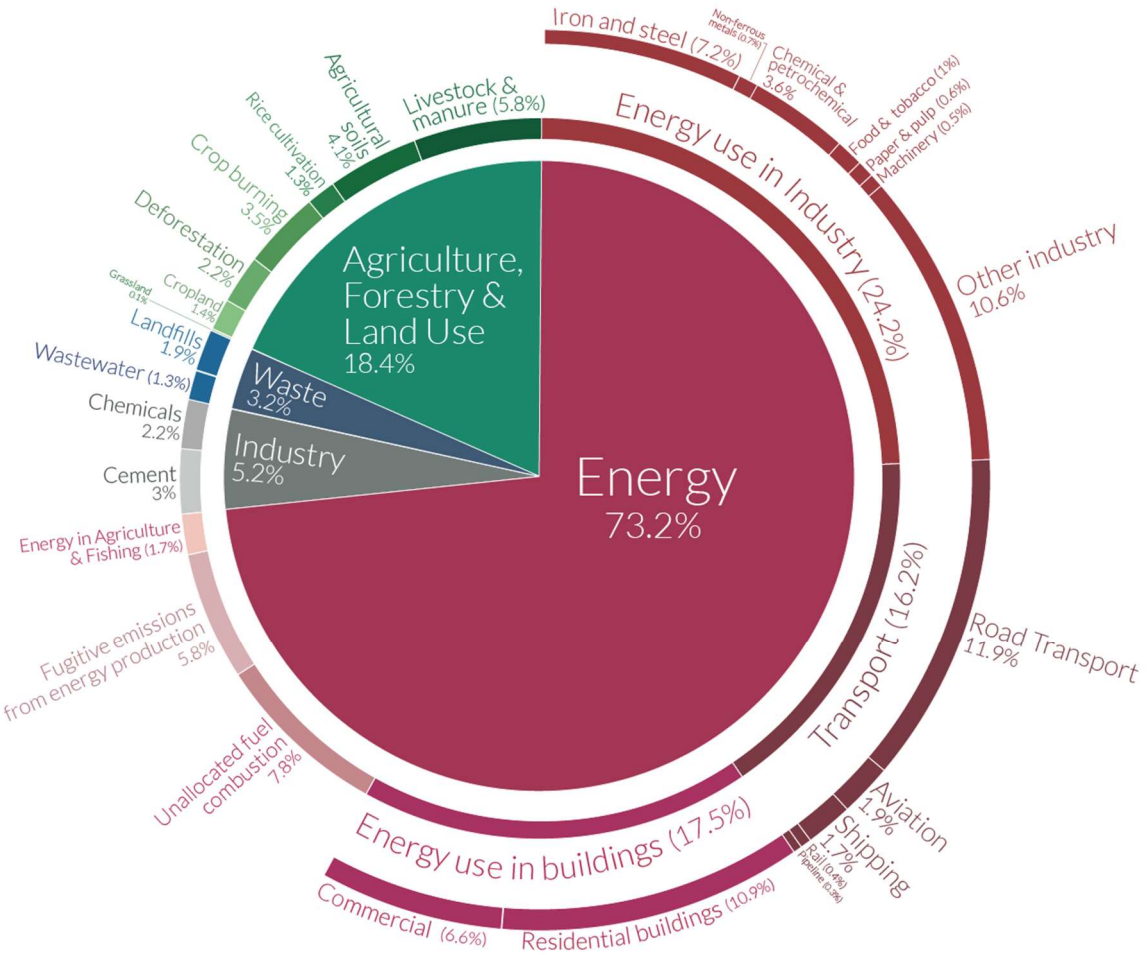

Figure 1.1. Global CO_2 emission by consumption sector in 2016. Total GHG emissions: 49.4 billion tons of CO_2. Source [8].

1.1. The role of carbon capture in the energy transition

As already mentioned, carbon capture utilization and storage (CCUS) technologies are expected to play a significant role in the energy transition, since they serve as a powerful tool for the decarbonisation of the already existing large stationary plants and the ones under construction. Moreover, if combined with bioenergy (BECCS) or direct air capture (DAC), they could even lead to negative emissions [9].

The analysis conducted by REN21 in their annual Global Status Report [10] points out the contribution of RES and non-RES to the global final energy consumptions – intended as the total energy consumed by end-users (i.e., residential, commercial, industrial and

transportation sectors) cut off the energy required by the energy sector for deliveries and transformation processes.

As it is shown in *Figure 1.2*, three major sectors can be identified: thermal, transport and power. It can be clearly seen that the penetration of RES is very low, with the highest share observed in the power sector – not even arriving at 30%, though. Possible routes to achieve the decarbonisation of these sectors are described in the following, enlightening the role of CCUS.

1.1.1. Power sector decarbonisation

In 2018, the power sector accounted for 17% of the global final energy consumption, from which only 21.7% derived from RES [10]. Considering the contribution of the nuclear sector around a value of ~4% [11], the remaining 70% involved biofuels, biomass- and fossil fuel-based power plants, which can be all coupled with CCS.

In the first two cases – that fall in the wider category of bioenergy – bio-crops are transformed via physico-chemical, thermal or biochemical processes into biofuels; these

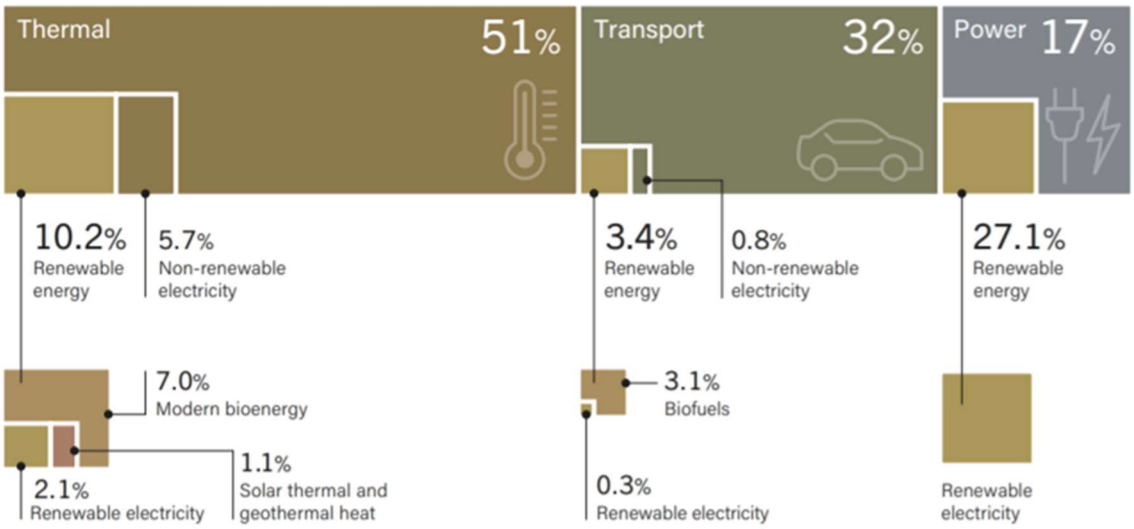

Figure 1.2. Contribution of RES and non-RES to total final energy consumption (by final energy use) by sector in 2018. Source [10].

are subsequently employed to generate electricity or as feedstock for industry, emitting the CO_2 captured during their growth and resulting in net-emissions in the optimal case. CCS technologies find their application in the biofuels conversion processes and combustion steps, possibly resulting in negative balances in the CO_2 emitted in the overall process. [12].

It has to be underlined, however, that in the case of BECCS – i.e., bioenergy coupled with CCS – two criticalities need to be faced: the energy-intensive bio-crop supply chain and the poor efficiencies of the plants. Studies [13] show that BECCs can present either positive or negative carbon emissions and energy balances according to the type of biomass utilised.

For what regards thermal power plants, the technologies available for decarbonisation are post-combustion CC, pre-combustion CC and oxyfuel combustion CC.

Post-combustion CC is usually coupled with traditional fossil fuel-based power stations for electricity production. In these configuration, the fuel undergoes complete combustion in air and the heat released during the process is utilised to produce high-pressure steam that feeds a turbine to produce electricity. The flue gases are then filtered to remove particulate matter and treated – usually by amine scrubbing – to sequestrate the CO_2 present in the stream (around 10% to 16% [14]). The advantage of post-combustion CC technologies is that they can be added to additional units without significant changes in the existing power plant.

Pre-combustion CC is combined with the integrated gasification combined cycle (IGCC). It presents an increased complexity, where the fuel is first gasified in an atmosphere of pure oxygen and steam in order to produce syngas. Then, the syngas – a stream of carbon monoxide (CO) and hydrogen (H_2) – is purified and sent to the water-gas-shift (WGS) reactor; here, thanks to the addition of steam, the CO and H_2O are converted to CO_2 and H_2. Lastly, the outlet stream is sent to the CC unit, which separates the CO_2 stream from the H_2 one, allowing the sequestration of the first and the combustion of the second in a gas turbine for electricity and heat production. The advantage of pre-combustion CC is that the CO_2 partial pressures at the CC stage are higher, resulting in favoured absorption

efficiencies. On the downside, it should be noted that this configuration cannot be employed for the retrofitting of existing plants.

The third configuration – the oxyfuel combustion – is a promising technology, but with still too low TRLs to be employed on an industrial scale. In this configuration, the fuel is burnt in a pure oxygen atmosphere. The heat produced during the combustion is again used to produce high-pressure steam that feeds a turbine to produce electricity – with no significant modifications in the eventually already existing plant. The outlet flue gases – after undergoing desulphurisation and water vapour condensation – are composed of pure CO_2, which can be stored underground or utilised in subsequent applications. In comparison to the previous two configurations, therefore, no CC is actually taking place here, but the relevant separation process is the N_2/O_2 at the furnace inlet. Furthermore, a replacement of the already existing boiler may also need to be considered in the case of retrofitting an existing plant.

Economic analyses [15]–[17] of the three configurations described above show that the pre-combustion CC is the least expensive option, though it presents the highest investment costs. Currently, the majority of the installed capacity sees the post-combustion CC configuration, since it allows the retrofitting of existing units.

1.1.2. Transport sector decarbonisation

In 2018, 32% of the global final energy consumptions were required from the transport sector, with the RES covering only 3.4% of the demand (see *Figure 1.2*.). Since the contribution to the total GHG emissions of this sector are around 20% (see *Figure 1.1*.) and transportation is dominated by fossils, the opportunities for decarbonisation are huge.

The three main options available – low-carbon electricity, low-carbon hydrogen, and biofuels – match with the three types of low-carbon mobility – electric mobility, hydrogen fuel cell mobility, and internal combustion engine mobility, respectively. In the following, the latter three are discussed.

Electric mobility – i.e., electric cars, buses, and rails – has nowadays a low share in the total fleet, however future projections see its steady increase. The achievement of net-zero

emissions in this sector requires low-carbon sources for the production of the power supplied, among which electricity from RES or large fossil plants coupled with CCS units.

Hydrogen fuel cell mobility technologies are commercially available for spacecraft and forklifts only, while passenger cars and buses are still in refinement [18]. Furthermore, the main barriers to market penetration of this low-carbon mobility type are the lack of infrastructure and the high costs. Low-carbon hydrogen can be produced from fossil fuel steam reforming coupled with CCS – known as blue hydrogen – or electrolysis with renewable energy – defined green hydrogen.

Internal combustion mobility nowadays holds the largest share in the mobility fleet. However, in order to decarbonise these vehicles it is necessary to substitute the current fossil fuels with biofuels (i.e., bioethanol and biodiesel) – by themselves or blended with gasoline and diesel. CCS technologies can be deployed in the biofuels production processes, as previously discussed.

1.1.3. Industry sector decarbonisation

The hardest sector to be decarbonised is the industrial one, which includes many processes as steel, cement and fertilizers production, refining, and chemicals synthesis . The latters rely on thermal energy that is currently supplied by the combustion of fossils and only a very small percentage have been electrified until now.

The possibilities for decarbonisation of industries see four paths: the further electrification of the heat sources involved in the processes, blue or green hydrogen employment as fuels, biomass utilisation, and fossil fuels utilisation coupled with CCS technologies

For what concerns the first option, it has to be recalled that the most carbon-intensive industries – i.e., chemicals, iron and steel, cement – are the hardest ones to be electrified. Indeed, these sectors see $\sim 45\%$ of emissions coming from the feedstocks, $\sim 35\%$ of emissions from the fossil fuels combustion for high-temperature heat production, and $\sim 20\%$ from the combustion for low- and medium-temperature heat production. As a result, electrification can act just in the reduction of the CO_2 from combustion processes. Moreover, the electrification of these processes would require a re-design of the

technologies involved, not to mention the significant increased prices of electricity that it would lead to.

The deployment of blue or green hydrogen may represent a very good alternative, since hydrogen can be both used as a feedstock and to supply heat to the industrial processes to be decarbonised. Furthermore, green hydrogen can be also considered as a tool for electrification, since renewable electricity is required for its production. Currently, however, the TRLs are still too low to allow the utilisation of hydrogen-fuelled processes.

Biomass can be utilised both as a heat source from its combustion or as a feedstock. Possible applications of biomass are in the steel, cement, glass and ceramics industries, however there are many barriers – among which the higher costs and the more complex processes in comparison with fossils-based ones – that hinder its penetration.

The last – and the most viable, at present – option sees the coupling of CCs technologies with fossil fuels-based industrial processes. CCS is in fact the only option nowadays to decarbonise the cement and the steel industries, until other energy- and cost-effective options will be developed.

A schematic of the considerations made until now about the possible routes to achieve net-zero, or at least to cut the CO_2 emissions from the power, transport and industry sectors is shown in *Figure 1.3*.

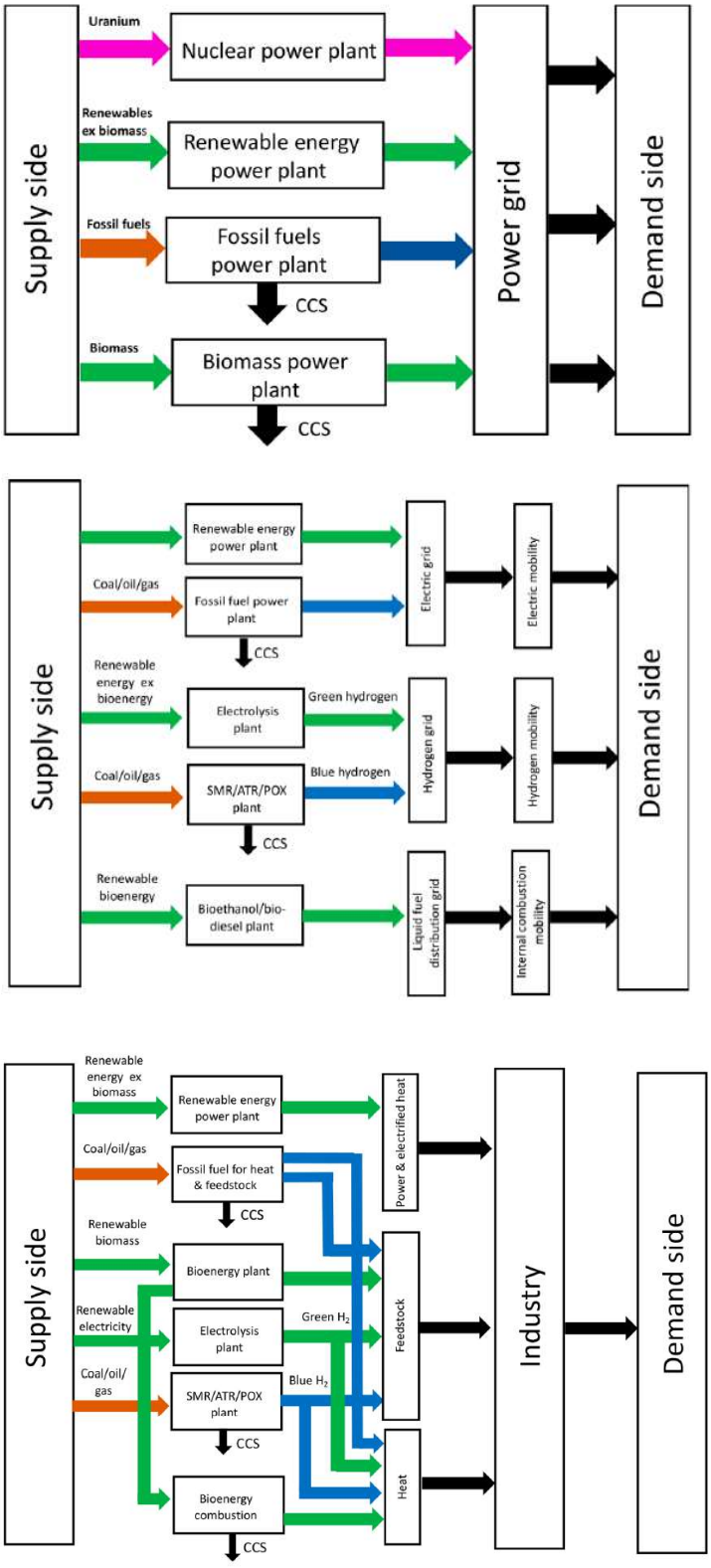

Figure 1.3. Schematic of the available options for the decarbonisation of the power, transport and industry sectors. Source [12].

2. State-of-the-Art of ILs for post-combustion carbon capture

Nowadays there is a strong urge to develop and efficiently design industrial processes able to curtail the carbon dioxide emissions from industrial flue gases. The possibilities are many – physical and chemical absorption, adsorption, membrane-based separation, electrochemical and cryogenic processes [19]; up to now, however, the technology which is most mature and allows the retrofitting of the existing fossil power plants is chemical absorption [20]. This leads to the need for enhanced and sustainable liquid absorbents for CO_2 capture.

The industrial applications are at present based on amine scrubbing, typically involving solutions of $30\%wt$ monoethanolamine (MEA) in water. CO_2 removal by absorption and stripping with aqueous amine is a well-known technology, having the basic process been patented in 1930 [21]. The main advantages of MEA solutions are the low costs – thanks to the high technology readiness level (TRL) achieved – and the fast kinetics and high mass transfer rates of the absorption, which result in large enthalpies involved in the reaction [22], [23]. The latters, on the other side, are the reason for the significant drop in energy efficiency of the power plants which include carbon capture from flue gases via aqueous amines solvents, since large amounts of heat are required to operate the regeneration step (ΔH ranges from $-80\ kJ/mol$ to $-64\ kJ/mol$ in case of bicarbonate formation in the absorption reaction and $-101\ kJ/mol$ in case of carbamate formation [24]). In this regard, it is estimated that the retrofitting of an operating power plant with amine scrubbing-based technologies lowers the energy output of the plant by $25-40\%$ [25]. This could result in increased prices of the electricity in absence of policies, besides.

Additional concerns must be taken into account when analysing MEA-based technologies, such as the corrosion of alloy steel components by the amines; the loss of active absorbents due to the thermal and oxidative degradation of MEA – with additional waste streams and operational costs linked to the necessity of additional fresh solvent; increased environmental impact due to evaporation losses into the gas stream – being amines and ammonia very volatile liquids [24], [26], [27].

As a consequence of the several drawbacks of the aqueous amine-based processes, research endeavours to develop alternative liquid absorbents, sustainable from the operational point of view, with limited synthesis costs and impacts, and with high absorption capacities – overcoming the $0.5\ mol_{IL}/mol_{amine}$ limit [28].

Within this framework, ionic liquids (ILs) are a new class of material that is considered to be very promising thanks to their remarkable and unique properties. By definition, ILs are salts which present melting points below $100°C$ [29], [30] . This difference in behaviour in comparison to the conventional inorganic molten salts is due to the lower lattice energies, which allows them to be liquid at room temperature [31].

Although discovered in 1914 with the studies of Paul Walden regarding the physical properties of ethylammonium nitrate ($[EtNH_3][NO_3]$), ILs did not prompt any significant interest until the late 1990s [32], [33]. The reason for that renewed attention was connected to an article published by Freemantle in 1998, which brought to light the potential of ILs as novel solvents for green chemistry [34]. From then onwards the advantages related to the distinctive features of ILs – i.e., the negligible volatility, the high thermal stability, the tunability of their physico-chemical character, the nonflammability, the extremely low saturated vapor pressure, the wide electrochemical window, and the high CO_2 solubility – spread their use in many fields of application [35]. ILs, in fact, show huge potential in analytical chemistry [36], [37], biochemistry [29], catalysis [38], [39], electrochemistry [40], [41], separation technology [42]–[44], and fluid engineering [45]–[47]. It needs to be underlined, moreover, that there are 10^{18} possible combinations of anions and cations which would be possible in theory; a proper study on what influences their performances appears to be crucial in the design of practical applications, therefore [34]. In line with the purposes of this study, the attention will be focused on the characterization and discussion of the ILs employed in carbon sequestration technologies.

The high solubility of CO_2 in an imidazolium-based ILs ($[bmim][BF_6]$) was first detected by Blanchard at al. in 1999 [48], [49]. Subsequently, numerous studies explored the possible applications of ILs in CO_2 absorption processes.

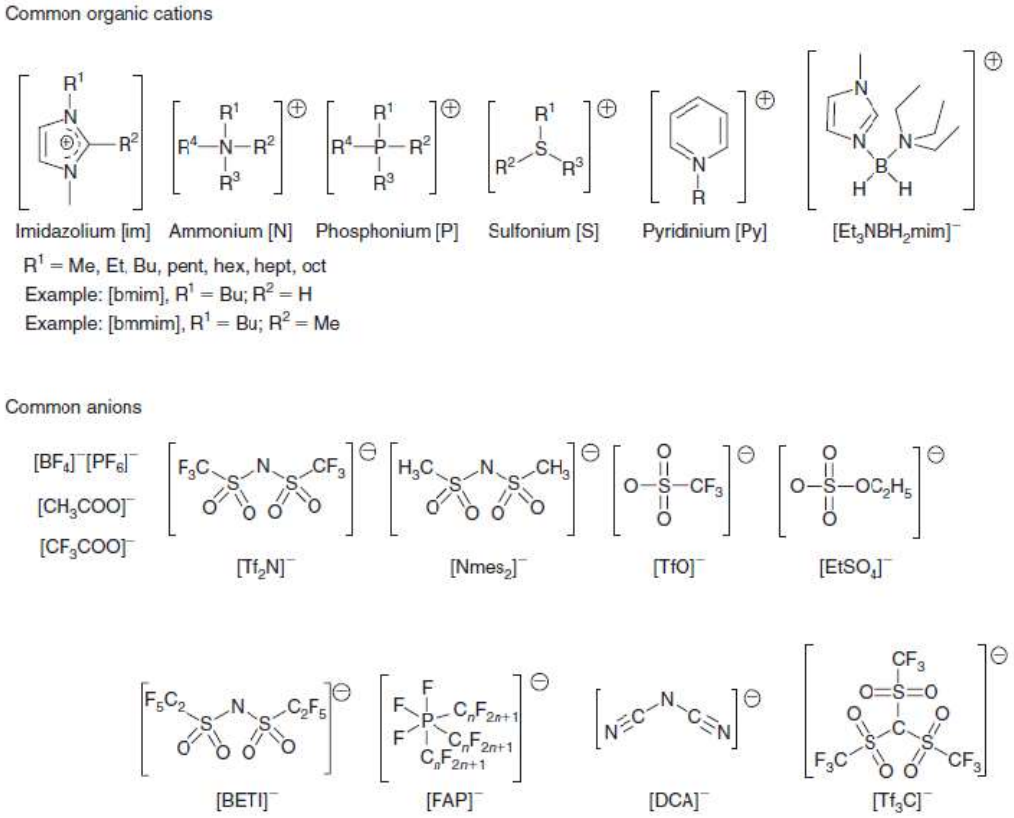

Figure 2.1. Molecular structures of common anions and cations employed for the synthesis of RTILs and TSILs. Source [24].

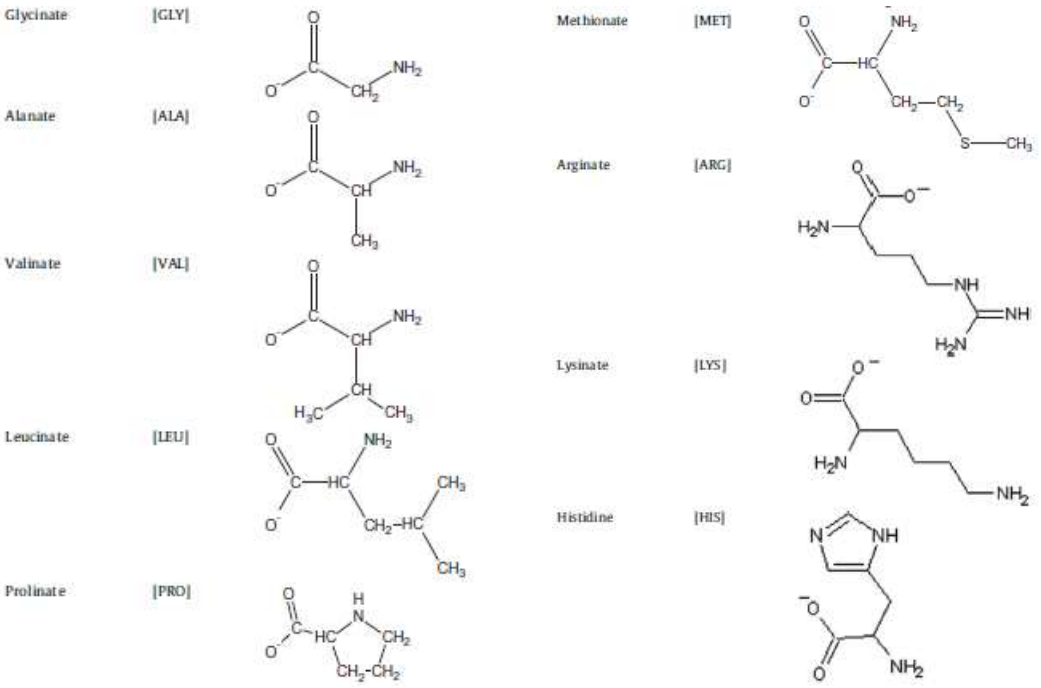

Figure 2.2. Molecular structures of common anions employed in amino acid ionic ILs (AAILs). Source [50].

Three generations of ILs can be distinguished. The first one coincides with the so-called room temperature (RTILs) or conventional ILs and is based on imidazolium cations. It is mainly centred on the physico-chemical properties of the IL itself and allows the physical absorption of CO_2 only.

The second-generation of ILs initiates the tunability of the properties of the IL by adding functional groups to the cation or the anion and is commonly referred to as task-specific (TSILs) or functionalised ILs. Both physical and chemical absorption take place in this case, resulting in much higher CO_2 capacity loadings.

The third generation consists of new compounds which contain hydrophobic anions from natural resources, like amino acids and organic acids; their main advantage is that they combine high absorption capacities – thanks to the functional groups they include in the structure – with ease of synthesis, low cost, low toxicity, and biodegradability. [24], [35], [51].

2.1. Conventional ILs (RTILs)

Conventional ILs or RTILs are made of cations and anions which do not present any functionality, thus CO_2 absorption is merely based on a physical mechanism. The number of possible combinations which gives origin to RTILs is huge, some of the possible cations and anions are displayed in *Figure 2.1.* As already mentioned, however, for this first generation of ILs the imidazolium-cation class is the most widely studied one.

The early studies on carbon capture with ILs are centred on the phase behaviour of RTILs with CO_2 in comparison to conventional organic solvents [48]. As it can be observed in the schematics reported in *Figure 2.3*., the remarkable difference of IL systems is the presence of a two-phase region (the liquid IL-CO_2 phase and the pure CO_2 phase) in the low-medium operating pressures and a single-phase (the liquid IL-CO_2 mixture phase) in the high operating pressures. This means that if for molecular organic solvents the CO_2 molecules are completely miscible at high pressures, in the case of IL applications the increase in pressure results in a slight or no increase in the solubility on the CO_2 rich side of the phase diagram.

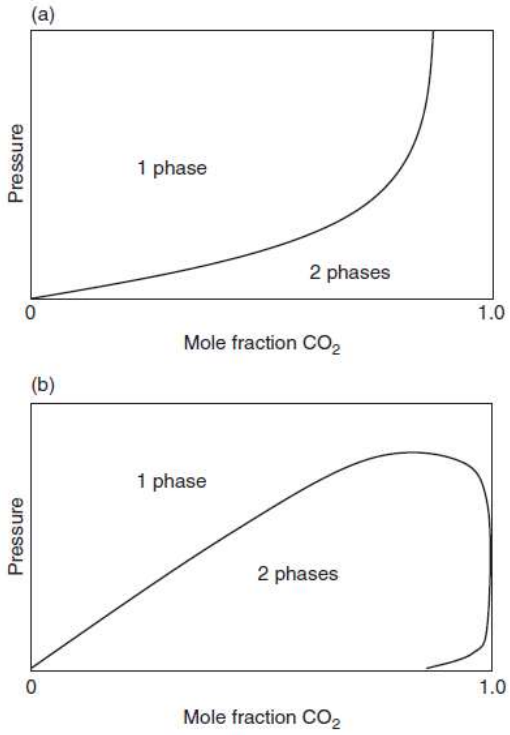

Figure 2.3. Schematic of the phase diagrams of (a) RTIL-CO_2 systems and (b) molecular organic solvent-CO_2 systems. Source [24].

An additional difference of ILs with respect to organic solvents concerning gas dissolution is that they do not show relevant volume expansion with increasing fractions of CO_2 dissolved [52]. Both of the considerations made up until now can be traced back to the internal structure which characterises ILs.

A packed structure results from the strong Coulombic interactions among anions and cations ILs are composed of, which is much more rigid if compared to the internal structure of organic solvents. The combination of the well-defined disposition of the ions and the electrostatic interactions among them leads to the small volume expansions when high mole fractions of CO_2 are dissolved.

Molecular dynamics studies about the absorption mechanism of $[\mathrm{bmim}][PF_6] - CO_2$ systems showed that the size of the cavities (i.e., the 'free volumes') available at the start is not sufficiently big; therefore, even though the differences are not significant in terms of radial distribution functions, the ionic network is slightly perturbed and the position of the anions changes by a small angular displacement in order to allow the arrangement of the

CO_2 molecules. Subsequently, the CO_2 molecules arrange themselves above and below the imidazolium rings [53].

These research findings suggest that, thanks to these internal arrangements, 'free volumes' are available in large quantities – which are occupied by the CO_2 absorbed molecules. This on the one side explains the reason behind the lower volumetric expansion upon dissolution and on the other one clarifies why the amount of CO_2 dissolved cannot be increased even by infinitely high pressures – since the amount of free volume initially available is finite

In addition to what was discussed until now, the utilisation of ILs as solvents for post-combustion carbon sequestration requires the proper evaluation of their performance in term of CO_2 capacity loading and selectivity. In the following, the factors which affect these properties are discussed, together with the concerns in practical applications involving RTILs.

2.1.1. CO_2 solubility

The dissolution of CO_2 in RTILs was studied by Palomar et al. [54], who provided an analysis of the intermolecular interactions among the species in the fluid phase – i.e., electrostatic interactions, hydrogen bonding and van der Waals interactions. Furthermore, they discussed the contribution of each of them to the total CO_2 solubility, proving that the CO_2 dissolution mechanism is dominated by van der Waals forces, while the electrostatic interactions are secondary and the hydrogen bonding are quite insignificant.

The studies available in the literature show that the carbon dioxide solubility in ILs is mainly affected by the characteristics of the anion – which is acknowledged to be the dominant factor both by molecular simulation studies [55] and experimental observations [56].

In situ attenuated total reflection infrared spectroscopy (ATR-IR) studies performed by Kazarian et al. [56] pointed out the favourable interaction between the anions and the CO_2 regardless of the structure of the cation. Furthermore, the study suggests that the interaction is of a Lewis acid-base type, with the anion serving as Lewis base (electron-pair

(a)

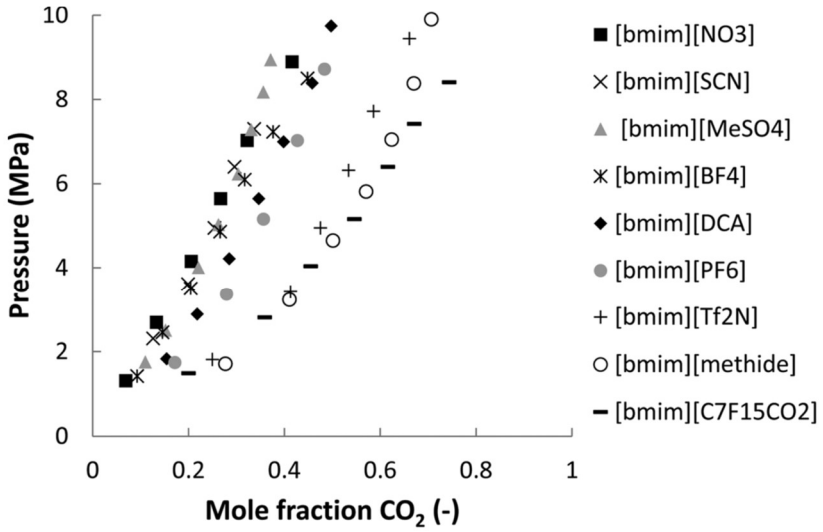

(b)

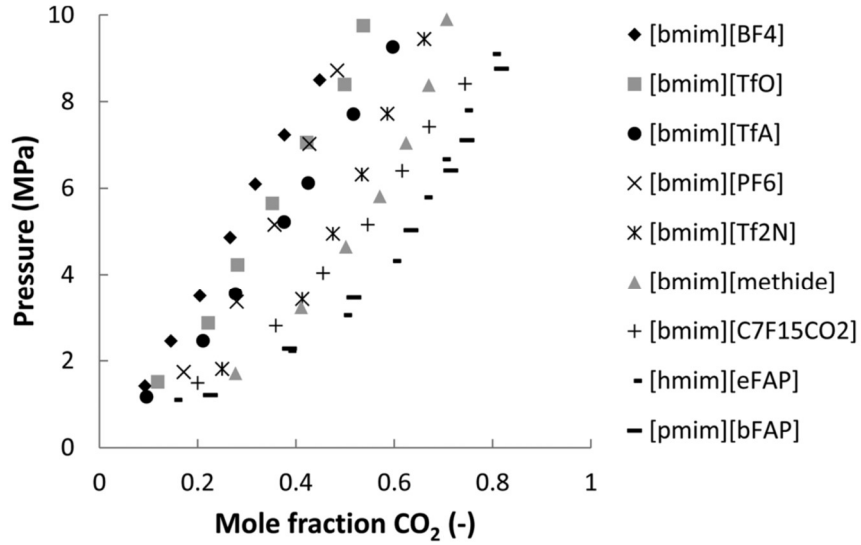

Figure 2.4. (a) Effect of the anion and (b) effect of the anion fluorination on carbon dioxide solubility in RTILs. (b) Source [34].

donor) and the carbon dioxide as Lewis acid (proton donor). In addition, it proved that the stronger the anion acts as a base, the stronger is the interaction with the CO_2. The effect which different anions have in terms of CO_2 solubility is shown in

Figure 2.4 (a). Based on the observations made above, it can be seen how the imidazolium-based ILs with $[BF_4]$ and $[NO_3]$ anions present the best performances among the cases examined.

Further observations demonstrated that ILs containing fluorine atoms present higher solubilities than those without it. The effect of fluorination was studied on ILs containing [bmim] cation and the results obtained are shown in *Figure 2.3 (b)*, confirming that the higher the number of fluor groups, the higher is the CO_2 solubility.

In this connection, additional studies on the effect of fluorination showed that the CO_2 solubility can be furtherly enhanced by adding fluoroalkyl chains in the anion structure, which has the double effect of both improving the interactions between the CO_2 and the ILs and of increasing the amount of available 'free volume' in the internal structure [57], [58].

The CO_2-philicity of fluorinated alkyl chains can again be described with the Lewis theory of acid-base interactions. In the case of the anion with no fluorine atoms within the alkyl chain, the carbon dioxide molecules are a weak Lewis base, with the oxygen atom interacting with the $C-H$ bond. In case electronegative fluorine atoms are included in the alkyl chain of the anion, on the contrary, the CO_2 molecules acts as a Lewis acid, with the carbon atom interacting with the $C-F$ bond. Since in the first case the Lewis base is weak, while in the second one the Lewis acid is strong, the intermolecular interactions between the anion and the CO_2 have different nature and result in the different solubilities performances observed.

Even though the nature of the anion has a predominant influence on the CO_2 dissolution mechanism than that of the cation, this last cannot be neglected. Its smaller effect on the CO_2 dissolution is displayed in *Figure 2.5*, from which the [choline] cation shows the best performances among the ones examined.

In this regard, studies showed that higher solubilities can be achieved when longer alkyl chains are present on the imidazolium ring, which is also associated with more negative sorption enthalpy and entropy values [59], [60].

The reason behind the considerations made above can be traced back to the 'free volume' mechanism, since longer alkyl chains result in larger 'free volumes' and more space available for the arrangement of the carbon dioxide molecules, consequently.

With regard to the intrinsic characteristics of the cation which enhance the CO_2 solubility, it is also necessary to point out the effect of the proton present on the imidazolium ring in the C2 position. It was in fact proved to be acidic, which involves the possibility of dissolving CO_2 via hydrogen bonds [61], [62].

The effect of this acidic site was studied by means of molecular simulations, which showed that substituting the hydrogen in the C2 position with a methyl group moderately decreased the CO_2 solubility at high pressures – that is, above $70\ bars$ [55]. The reason behind this behaviour is that the methyl groups changes the disposition of the anions, which would be bounded at the C2 sites via hydrogen bonding; at low operating pressures, the carbon dioxide molecules are mainly associated with the anions and are quite distant from the cations. When high operating pressures – and thus large amounts of CO_2 – are involved, some molecules occupy the secondary locations near the cations, enhancing the dissolution in this manner.

The fluorination of the alkyl chains on the cations has been studied as well [63], [64]; the effects observed, though, were not as significant as in the case of anion fluorination since, as said above, the CO_2 molecules mainly interact with the anions.

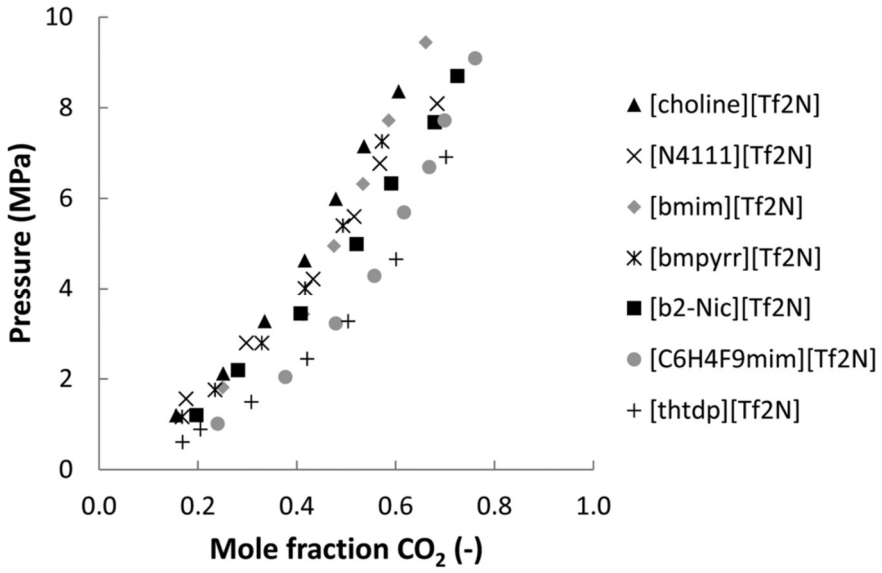

Figure 2.5. Effect of the cation on carbon dioxide solubility in RTILs. Source [34].

2.1.2. CO_2 selectivity

Since the ultimate aim of carbon capture technologies is to separate the carbon dioxide from the mixture of multiple gases present in the stream to be treated, the selectivity performance of the solvent employed in the process is fundamental.

In general, the solubility of nitrogen, oxygen, hydrogen, carbon monoxide, and hydrocarbons in RTILs is significantly low [65]–[67].

Table *2.1* reports the Henry's constant values for some gases which may be present in practical applications of post-combustion processes. It is recalled that the lower the Henry's constant value, the higher is the solubility of the gas in the liquid.

The most relevant selectivities in the field of post-combustion CO_2 capture processes are the CO_2/N_2, the CO_2/O_2, CO_2/CO and the CO_2/SO_x ones. Hydrogen and syngas purification and pre-combustion carbon capture applications are also interested in the CO_2/H_2, the CO_2/CH_4 and the CO_2/H_2S ones, respectively; however, this will not be discussed in detail in the following, since it lies outside the scope of this study.

Broadly speaking, the N_2, the CO and the O_2 solubilities are much lower in comparison to the CO_2 one – with Henry's constant values differing of orders of magnitudes (see Table *2.1*). Therefore the CO_2/N_2, the CO_2/O_2, CO_2/CO selectivities are proved to be very good.

Table 2.1. Henry's constant for different gases at $p = 1\ bar$ and $T = 25°C$ in [bmim]-based ILs . Source[24].

	$[bmim][PF_6]$	$[bmim][BF_4]$
CO_2	53.4	55.7
CO	>20 000	1728
O_2	8000	1580
N_2	>20 000	1703
H_2	>1500	2037
CH_4	1690	887
C_2H_4	173	-
C_2H_6	355	300

The main issue which affects CO_2 selectivity in post-combustion carbon capture processes is attributed to the sulphur-containing compounds, which show higher solubilities in RTILs and are twice or three times more soluble than CO_2 one in some cases [66]. Nonetheless, it must be taken into account that the partial pressure of the CO_2 in the flue gases stream is much higher in comparison to the SO_x one, which reduces this drawback significantly. In any case, it is necessary to separate the sulphur compounds from the flue gases before the carbon capture takes place in a flue gas desulphurisation (FGD) unit. An alternative option consists in removing the CO_2 and the SO_x from the stream at the same time by absorbing them in the RTILs and separating them after their release at the end of the regeneration step [68], [69].

Water solubility is an additional aspect that needs to be discussed; all ILs are hygroscopic, therefore they collect the water vapour contained in the flue gases, drastically lowering the CO_2 capacity of the IL [70]. Just to give an example, Blanchard et al. [52] showed that the capacity decreases from a 0.54 molar fraction in dried $[\mathrm{bmim}][PF_6]$ to a 0.13 molar fraction in water-saturated samples.

Furthermore, the energy requirements that occur at the regeneration step increase significantly, since water needs to be evaporated in the stripper. It is of utmost importance, thus, to condensate the vapour phase present in the flue gases before they enter the absorption column for the carbon capture step.

2.1.3. Critical issues affecting RTILs in practical applications

The most relevant concern which affects the utilisation of RTILs in post-combustion carbon capture processes is linked to the very low capacity achievable when the CO_2 partial pressure is lower than the ambient pressure one. Indeed, even though the absorption capacity performances are very good at CO_2 pressures above $10\,bar$, these operating conditions are hard to be reached in normal applications, where the flue gases are usually at ambient pressure and the CO_2 fraction is around values of $\sim 10\% \div 15\%$ – thus significantly decreasing its partial pressure [71], [72].

The poor absorption capacity exhibited by RTILs can be attributed to the physical mechanism which occurs. As it has been proved by molecular dynamic simulations, in fact, only a very small number of CO_2 molecules can be arranged within the internal structure of anions and cations. In this regard, Zhang et al. [73] showed that 192 molecules of IL are necessary to physically absorb 10 molecules of CO_2 when $[bmim][PF_6]$ is employed.

Despite the much higher absorption performances which could be obtained, increasing the operating pressures far beyond the ambient one is inconceivable, since the decrease in energy efficiency and the increase in capital cost of the plant would occur simultaneously.

To overcome these problems, one way consists in developing ILs with a better internal structure in order to allow the arrangement of a higher number of molecules; this, however, would lead to limited performances in any case.

A more effective option is to develop TSILs with functional groups able to chemically absorb the CO_2 from the flue gases to be treated. An overview in this regard is given in the following section.

2.2. Functionalised or Task-Specific ILs

The limited absorption capacity values which distinguish conventional ILs have led to the necessity of including functional groups in their internal structure to increase the number of molecules sequestrated by the absorbent.

The selection of the functional groups which can be employed is driven by the thermodynamics and the kinetics of the absorption process. The energy profile for the absorption and desorption reactions occurring at the functional group site is shown in *Figure 2.6*. Clearly, the difference in enthalpy between the absorption and the desorption phases must be limited. Furthermore, the ideal condition requires the low exothermicity of the absorption phase, so that the energy requirements during the subsequent regeneration are limited. Either way, TSILs show much lower sorption enthalpy values in comparison to conventional aqueous amine solutions – which can release up to $100\ kJ/mol$ when the reaction between the CO_2 and the functional group takes place [74].

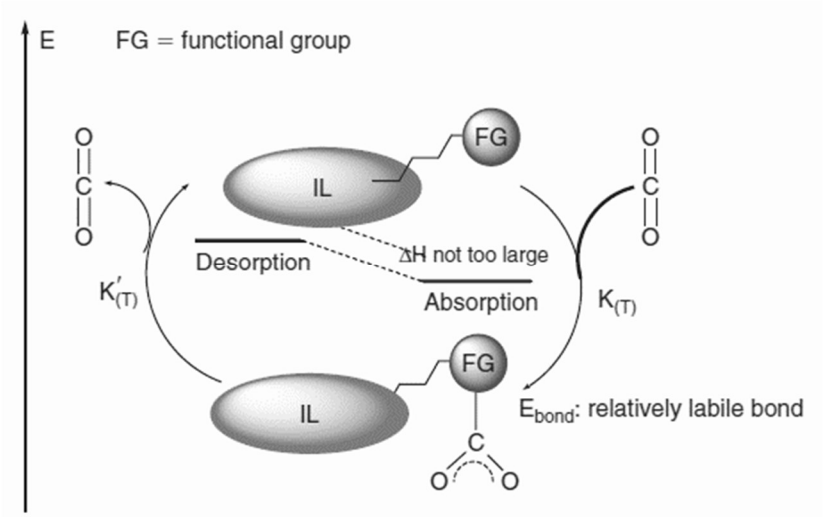

Figure 2.6. Energy profile for the absorption and desorption reactions in TSILs. Source [24].

Before discussing the possible functionalities that can be included in the IL structure, the ambivalent nature of the CO_2 molecule needs to be recalled. CO_2 can, in fact, act as a Lewis acid, due to the presence of the electron-deficient carbon atom; or as a Lewis base, due to the electron-rich oxygen. This enhances the total solubility and renders both amine and carboxylate functionalities possible.

2.2.1. Amine functionalised ILs

The first studies which combined the advantages of conventional ILs with the well-performant amines were initiated by the group of Davis in 2002 with the synthesis of an imidazolium-based cation with an amine functionality bonded through an alkyl chain [75], [76].

The reaction observed is shown in *Figure 2.7*. The functionalised IL reacted in a 2:1 stoichiometry, with two IL molecules necessary for the absorption of a CO_2 molecule; this led to the theoretical maximum uptake for amine-based absorbents of $0.5\, mol_{CO_2}/mol_{amine}$. The carbamate formation was detected as well, according to the conventional reaction scheme and confirmed by FT-IR spectra analysis.

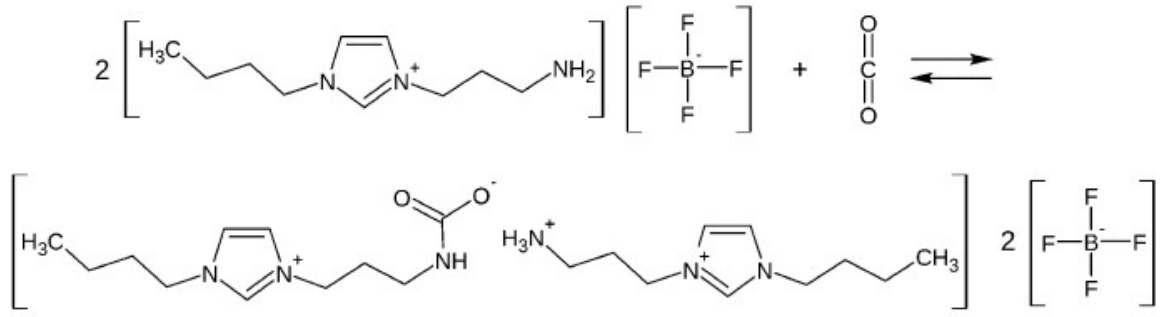

Figure 2.7. Absorption reaction between a functionalised IL and CO_2 with formation of a carbamate salt. Source [34].

The reversibility of the reaction is an additional important finding observed by the authors, with the CO_2 releasing taking place at temperatures of $80°C - 100°C$.

The significant drawback that was detected, though, is the higher viscosity of the synthesised TSIL in comparison to the conventional ones, resulting in hindered absorption mechanisms and higher energy demands from the fluid circulation system of the plant. However, no increase in viscosity was detected with the increase in the amount of CO_2 absorbed.

Sánchez et al. [77] investigated the difference in absorption performances resulting from the functionalisation of the [bmim] cation with primary or tertiary amines. Different anions – tetrafluoroborate [BF_4] and dicyanamide [DCA]) – were employed for the experiments performed. The study demonstrated that the CO_2 solubility of the tertiary amine-functionalised system is much lower in comparison to the primary amine one, due to the higher reactivity of the latter towards CO_2 [78]. Moreover, it was proven that the absorption performance of the primary amine-functionalised IL at ambient pressure is 13 times better in comparison to the same non-functionalised IL in case of [BF_4] anion. The possibility of regenerating the solution at $80°C$ without any decrease in absorption capacity was confirmed. The drawbacks linked to the high viscosities were still noted, with further increases occurring after the CO_2 absorption.

In order to figure out the reasons behind the high viscosities in cation-amine-functionalised ILs, Yu et al. [79] performed molecular dynamic simulations. Their study showed that the increase in viscosity is due to the internal arrangement of the anions around the $-NH_2$

functional groups and the subsequent formation of a strong hydrogen bonding network. The simulations, however, did not show any relevant change in the arrangement of the anions around the imidazolium cation.

Gutowski et al. [80] investigated the mechanism responsible for the relevant viscosity increase upon contact with CO_2. Through an accurate analysis of the simulations run, they found out that a strong hydrogen-bonded network is formed between the zwitterions, the intermediate molecules formed during the absorption mechanism.

Besides the cation functionalisation discussed until now, the anion functionalisation is also possible, leading to even better performances.

Gurkan et al. [81] studied the effects induced by cation and anion functionalisation in terms of absorption performances. They showed that in the first case the carbamate formation was prevailing, resulting in a $1:2$ reaction stoichiometry, while in the second case the CO_2 uptake was higher than one mole of CO_2 per two moles of IL, getting closer to the $1:1$ stoichiometry. Furthermore, it was observed that the CO_2 capacity loading curve presented two different parts: a steep increase occurring at the beginning of the experiment due to the chemical absorption, followed by an almost flat curve with slight capacity increases due to the predominance of the physical absorption.

As before, also in the case of anion functionalisation there is a significant increase in the enthalpy of reaction and viscosity values due to the presence of the amine functional groups.

2.2.2. Carboxylate functionalised ILs

IL functionalisation was also experimented through carboxylate functional groups. In particular, almost all the applications see the acetate anions $[CH_3COO]^-$ paired with imidazolium cations.

Chinn et al. [82] studied the [bmim][acetate] IL in a $14\%wt$ water solution; the experimental evidence they found confirmed that chemical absorption was occurring, since the CO_2 absorption profile presented the typical initial steep increase followed by a plateau

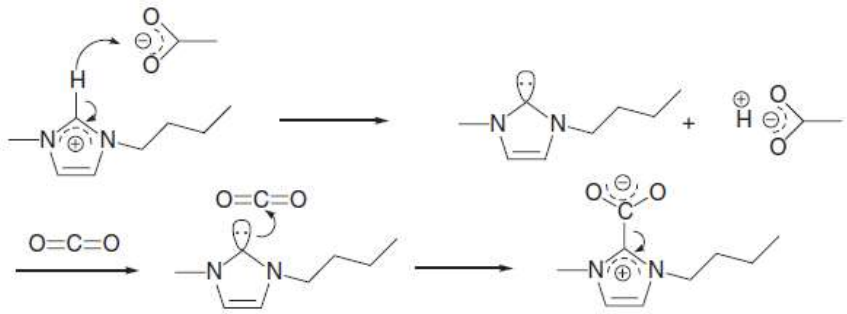

Figure 2.8. Reaction of CO_2 at the C2 site of the imidazolium in an in situ-generated carbene. Source [24].

when the physical absorption started to be predominant. They explained the complexation process with a mechanism where the acetate groups interact with water and the CO_2 molecules bind as bicarbonate.

Maginn et al. [83] also studied the [bmim][acetate]interaction with CO_2, hypothesising a different reaction mechanism in which the acetate anion extracts a proton from the C2-site of the imidazolium ring and the forms of acetic acid; in this mechanism, the CO_2 is captured in the form of bicarbonate through the reaction with carbene. The reaction is shown in *Figure 2.8*.

2.3. Amino acid ionic liquids (AAILs)

Since they emerged in the research field, ILs have been generally referred to as 'green solvents', though neither the fluorine-based anions nor the imidazolium cations discussed until now and extensively employed in practical applications show good biodegradability, but are on the contrary proved to be toxic [84].

In this view, many efforts are being made to develop truly biocompatible ILs, while maintaining optimal absorption performances and good regeneration efficiencies of the materials, together with guaranteeing recyclability.

In 2004, Abbott et al. [85] synthesised the first fully biocompatible IL by coupling choline chloride with succinic and oxalic acids, naturally-occurring organic substances. Thereafter, the imidazolium cation started to be replaced with the biodegradable and less expensive cholinium cation [86]. In concomitance, the idea of replacing the fluorinated anions with organic acids arose – with particular focus on amino acids (AA) [87], [88]. These choline-based AAILs were – and still are – believed to be able to accomplish a green chemistry cycle, starting from the synthesis process and ending with their use in carbon capture processes.

Cholinium-amino acid ionic liquids ([Cho][AA] ILs) consist of a quaternary ammonium choline cation and a deprotonated amino acid anion. The general structure is shown in *Figure 2.9.* Before discussing in detail the inherent nature of cation and anion, the overall structural features are pointed out.

The analysis of the electrostatic potential in the cation shows that the positive charge is located on the $N-(CH_3)_3$ fragment and on the terminal hydroxyl hydrogen $-OH$. Due to its large extension, the first fragment is not densely charged and thus is polarizable, while the hydroxyl group is highly polar. In the anion, instead, the charge results to be denser on the carboxylate group $-COO^-$ site and the remaining part of the chain has a little polar character. Moreover, it has been noticed that the $-COO^-$ functional group can act as a hydrogen bond acceptor, while the $-OH$ group on the choline can be both hydrogen bond acceptor and donor [89].

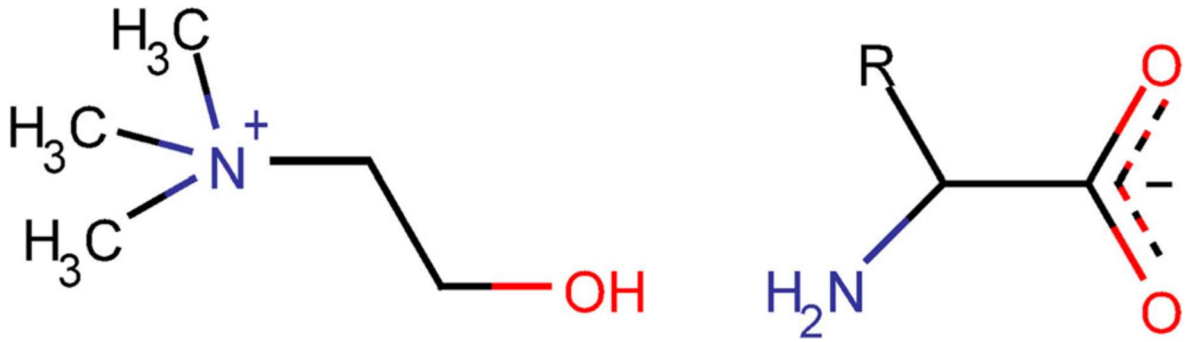

Figure 2.9. The general structure of choline-amino acids. Source [89].

The multiple interactions enumerated above have been confirmed by theoretical and experimental studies, which showed that ion coupling, strengthened by the hydrogen bonding network between the carboxylate groups in the anion and the hydroxyl groups in the cation, play a major role in the interactions discussed [89].

Furthermore, these possible interaction patterns explain both the large solvating power of [Cho][AA] ILs and the extreme viscosity which distinguishes them and makes the use of solvents unavoidable.

2.3.1. Nature and characteristics of the choline cation

Choline belongs to the class of quaternary ammonium salts and is one of the most important biodegradable, inexpensive and water-soluble organic salt [89].

AA ILs with ammonium cations, besides having low toxicities, show very good CO_2 capture performances thanks to the fast reactivity towards CO_2 [90], [91]. Choline – or N,N,N-trimethylethanolammonium – consists of an ethanolamine with three methyl substituents attached to the amino function, thus is an optimal candidate in this sense.

Thanks to their reduced cost and greener properties, cholinium-based ILs are gaining more and more attention as solvents in the field of organic synthesis [92]. Just to cite some studies in this field, Pernak et al [93] synthesised sixty-three choline derivative-based IL in the form of chlorides, acesulfamates, and imides and determined their physical properties; García-Suárez et al. [94] studied the chemical stability of choline-based ILs intending to use them as catalysts to conduct liquid-phase synthesis; Gadilohar et al. [95] provided a detailed analysis of choline-based ILs and their applications in organic transformation; De Santis et al. [96] described the correlation between experimental properties (density, viscosity, conductivity, refractivity) and AA; Gontrani [89] reviewed the achievements made in the structure and properties; Le Donne et al. [97] presented a state-of-the-art of the choline-based AA ILs, reporting synthesis process, physico-chemical properties, toxicity and biodegradability, interaction with complex biological molecules, different applications in which they can be involved, structure and computational studies.

There is also recent work about cholinium-base AA ILs in the carbon capture field [98]–[102]; however, being the system mostly ruled by the aminate anion, a more detailed review of the mechanisms involved and the work done until done is reported in the following section.

2.3.2. Nature and characteristics of the amino acid anion

AAs have a low environmental impact, high biodegradability, negligible volatility and high resistance to oxidative degradation. Their biocompatibility is a direct consequence of their metabolic nature, being them the building unit of proteins and essential components of many nutrients [97].

In terms of internal structure, the common feature of all AA is that they are composed of at least one amino ($-NH_2$) and one carboxylic acid ($-COOH$) group. Both inter- and intramolecular interactions between the basic and acidic sites determine the physical and chemical properties of these compounds [103].

The most common AA anions employed in ILs are shown in *Figure 2.2*.

A relevant characteristic of AAs is their amphoteric character – that is, they can act as either acids or bases depending on the environment they are in. AAs, in fact, exist as inner salts (zwitterions), with the positive charge located on the amino group and the negative charge located on the carboxylic acid group.

The internal structure of AAs is a result of the pH of the medium in which they find themselves. At low pH (<1), they exist as protonated cations, at high pH (>12) they are in the amino carboxylate anion form; in the middle, the inner salt – with both the positive and negative charges dislocated on the functional groups – is present along with varying amounts of protonated cations and amino carboxylate anions. The mechanism described is resumed in equation (2.1).

$$H_3N^+CH_2COOH \overset{H^+}{\longleftrightarrow} H_3N^+CH_2COO^- \overset{H^+}{\longleftrightarrow} H_2NCH_2COO^- \quad (2.1)$$

In ILs, AAs are already found in the deprotonated form; however, depending on the cation they are paired with, they can be more or less basic. Studies [104] proved that enhancing the basicity of the AA anion leads to better CO_2 absorption performances by facilitating the carbamic acid-formation reaction and thus the $1:1$ reaction mechanism.

Within this framework, it is important to revise the possible CO_2 absorption mechanisms. It is agreed on the fact that the greater part of reactions involved are due to the interaction of the CO_2 molecules with the amine groups, however different mechanisms have been proposed.

According to Kumar et al. [105], the reaction of CO_2 with the AA is different from the zwitterion mechanism, which typically occurs for alkanolamines. The reaction suggested is reported in equation (2.2) and it presents a direct $1:2$ mechanism, with the formation of carbamate and protonated amine.

$$2RNH_2 + CO_2 \leftrightarrow RNHCOO^- + RNH_3^+ \tag{2.2}$$

Vaidya et al. [106], on the contrary, reported the zwitterion mechanism, with the two-step reaction based on the $1:2$ mechanism shown in equations (2.3) and (2.4). B in equation (2.4) stands for any base and in a non-aqueous medium is the AA itself.

$$^-OOC - R - NH_2 + CO_2 \leftrightarrow \ ^-OOC - R - N^+H_2COO^- \tag{2.3}$$

$$\begin{aligned} ^-OOC - R - N^+H_2COO^- + B \\ \rightarrow \ ^-OOC - R - NHCOO^- + \ ^-OOC - R - NH_3^+ \end{aligned} \tag{2.4}$$

Gurkan et al. [107] claimed that the reaction of CO_2 with the AA ends with the formation of carbamic acid, without the intermediate formation of the zwitterion. The reactions suggested are reported in equations (2.5) and (2.6).

$$^-OOC - R - NH_2 + CO_2 \leftrightarrow \ ^-OOC - R - NHCOOH \tag{2.5}$$

$$\begin{aligned} ^-OOC - R - NHCOOH + B \\ \rightarrow \ ^-OOC - R - NHCOO^- + \ ^-OOC - R - NH_3^+ \end{aligned} \tag{2.6}$$

Anyway, it has to be said that most of the literature supports the formation of zwitterion intermediate as the most likely route, rather than the one-step carbamate formation or the carbamic acid formation in the intermediate step [108], [109].

Whether the reaction is characterised by a $1:2$ stoichiometry ($0.5\ mol_{CO_2}/mol_{IL}$) or a $1:1$ stoichiometry ($1\ mol_{CO_2}/mol_{IL}$) depends on the extent to which the second step of the reaction takes place (equation (2.4)) – with the formation of carbamates. With the aim of enhancing the CO_2 absorption capacity, research is now focusing on the deep understanding of the factors which favour the carbamic acid formation instead of the carbamate one.

Shaikh et al. [110], [111] showed the existence of activation barriers associated with the proton transfer between the NH_2 of the zwitterionic pre-complex and the carbonyl oxygen which leads to the formation of the final carbamate.

Yang et al. [104] showed that little differences in the local structure of the amine group in AA ILs lead to different absorption mechanisms, providing the opportunity for achieving higher absorption capacities by structure design. Indeed, they demonstrated that the CO_2 absorption mechanism by AA ILs exceeds the CO_2/amine stoichiometry, since a rigid ring structure around the amine functionality creates a unique electrostatic environment that hinders the carbamate formation by inhibiting the deprotonation of the carbamic acid. In this way the $1:1$ reaction mechanism is favoured.

Additional relevant evidence they found is that also the carboxylate group $-COO^-$ is implied in the CO_2 absorption. They observed, in fact, that about $10-25\%$ of the CO_2 was not absorbed as carbamic acid through the $1:1$ mechanism, nor as carbamate through the $1:2$ mechanism. Given the number of moles involved, the discrepancy could not be ascribed to the physical absorption mechanism only and it proved that some amount of CO_2 was captured by the carboxylic group thanks to its strong basicity.

In comparison to the amine-functionalised ILs described in *chapter 222.2.1*, therefore, AAILs present the double advantage of allowing multiple amine sites – as in the case of arginate and lysinate, for example (see *Figure 2.2*) – and including carboxylate functional group, furtherly enhancing the CO_2 uptake.

The biggest issue of [Cho][AA] ILs is their extremely high viscosity, which limits their applicability because of the limited diffusion in the liquid absorbent. Some attempts have been made to reduce this drawback by reducing the strength of the hydrogen bonding network [112], however the option of using co-solvents seems more viable.

The addition of water turned out to have beneficial effects. Zhang et al. [113] studied the effect of the addition of water on the CO_2 absorption behaviour and found out that small amounts of it increase the mass transfer due to the decrease in the viscosity of the system. Moreover, Li et al. [114] showed that the addition of water on the one side reduces the viscosity and hydrogen bonding – thus enhancing the diffusion mechanisms and rendering the reaction sites more available; on the other one, it catalyses the CO_2 absorption reaction.

Li et al. [74] studied the absorption/desorption in a solution of [Cho][Pro] in polyethylene glycol (PEG 200) mixture and showed that the addition of PEG200 significantly accelerated the absorption and desorption processes.

Davarpanah et al. [115] introduced the use of solutions of 12.5%wt [Cho][AA] ILs in dimethyl sulfoxide (DMSO), chosen as a solvent because of high boiling point, low toxicity, low vapour pressure, and relatively low price. Despite the good results in terms of cost, environmental impact, energy consumption, and regenerability, however, the absorption capacities obtained were not satisfactory, with values of 0.3 mol_{CO_2}/mol_{IL}.

2.4. Absorption studies performed with [Cho][Pro] solutions

Although [Cho][Pro] is a promising candidate as post-combustion carbon capture solvent, the studies which assess its absorption capacity and regeneration efficiency are not numerous.

Li et al. [102] studied the solubility of CO_2 in $30\%wt$ aqueous solutions of five [Cho][AA] ILs ([Cho][Ser], [Cho][Gly], [Cho][Pro], [Cho][Asp], [Cho][Lys]) at temperatures from $303.15\,K$ to $333.15\,K$ and pressures up to $7\,bar$. Moreover, they derived the thermodynamics parameters (Henry's law constants, reaction equilibrium constants, enthalpy of physical dissolution and chemical reaction) required for the reaction equilibrium thermodynamic model (RETM) and investigated the recyclability of the

solution. They calculated the solubilities in molality terms (i.e., $mol_{CO_2}/kg_{solution}$), obtaining a minimum value of $0.5628\,mol/kg$ at $0.1570\,bar$ and $333.15K$ and a maximum value of $1.1540\,mol/kg$ at $6.7918\,bar$ and $303.15\,K$. The results they obtained are shown in *Figure 2.10*. They also investigated the regeneration of the solution with [Cho][Lys], stating that it maintained a quite steady CO_2 absorption capacity. They operated the regeneration of the aqueous [Cho][Lys] solution in a three-neck flask with a magnetic stirrer in oil bath at $353K$ and atmospheric pressure for $1\,hour$.

Yuan et al. [98] investigated aqueous solutions of three [Cho][AA] ILs ([Cho][Gly], [Cho][Ala] and [Cho][Pro]). They assessed the CO_2 absorption loadings, in terms of molarity (i.e., mol_{CO_2}/mol_{IL}) and molality (i.e., mol_{CO_2}/kg_{sol}), at varying concentrations of the solutions ($5\%wt,\ 10\%wt,\ 20\%wt,\ 30\%wt$) and at a temperature of $308.2\,K$. The results obtained are shown in *Figure 2.11*. Furthermore, the CO_2 absorption mechanism in the aqueous solution of [Cho][Gly] was studied by Nuclear Magnetic Resonance (NMR), showing that the formation of carbamate takes place at low absorption loadings and is then followed by the hydrolysis of carbamate and CO_2 hydration reactions at high absorption loadings. Lastly, they regenerated the aqueous [Cho][Gly] solution at $383\,K$ and atmospheric pressure and derived the regeneration efficiencies, observing a decrease with increasing concentration and regeneration cycles.

Latini et al. [116] studied the absorption and desorption reaction mechanisms in [Cho][Gly] and [Cho][Pro] in DMSO solutions; via ATR-IR spectroscopy they showed the different absorption pathways occurring for the two AA anions. They also performed CO_2 absorption experiments through a gravimetric method using a $\sim 4.5\,ml$ reactor. Different IL concentrations were tested ($16\%wt,\ 20\%wt,\ 33.3\%wt,\ 50\%wt$) and the absorption capacities ($\%kg_{CO_2}/kg_{solution}$) and molar efficiencies (mol_{CO_2}/mol_{IL}) were calculated. Subsequently, they investigated the effect of temperature on the absorption process in a $16\%wt$ [Cho][Pro]-DMSO solution at $25°C, 30°C$ and $40°C$ The synthetic gas sent to the reactor was composed of 20% CO_2 and 80% N_2. As saturation was reached, the solution was completely regenerated with a N_2 stream at $80°C$. The result obtained are reported in *Table 2.2*.

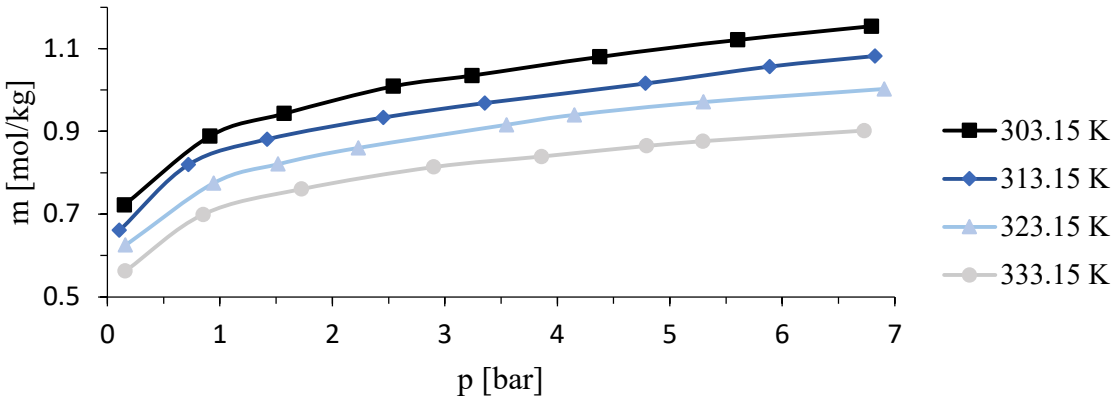

Figure 2.10. CO_2 solubilities in aqueous 30%wt [Cho][Pro] solutions for varying temperatures as functions of pressures. Results obtained by Li et al. [102].

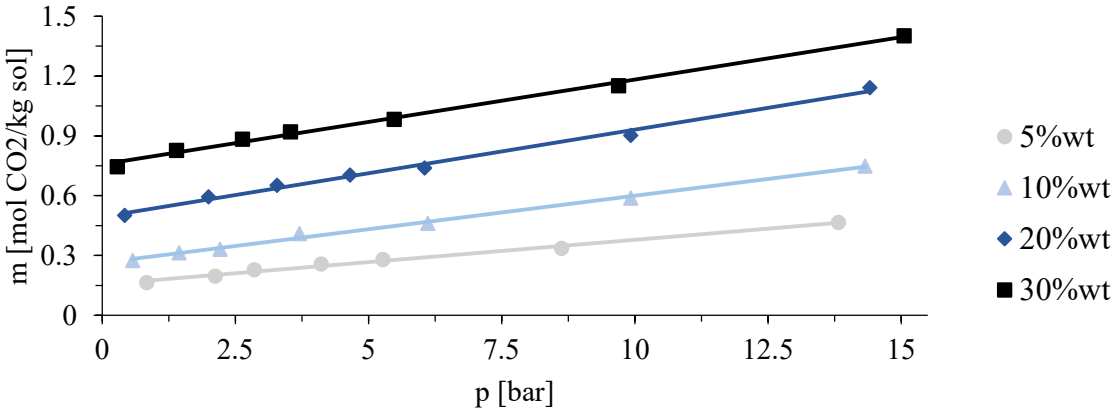

Figure 2.11. CO_2 solubilities in aqueous [Cho][Pro] solutions at $308\,K$ for varying concentrations as functions of pressure. Results obtained by Yuan et al. [98].

Table 2.2. CO_2 absorption performances of [Cho][Pro] in DMSO (a) for varying concentrations at ambient temperature and ambient pressure (b) for varying temperatures $(25°C, 30°C, 40°C)$ at 16%wt concentration and ambient pressure. Results obtained by Latini et al. [116].

(a)

	$AC\ [\%\ kg_{CO_2}/kg_{solution}]$	$ME\ [mol_{CO_2}/mol_{IL}]$
16%wt [Cho][Pro] in DMSO	2.39	0.75
20%wt [Cho][Pro] in DMSO	2.95	0.73
33.3%wt [Cho][Pro] in DMSO	4.63	0.69
50%wt [Cho][Pro] in DMSO	7.03	0.7

(b)

	$AC\ [\%\ kg_{CO_2}/kg_{solution}]$	$ME\ [mol_{CO_2}/mol_{IL}]$
25 [°C]	2.39	0.74
30 [°C]	2.27	0.71
40 [°C]	2.14	0.66

2.5. Aim of the thesis

This study is part of the common effort to develop reliable, cost- and energy-efficient post-combustion CC solvents able to replace the toxic MEA solutions currently employed in the installed capacities.

In continuation with the work previously done on the test-bench employed for the absorption/desorption experiments, a 50%wt [Cho][Pro] in DMSO solution will be employed. The cyclability and the effect of temperature on the absorption process will be assessed and a comparison with the performances formerly shown by the 12.5%wt solution will be carried out, intending to identify the concentration of the solution that leads to the best results in terms of capacity loading and regeneration efficiency.

Furthermore, being the thermophysical properties of [Cho][Pro] and the solutions at varying concentration not available in the literature, their experimental assessment will be performed and empirical formula will be derived to allow their future calculations.

3. Experimental assessment of the thermophysical properties of Choline Proline and its CO_2 absorption quantification

In order to understand the behaviour of materials and to engineer the processes in which they are involved, it is of utmost importance to define their basic thermophysical properties. By way of example, the equipment sizing requires the knowledge of the density values, the setting of the feasible temperature operating ranges needs the phase change temperatures and the thermal decomposition one, while the study of the flow characteristics and the gas diffusion properties relies on the proper estimation of the kinematic and dynamic viscosities.

The following chapter reports the experimentally assessed values of density, viscosity and CO_2 absorption of pure [Cho][Pro] and of solutions of the latter in DMSO at varying concentrations (12.5%wt, 25%wt and 50%wt).

The method for the synthesis of the IL is reported below and it follows the one described in [116]; this constitutes an innovation in comparison with the previous procedures since it replaces the expensive and corrosive choline hydroxide with choline chloride as a mean of cation source.

3.1. Synthesis of [Cho][Pro]

The procedure described below considers the quantities of reactants and reagents required for the synthesis of 0.5 $moles$ of [Cho][Pro].

1- In a 500 ml flask, 56.2 g of potassium hydroxide pellets (supplied by Carlo Erba, purity ≥85%) are dissolved in 300 ml of methanol (supplied by Merck, purity ≥99.8%) with the auxilium of a stirrer; 57.57 g of L-proline (supplied by Merck, purity ≥ 99%) are then added to the solution. It can be noticed that the suspension turns white and there is the formation of some precipitate, hence the potassium salt of the proline is formed and its excess separates from the solution. With the stirrer still powered on, the flask is covered with an aluminium foil and left there for 2 hours.

Figure 3.1. Synthesized [Cho][Pro]

2- After 2 hours under continuous stirring, the potassium hydroxide pellets are completely dissolved and the choline chloride (69.81 g, supplied by Alfa Aesar, purity ≥98%) can be added. It is important to perform the operation very fast, in order not to contaminate the whole initial mixture with the moisture present in the surrounding environment, which would lead to the formation of water.

3- The mixture is left under stirring for 4 $hours$, with the aim of ensuring the complete dissolution of the potassium salt of proline, the formation and precipitation of the potassium chloride and the formation of choline proline in the solution.

4- The mixture is poured into 8 flacons of 50 ml each; centrifugation is carried out for 15 $minutes$ in order to separate the potassium chloride crystals.

5- The solution of choline proline, methanol and eventual water produced during the procedure is poured into a round bottom flask and introduced into the rotary evaporator; the device allows to remove the 2 solvents by evaporation and to obtain the pure desired ionic liquid.

6- The obtained [Cho][Pro] is outgassed overnight under dynamic vacuum at a temperature of $30°C$, in order to remove any trace of methanol and water which might be still present.

Table 3.1. Reactants and solvent required for the synthesis of 0.5 mol of [Cho][Pro].

		supplier	**molecular weight**	**quantity**
	potassium hydroxide	Carlo Erba	56.1056 [g/mol]	56.2 [g]
reactants	L-proline	Merck	115.13 [g/mol]	57.57 [g]
	choline chloride	Alfa Aesar	138.62 [g/mol]	69.81 [g]
solvent	methanol	Merck	32.04 [g/mol]	300 [ml]

3.2. Density

The density of a liquid is formally defined as

$$\rho = \frac{m}{V} \tag{3.1}$$

where ρ is the density, m is the mass and V is the volume. The experimental measurement of the density of a substance requires thus the knowledge of its mass and volume.

3.2.1. Methods

The density values of the pure [Cho][Pro] and the other solutions at varying concentrations of the latter in DMSO were determined by means of a Gay-Lussac pycnometer – a glass flask with a capillary stopper to be put into the opening.

The procedure consists of 2 main steps.

1- Estimation of the volume of the pycnometer using the well-known values of the water density:

- the mass m_0 of the dry and empty pycnometer is precisely weighted;
- the instrument is filled with distilled water and its mass m_1 is weighted;
- the mass of the distilled water m_w is calculated as the difference between the mass of the filled instrument m_1 and the empty one m_0;
- the temperature of the water T_w at which the measurement is performed is established;

- the value of density ρ_w at the temperature T_w is defined from tables available in the literature;
- the volume of the pycnometer V is derived, calculated as the ratio of the mass m_w over the density ρ_w.

2- Estimation of the density of the pure [Cho][Pro] and the other solutions at varying concentrations of the latter in DMSO and definition of experimental formulas of the densities in the function of temperature:

- the pycnometer is accurately filled with pure [Cho][Pro] and put in the oven at the desired temperature T;
- once the set temperature is reached, the instrument is taken out and eventual excesses of the IL due to thermal expansion are removed;
- the mass m is measured. The measurements are repeated three times and an average value is considered; the mass of the IL $m_{[Cho][Pro]}$ can be calculated, since the mass of the pycnometer is defined in the first step;
- the density $\rho_{[Cho][Pro]}$ at the temperature T can be calculated as the ratio of the mass $m_{[Cho][Pro]}$ over the volume V;
- the mass of the IL is measured for at least 3 different values of temperature, making sure that the instrument is always well-filled and there are no excesses on the stopper;
- the [Cho][Pro] density in function of temperature can be plot and the experimental formula can be derived; the procedure is repeated for the other solutions of [Cho][Pro] in DMSO at varying concentrations – 12.5%wt, 25%wt, 50%wt.

- **Figure 3.2**. Pycnometer used for the measurements of density.

3.2.2. Results and discussion

The data obtained from the measurements performed are reported in *Figure 3.3*. The data points well match a straight line, thus a linear dependence of density with temperature is assumed and the empirical equation (3.2) is obtained. The values of the two fitting coefficients A_1 and A_2, the correlation coefficients R^2 and the standard deviations SDs are reported in *Table 3.2*.

$$\rho(T) = A_1 \cdot T + A_2 \tag{3.2}$$

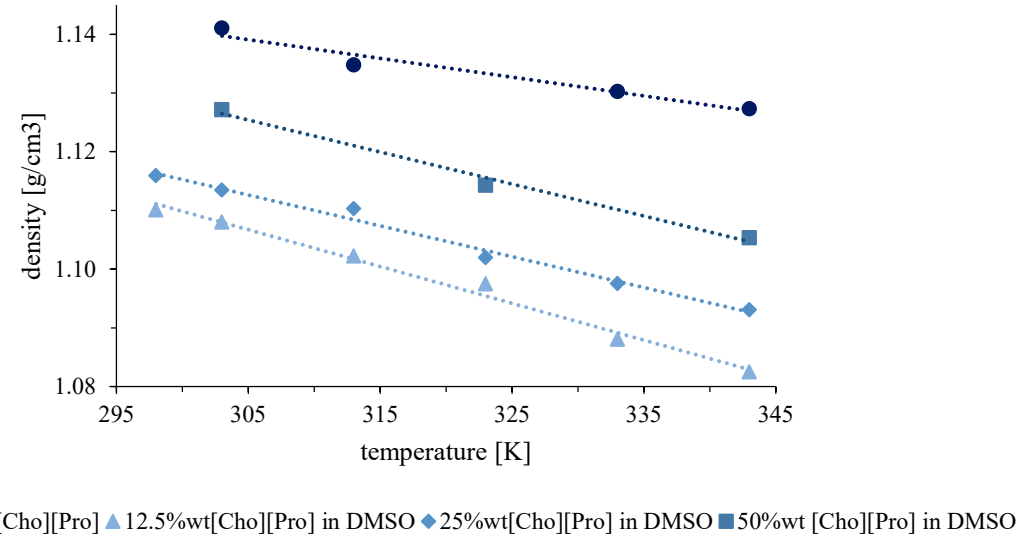

Figure 3.3. Density ρ as a function of temperature.

Table 3.2. Fitting parameters A_1 and A_2, SDs and R^2 of the obtained empirical equations of density as functions of temperature for the solutions at varying concentrations considered.

solution	A_1	A_2	SD	R^2
100%wt [Cho][Pro]	-0.0003	1.2364	0.006	0.95323
12.5%wt [Cho][Pro] in DMSO	-0.0005	1.2915	0.034	0.98874
25%wt [Cho][Pro] in DMSO	-0.0005	1.2727	0.008	0.98704
50%wt [Cho][Pro] in DMSO	-0.0006	1.2978	0.012	0.98954

As expected, a general decreasing trend can be observed with increasing temperatures, with the correlation coefficient assuming values over 0.98 for the three solutions at varying concentrations.

Furthermore, the data show an increase of density for increasing concentrations, due to the much higher molecular weight of [Cho][Pro] in comparison to DMSO – respectively 219.3008 g/mol and 78.13 g/mol.

3.3. Viscosity

The viscosity of a fluid is a measure of its resistance to deformation under shear stress and it is commonly intended as its resistance to flow [117].

Dynamic and kinematic viscosities can be distinguished. The first one – also referred to as absolute viscosity – is a measure of the resistance to movement of one layer of fluid over another and it coincides with the tangential force per unit area necessary to move one horizontal plane with respect to another one at a unit velocity. The kinematic viscosity is a measure of the internal resistance of a fluid to flow under gravitational forces; it is obtained from the ratio of the dynamic viscosity over the density of the fluid.

3.3.1. Methods

In this work, the kinematic viscosities of the pure [Cho][Pro] and the other solutions have been measured through a Cannon-Fenske viscometer according to the method indicated in the ASTM D445 and D446 standards and described below. The dynamic viscosity has been obtained by dividing the kinematic viscosities for the proper values of density calculated through the empirical formula found in the previous section.

The procedure is reported in the following:

1- the bath is filled with distilled water and the desired temperature is set;
2- the proper viscometer is chosen among the available ones, cleaned with ethanol and dried in a stream of filtered N_2;

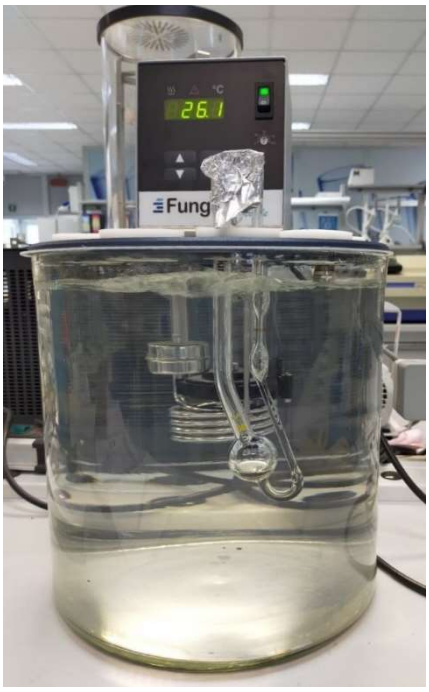

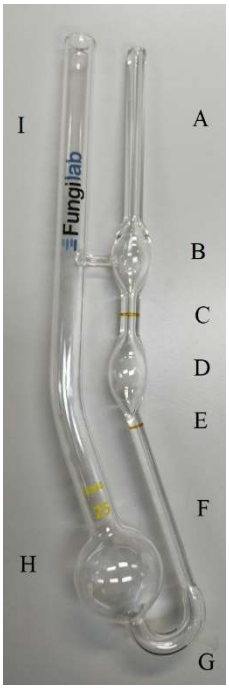

Figure 3.4. Experimental setup and viscometer used for the measurements.

3- the IL is introduced into the viscometer by inverting the instrument, immerging side *A* of the tube (see *Figure 3.4*) into a flask containing the liquid and applying suction to the side *I* of the tube until the IL rises to the line *E*; the viscometer is turned to its normal position and the tube *A* is cleaned; an aluminium foil is applied on tube *A* and tube *I* in order for the IL not to absorb the CO_2 present in the surrounding environment and change its properties;

4- the viscometer is inserted into a holder and immersed in the bath at constant temperature;

5- when an adequate amount of time has passed (approximately $15\ minutes$) and the sample reached the set temperature, suction is applied to tube *A* and the IL is brought in the section *B* above the line *C*;

6- suction is released and the efflux time required by the IL to flow from line *C* to line *E* is measured with a chronometer. Three measurements of the efflux time are taken for each temperature – ranging from $30°C$ to $70°C$ – and an average value is considered;

7- the kinematic viscosity is obtained by multiplying the average efflux time by the viscosimeter constant – appropriately calculated for the considered temperature; the

dynamic viscosity is determined by multiplying the kinematic viscosity for the dynamic one.

8- the viscometer is taken out of the holder, inverted and the side *A* of the tube is put into a flask; pressure is applied to tube *I* and the IL is released into a flask; the viscometer is cleaned with a proper solvent (methanol, ethanol, acetone) and dried with N_2;
9- the procedure is repeated for the remaining solutions at different concentrations.

It needs to be remarked that it is important to consider the viscometer of the correct size – being the instrument optimized for the operations around the centre of its range; the use of too much or too little quantity of sample gives in fact inaccurate values, thus it must be avoided as far as possible.

3.3.2. Results and discussion

The data obtained from the measurements performed are reported in Figure *3.5*. The data points show an exponential trend and well match the empirical formula (3.3). The values of the two fitting coefficients A_3 and A_4, the standard deviations SDs and the correlation coefficients R^2 are reported in *Table 3.3.*

$$\mu(T) = A_3 \cdot e^{A_4 \cdot T} \tag{3.3}$$

As predictable, the curves show decreasing viscosity values for increasing temperatures; the correlation coefficient is above 0.99 for all the solutions.

It is interesting to observe the remarkable differences in viscosity among the pure [Cho][Pro] and the other solutions – which results to be of three orders of magnitude when considering the 12.5%wt solution. This supports the unavoidable necessity of diluting it in a solvent when IL are implied in carbon capture processes and mass transfer phenomena have to be optimized.

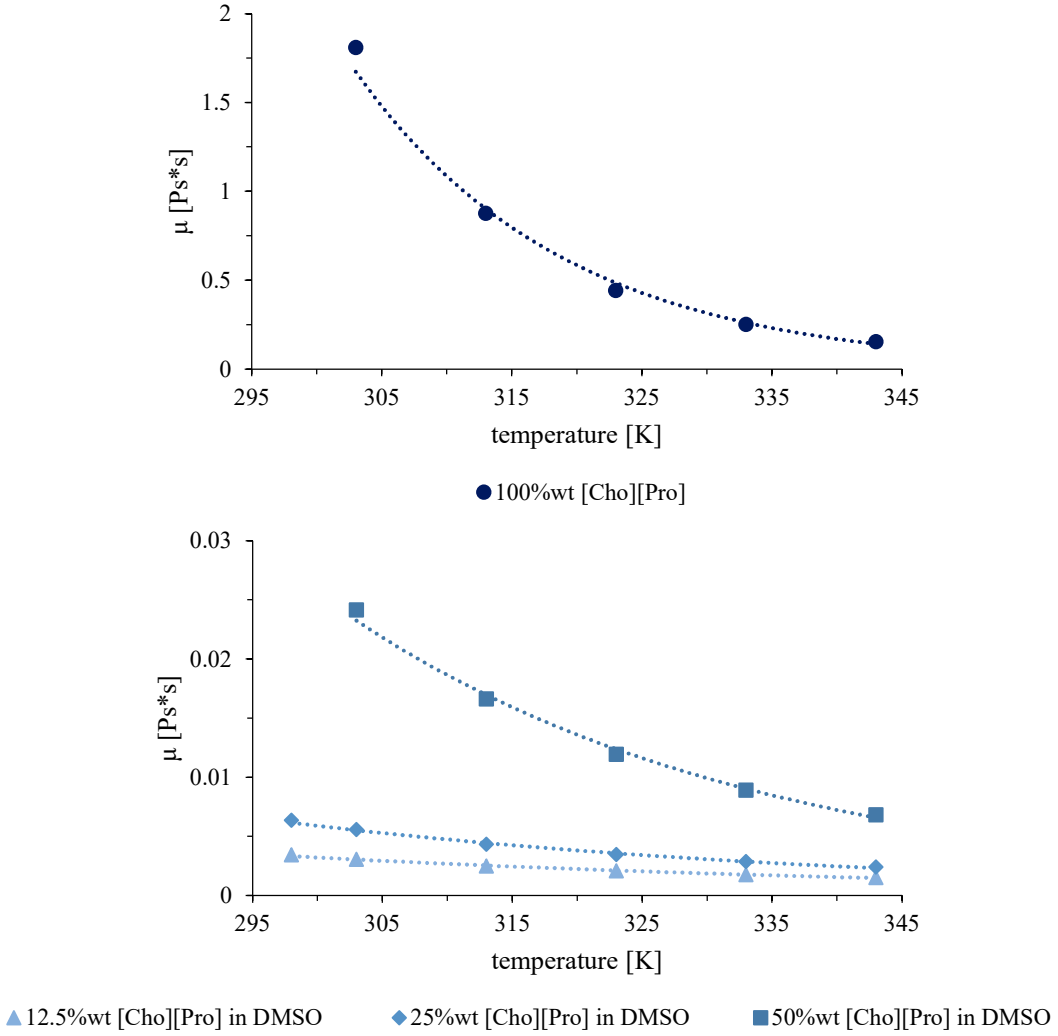

Figure 3.5. Dynamic viscosity μ as a function of temperature.

Table 3.3. Fitting parameters A_3 and A_4, SDs and R^2 of the obtained empirical equations of viscosity as functions of temperature for the solutions at varying concentrations considered.

solution	A_3	A_4	SD	R^2
100%wt [Cho][Pro]	2.00E+08	-0.062	1.99E-01	0.998154
12.5%wt [Cho][Pro] in DMSO	0.7155	-0.018	5.15E-05	0.99882
25%wt [Cho][Pro] in DMSO	3.966	-0.022	4.20E-04	0.998441
50%wt [Cho][Pro] in DMSO	325.3	-0.032	2.30E-03	0.999009

3.4. CO_2 absorption quantification

Once established the need for using [Cho][Pro] in solutions with a solvent able to properly offset the problems caused by the high viscosity values without limiting the absorption performances, the optimal concentration needs to be evaluated.

Two parameters can serve to this end: the absorption capacity AC and the molar efficiency α. The first one is expressed in percentage terms as the mass of the absorbed carbon dioxide over the mass of the employed solution, while the second one considers the moles of CO_2 per mole of IL present in the solution at the end of the absorption process. In the following, the experiment performed to quantify the CO_2 absorbed by means of a gravimetric test is described and the results obtained are reported and discussed.

3.4.1. Methods

The quantity of CO_2 absorbed by the samples of pure [Cho][Pro] and by the solutions of the latter in DMSO at varying concentrations – 12.5%wt, 25%wt, 50%wt – has been tested by means of a gravimetric method.

The procedure followed is described below:

1- m^r_{empty} – the mass of the vial (volume $\sim 5\ ml$) with the magnetic bar inserted and the cap screwed – is acquired;
2- the volume of the reactor V_r is measured using a volumetric pipette filled with water;
3- $2\ ml$ of [Cho][Pro] – V_{sol} – are poured into the reactor through a volumetric pipette;
4- the sample is purged with a $20\ ml/min$ nitrogen flow for $10\ minutes$ with the stirrer powered on at $200\ rpm$; the mass $m^r_{N_2}$ is afterwards acquired. The mass of the solution m_{sol} which will be considered in the AC calculations can be determined according to the formula (3.4), where d_{N_2} and d_{air} are the densities of N_2 and air at 25°C respectively.

$$m_{sol} = \left[m^r_{N_2} - (V_r - V_{sol}) \cdot d_{N_2}\right] - \left[m^r_{empty} - V_r \cdot d_{air}\right] \quad (3.4)$$

The mass of the IL contained in the solution – from which the moles can be derived for the α calculation – is determined by multiplying for the corresponding percentage of concentration;

5- the IL is bubbled with a $20\ ml/min\ CO_2$ flow under continuous stirring and the mass $m^r_{CO_2}$ is acquired every 15 minutes until there is no increase anymore;

6- the quantity of the CO_2 absorbed – m_{CO2} – is calculated as the mass difference of the measurements acquired after the N_2 purging and the CO_2 bubbling, considering the headspace of the vial, according to the formula (3.5), where d_{CO_2} is the density value of carbon dioxide at 25°C;

$$m_{CO_2} = \left[m^r_{CO_2} - (V_r - V_{sol}) \cdot d_{CO_2}\right] - \left[m^r_{N_2} - (V_r - V_{sol}) \cdot d_{N_2}\right] \tag{3.5}$$

7- by means of the molecular weights, the moles of absorbed CO_2 and [Cho][Pro] in the solution can be derived. The absorption capacity and the molar efficiency are calculated according to the formulas (3.6) and (3.7), where n_{CO2} are the moles of CO_2 absorbed and n_{IL} are the moles of [Cho][Pro] in the solution;

$$AC = \frac{m_{CO_2}}{m_{sol}} \cdot 100 \tag{3.6}$$

$$\alpha = \frac{n_{CO_2}}{n_{IL}} \tag{3.7}$$

8- the procedure is repeated for the 12.5%wt, 25%wt and 50%wt solutions.

Figure 3.6. 5ml reactor employed for the gravimetric quantification of the CO_2 absorbed by the different solutions.

3.4.2. Results and discussion

The evolution in time of the carbon dioxide absorbed in terms of moles of CO_2 per moles of [Cho][Pro] present in the solution is reported in *Figure 3.7*. It is very apparent at first glance that the pure [Cho][Pro] cannot be used for practical application if not diluted in a proper solvent. The too high viscosity values, in fact, drastically reduce the molar efficiency and the absorption capacity due to the hindered diffusion of the CO_2 in the IL and the slow reaction kinetics that comes with it.

It is also interesting to observe that the evolution curves of the three solutions of [Cho][Pro] in DMSO present a peak, particularly visible for the 12.5%wt and the 25%wt ones. A reason for this may be that in a first phase the CO_2 is physically trapped in the solvent and then it is released until equilibrium is reached – that is after approximately $30\ minutes$. This phenomenon is less and less visible as the concentration of the solution – and thus the viscosity – increases. In the case of the pure [Cho][Pro] the CO_2 keeps being slowly absorbed even after $120\ minutes$.

Figure 3.8 and *Table 3.4* compare the performances of the four solutions in terms of absolute mass of CO_2 absorbed, absorption capacity and molar efficiency. It shall be underlined the different behaviour of the absorption capacity and the molar efficiency with the increase in concentration. If on the one side the CO_2 absorbed and the absorption capacity show an increasing trend with concentration, on the other one the absorption reactions are less and less efficient – as it is shown by the decrease in molar efficiency. This is again ascribable to the problems raised by the increase in viscosity.

When designing practical applications, it is thus necessary to find the optimum – enhancing the process and the reaction kinetics for optimal use of the IL and guaranteeing an adequate carbon dioxide sequestration from the flow to be purified at the same time.

Table 3.4. CO_2 absorption performances of the four solutions of [Cho][Pro] in DMSO at varying concentrations in terms of mass of CO_2 absorbed, molar efficiency and absorption capacity.

solution	m_{CO_2} $[g]$	α $[mol\ CO_2/mol_{IL}]$	AC $[\%g_{CO2}/g_{sol}]$
100% [Cho][Pro]	0.0514 ± 0.0002	0.1128 ± 0.0003	2.26 ± 0.01
12.5%wt [Cho][Pro]	0.0437 ± 0.0002	0.772 ± 0.003	1.94 ± 0.01
25%wt [Cho][Pro]	0.0756 ± 0.0002	0.669 ± 0.001	3.36 ± 0.01
50%wt [Cho][Pro]	0.1328 ± 0.0002	0.528 ± 0.001	5.84 ± 0.01

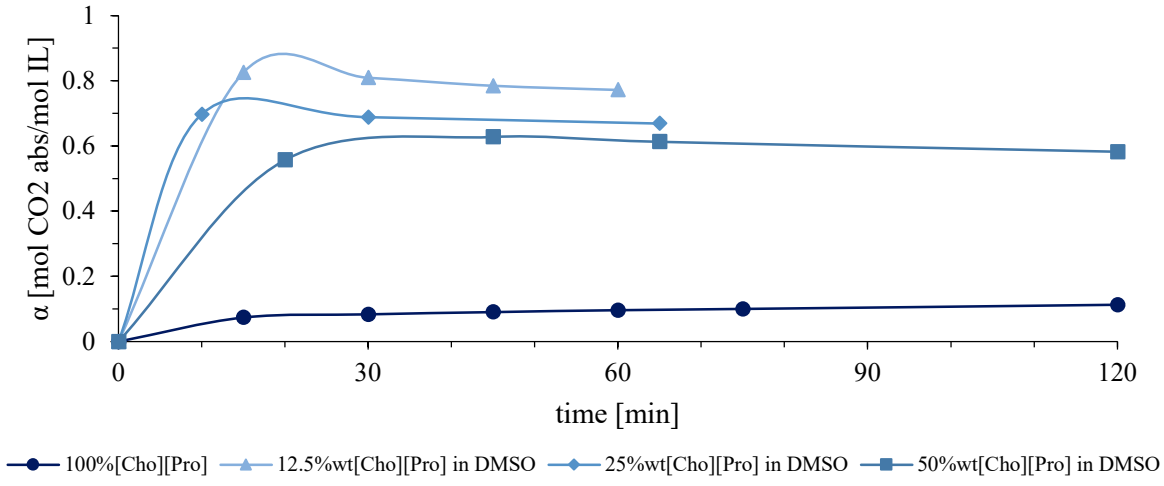

Figure 3.7. Evolution in time of the moles of CO_2 absorbed per moles of [Cho][Pro] present in the four solutions (concentrations: 100%wt, 12.5%wt, 25%wt, 50%wt [Cho][Pro] in DMSO).

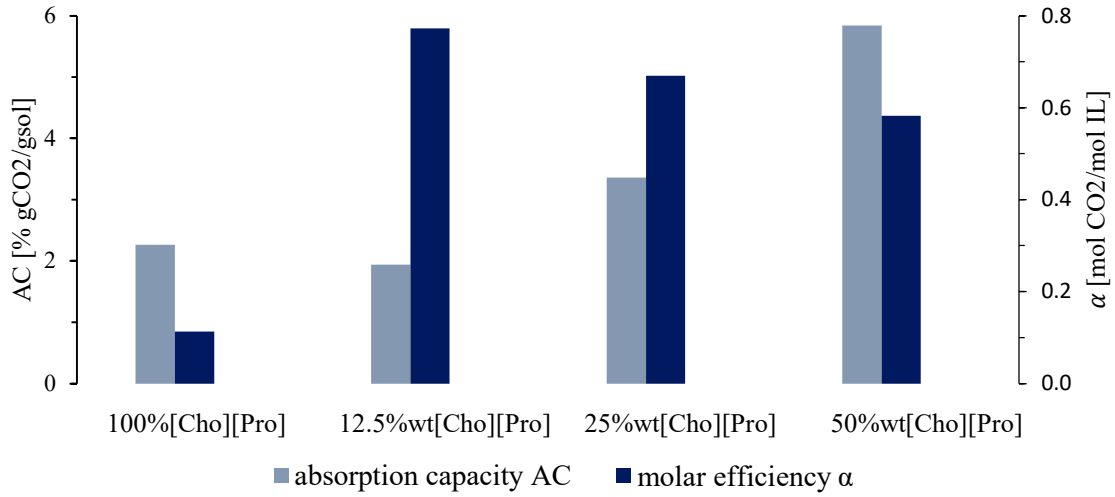

Figure 3.8. CO_2absorption performances of the four solutions in terms of absorption capacities and molar efficiencies (concentrations: 100%wt, 12.5%wt, 25%wt, 50%wt [Cho][Pro] in DMSO).

4. Experimental assessment of the performance of a bench-scale post-combustion carbon capture plant

The experiments were performed by means of a bench-scale test plant supplied and installed in the CO_2 Circle Lab (CCL) by Technodelta Srl.

The test bench is a reproduction of a post-combustion carbon capture plant based on chemical absorption. It has been designed according to the data available in literature concerning amine solvents technologies and it presents the typical double-column scheme composed of an absorption unit and a desorption one. In order to simulate different streams and accurately reproduce specific industrial applications, the plant allows to set the desired percentages of carbon dioxide, nitrogen, methane, carbon monoxide, and oxygen or hydrogen of the flow to be processed – for safety reasons the latter two cannot be present simultaneously. A more detailed description of the test bench, its main components, and operational conditions are reported in *chapter 4.1*.

The plant has been previously validated by performing a set of absorption and desorption experiments with aqueous monoethanolamine (MEA) solutions, used as the benchmark. Since at the time the results were considered to be consistent with those reported in the studies found in literature, the reliability of the test bench has been taken for granted a priori.

The experiments performed for the study are part of the wide research on the development of green solvents for post-combustion carbon capture, intending to think up sustainable and non-toxic processes. In particular, it aims at furtherly understanding the characteristics and behaviour of amino acid based ILs – in this case [Cho][Pro] – as a means of replacing the above mentioned MEA solutions, which are known for the high energy consumptions, large evaporation losses, corrosiveness and toxicity [26], [28].

In the following chapter, the experimental assessment of the performance of a 50%wt solution of [Cho][Pro] in DMSO is presented and discussed – in continuity with the work formerly done on the same test bench which employed a 12.5%wt solution of the same IL and solvent. The results obtained in the two sets of experiments are then compared, showing the criticalities which arose in the interim.

4.1. Description of the plant

4.1.1. Main components and operational ranges

The plant consists of the following main components:

- two stainless steel packed columns – where one is the absorption reactor ($V = 2\ l$, $p_{max} = 25\ bar$, $T_{max} = 100°C$) and the other is the desorption reactor ($V = 4\ l$, $p_{max} = 4.5\ bar, T_{max} = +150°C$) – and a stainless steel solvent tank ($V = 5\ l$, $p_{max} = 4.5\ bar$);
- a gas line – which supplies the inlet gas flow to the absorption and desorption reactors (pure or as a mixture of the desired percentages of gases, according to the process to be simulated), carries the outlet gas to the mass spectrometer, and allows to send the N_2 flow to the two reactors for the desorption operation and the clean-up of the tanks;
- a fluid recirculation system with a gear pump – which connects the solvent tank, the absorption tank and the desorption one – and a vacuum pump – in case the stripper works in depression;
- a heating system – which brings the gas and the fluid flows at the desired temperatures by means of electrical resistors;
- a system of valves – which allows to connect the different lines according to the required configuration (three-way valves), to regulate the mass flows (flow-control valves), to impose the direction of the flow (non-return valve), and to ensure the safety of the plant (safety valves);
- a system of temperature, pressure and flow meters – which allows the measurement of the corresponding values.

The different parts are interrelated and the system is controlled by an electric panel, which is connected to a computer; by means of a software it is then possible to set the operational values of the process, monitor the correct functioning, and extrapolate the data to analyse the performance. The scheme plant is reported in *Figure 4.1.*

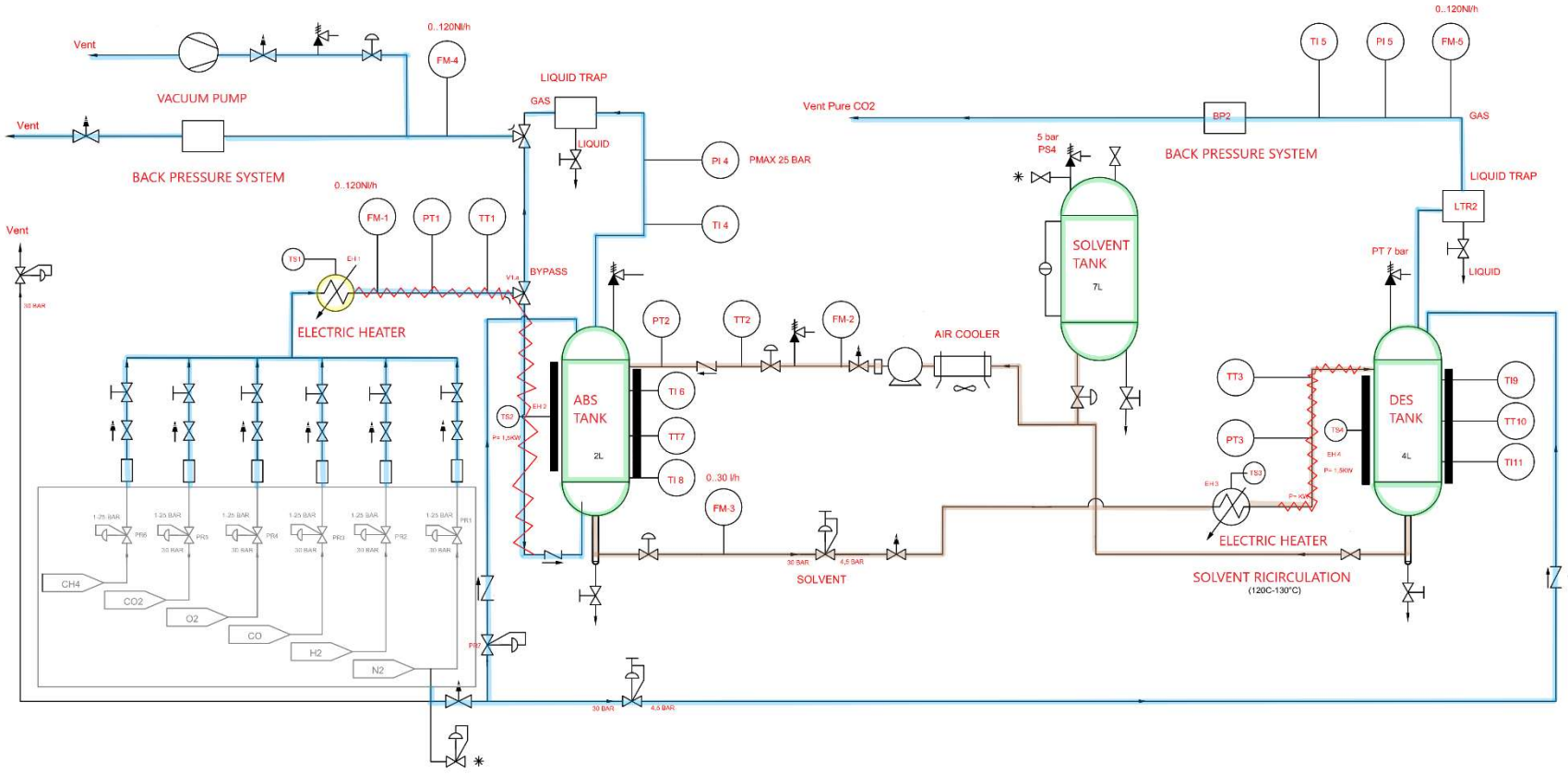

Figure 4.1. Scheme plant of the test bench. Adapted from the instruction manual provided by Technodelta Srl.

Two working conditions are possible – the continuous and the batch configurations. In the first one, the carbon capture from the stream to be purified and the regeneration take place simultaneously. The solution rich in carbon dioxide is sent to the stripper, where it is regenerated under the combination of high temperatures and low pressures; thereafter the lean solution is continuously recirculated to the absorption reactor, with no interruption of the overall process.

In the batch configuration, the absorption column is employed only. The process takes place in two stages: first, the absorption column is crossed across by the stream rich in carbon dioxide until the solution reaches saturation, then the temperature is raised and the solution is regenerated. If on the one side the second setup requires to interrupt the process in order release the carbon dioxide previously captured, on the other one it allows to study the two processes separately, in order to identify the critical issues of the processes themselves, without any superposition of the effects or influences on each other.

4.1.2. Phases of operation

Every experiment conducted using the test bench described above consists of three main phases: set-up of the plant, test run, and clean-up of the plant.

The first one coincides with the preparation for the test and the correct setting up of the desired configuration according to the test that needs to be performed. The three-way valves are turned depending on whether the continuous or the batch operation are needed, or on the basis of the plant layout required if other working conditions have to be checked for the experiment (e.g., proper functioning of the inlet and outlet flow meters). Then the computer is turned on and the software is run; once it is ensured that no problems occur, the percentages of the composition of the stream to be simulated and the corresponding flow rates are introduced – verifying that the gas cylinders are able to provide the desired flow rate for the entire duration of the test. The initial temperatures of the process are imposed and it is waited until they are reached.

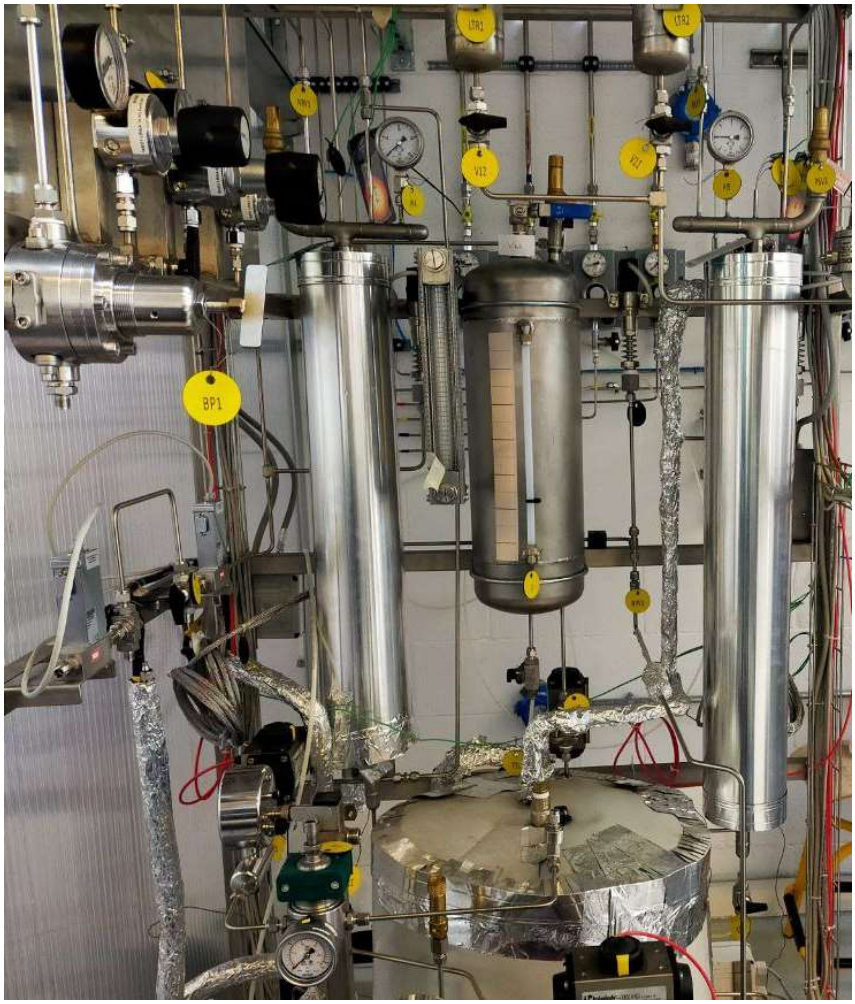

Figure 4.2. Test bench installed at the CO_2 Circle Lab (CCL), part of the lab A1 at the Environment Park in Turin.

As soon as all the initial operating conditions are reached, the second phase – the test run – can start. By means of the software, the test is initiated and the data is acquired according to the sampling frequency set in the previous step (one second in the tests performed for this study). Although the plant is equipped with safety systems, the proper functioning should be monitored for the whole duration of the test. Upon completion, the heating system is eventually turned off, the test is concluded and the data are saved and furtherly analysed.

The third phase is the clean-up of the plant. It occurs when the experiment – which may comprise a single test or a set of tests with the same solution – is completed. In this case it is necessary to drain the two packed-column and the solvent tank and to clean them with an appropriate solvent. A nitrogen-based cleaning is then performed – both of the gas lines

and the circulation system. The mass spectrometer lines need to be nitrogen-cleaned as well, in order to remove the possible residues and not to compromise the future analyses.

4.2. Methods: set of tests carried out and operational conditions employed in the experiments performed

The objective of the experiments performed is to evaluate the cyclability and the CO_2 loading capacity of a solution of 50%wt [Cho][Pro] in DMSO for varying working temperatures. The experiments carried out are still part of the preliminary studies on this test bench on the evaluation of the performance and behaviour of [Cho][Pro] as a potential candidate to substitute the MEA aqueous solutions in post-combustion carbon capture plants. Other than comparing the results obtained with the previous ones in a process-optimisation perspective, one of the goals of the study is thus to understand the ranges of operation in case the process is run in a real plant and to better point out the criticalities of the test bench utilised.

In order to study the absorption and the desorption processes separately, the plant is set up in the batch configuration – hence a single column is employed. The tests are run at ambient pressure, with a constant flow rate of $71\ Nl/h$ for both the absorption and the desorption operations. Moreover, it was chosen to set the inlet streams as pure CO_2 flows, so that the chemical and the physical absorption which take place are attributed to the carbon capture and release only.

In order to assess the absorption performance and the solvent regeneration efficiency with the related changes in CO_2 loading capacities, basically two types of tests have been performed. The first one consisted of a set of three consecutive absorption, desorption and cooling stages with an initial absorption temperature of $30°C$ and an initial desorption temperature of $80°C$. The aim of it was to assess the absorption capacity of the fresh solution and the regeneration efficiencies after each cycle. The second type of test is aimed at evaluating the absorption and desorption performances for varying operating temperatures. To this end, the absorption and the desorption were carried out at

progressively increasing temperatures. To better clarify the tests performed, the operating conditions of each test are summed up in *Table 4.1*.

Table 4.1. Summary of the operating conditions of the test carried out.

			T_0 [°C]	p_0 [bara]	flow composition [%]	flow rate [Nl/h]
1st set	1st cycle	absorption	30	1	100% CO_2	71
		desorption	80	1	100% N_2	71
		cooling	T_{amb}	1	-	-
	2nd cycle	absorption	30	1	100% CO_2	71
		desorption	80	1	100% N_2	71
		cooling	T_{amb}	1	-	-
	3rd cycle	absorption	30	1	100% CO_2	71
		desorption	80	1	100% N_2	71
		cooling	T_{amb}	1	-	-
2nd set		complete regeneration	110	1	100% N_2	71
		absorption	30	1	100% CO_2	71
			40	1	100% CO_2	71
			50	1	100% CO_2	71
			60	1	100% CO_2	71
		complete absorption	30	1	100% CO_2	71
		desorption	70	1	100% N_2	71
			80	1	100% N_2	71
			90	1	100% N_2	71
			100	1	100% N_2	71
			110	1	100% N_2	71

The analysis of the data acquired from the process by means of the software allows to derive the following quantities:

- absorbed CO_2 flow rate

$$\dot{m}_{CO_2}^{abs} = \dot{m}_{CO_2}^{in} - \dot{m}_{CO_2}^{out} \tag{4.1}$$

where $\dot{m}_{CO_2}^{abs}$ $[Nl/h]$ is the flow rate of the CO_2 absorbed, $\dot{m}_{CO_2}^{in}[Nl/h]$ is the flow rate of the CO_2 in the inlet stream and $\dot{m}_{CO_2}^{out}[Nl/h]$ is the CO_2 flow rate in the outlet stream;

- CO_2 removal rate

$$\psi = \frac{\dot{m}_{CO_2}^{abs}}{\dot{m}_{CO_2}^{in}} \cdot 100 \tag{4.2}$$

where ψ [%] is the CO_2 removal rate, $\dot{m}_{CO_2}^{abs}$ $[Nl/h]$ and $\dot{m}_{CO_2}^{in}$ $[Nl/h]$ are the same as above;

- absorption loading – expressed in terms of molality as

$$m = \frac{n_{CO_2}}{m_{IL} + m_{DMSO}} \tag{4.3}$$

where m $[mol_{CO_2}/kg_{sorb}]$ is the CO_2 absorption loading, n_{CO_2} $[mol]$ are the moles of CO_2 absorbed in the solution, m_{IL} $[kg]$ and m_{DMSO} $[kg]$ are the [Cho][Pro] and DMSO masses respectively; or in terms of molar efficiency

$$\alpha = \frac{n_{CO_2}}{n_{IL}} \tag{4.4}$$

where α $[mol_{CO_2}/mol_{IL}]$ is the CO_2 absorption loading, n_{CO_2} $[mol]$ and n_{IL} $[mol]$ are the moles of CO_2 and [Cho][Pro] respectively in the solution;

- regeneration efficiency

$$\eta = \frac{m_n}{m_1} \cdot 100 \tag{4.5}$$

where η [%] is the regeneration efficiency, m_n is the m_n $[mol_{CO_2}/kg_{sorb}]$ and m_1 $[mol_{CO_2}/kg_{sorb}]$ are the absorption loading at the end of the nth cycle and the first one with the fresh solution.

4.3. Results and discussion

4.3.1. CO_2 loading capacity of the fresh 50%wt [Cho][Pro] in DMSO solution

The first set of tests performed on the test bench aimed at evaluating the CO_2 absorption capacity of the fresh 50%wt [Cho][Pro] in DMSO solution. To this end, a $71\ Nl/h$ flow rate of CO_2 was sent to the absorption reactor for a duration of $90\ minutes$.

The results obtained are reported in *Figure 4.3*, pointing out the poor absorption capacity of the 50%wt concentration solution. It can be seen, in fact, that α stabilises even below the value of $0.5\ mol\ CO_2/mol_{IL}$, which is considered to be the lower acceptable threshold since it is the usual absorption efficiency of the amine aqueous solutions. Moreover, it has to be underlined that according to research evidence [Cho][Pro] is expected to be more inclined to the 2:1 rection mechanism, rather than the 1:1 one. This is indicative of the inefficient diffusion of the carbon dioxide inside the solution due to the high viscosity of the latter. The increase in moles of [Cho][Pro] does not imply an increase in absorption capacity – as one would intuitively expect.

The high volume employed for the experiment ($\sim 1\ l$) may also have an influence on the results obtained, since it may be one of the reasons for which the CO_2 molecules were not able to reach all the amine functionalities present in the solution and to react with them.

Higher operating pressures could countereffect the problems discussed above, as they would act on the concentration gradient increasing the driving force which controls the diffusion mechanism and consequently enhancing the chemical absorption reactions.

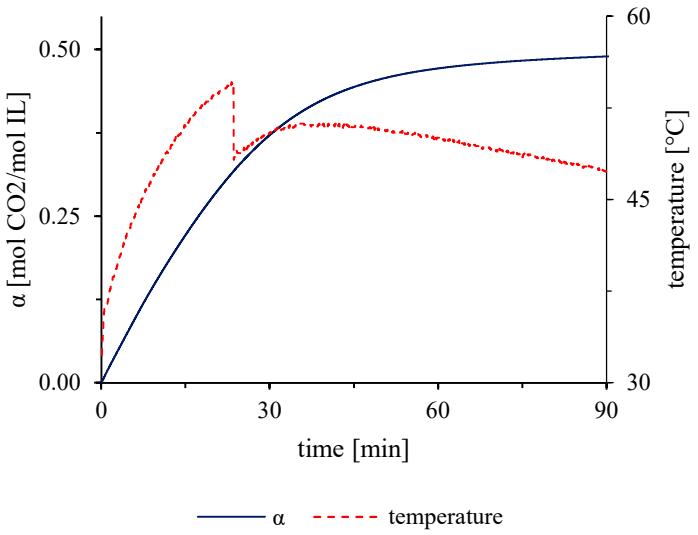

Figure 4.3. CO_2 loading capacity of the 50%wt [Cho][Pro] in DMSO solution in terms of molarity. (Initial absorption temperature: 303 K; CO_2 mass flowrate: 71 Nl/h; volume of the solution: 0.916 l; duration of the test: 90 min).

During the absorption run, the CO_2 flowrate has been interrupted for approximately 30 min because of dysfunctionality of the test bench – which explains the $6°C$ temperature drop of the solution in the absorption reaction that takes place after 25 $minutes$ from the beginning of the experiment. Despite this, the capacity load curve does not show a change in terms of absorption rate, as the slope remains constant. This implies that the kinetics of the reaction and the correlated mass transfer phenomena are not susceptible to such small variations in temperature.

Furthermore, it is to be pointed out that the difference in temperature during the operation is very little, proving the low exothermicity of the CO_2 absorption reaction by means of [Cho][Pro] – especially when compared to the ones via aqueous amine solutions.

It can also be observed that the loading curve changes concavity after approximately 45 $minutes$ of absorption, with very little changes in the loading capacity afterwards. As a consequence, the CO_2 removal from the stream to be purified would not be acceptable from this point on and the solution should be regenerated within these limits.

4.3.2. Cyclability performance

Practical applications of carbon capture solvents strongly require an efficient solvent regeneration process – in which the energy requirements, the losses and the degradation of the materials involved are minimised as much as possible.

The efficiency loss and the cyclability of the 50%wt [Cho][Pro] in DMSO solution was studied in terms of regeneration efficiency – that is the ratio of the capacity loading at the nth cycle over the one at the first cycle. Three cycles have been performed, with an absorption duration of $90\,minutes$ at an initial temperature of the solution of $30°C$ and a desorption duration of $90\,minutes$ at an initial temperature of $80°C$. Pure CO_2 and N_2 flow rates were utilised for the two operating conditions, in order to remove the effects of other possible gases involved in the stream in these preliminary studies.

The evolution of the CO_2 loading in the [Cho][Pro] in DMSO solution is reported in *Figure 4.4*. The first thing that catches the eye is that if on the one side α does not exceed the value of $0.5\,mol_{CO_2}/mol_{IL}$ for any of the cycles, on the other one it does not even decrease with increasing cycles – even though the solution is not completely regenerated.

It is also noticeable that the moles of CO_2 desorbed during the regeneration process is almost constant and is roughly equal $0.25\,mol_{CO_2}/mol_{IL}$ – which corresponds to half of the amount absorbed in the first step. It can also be seen that at the end of the regeneration step the α curve is still downwards sloped, indicating that the desorption is still remarkably going on.

Based on the considerations made until now, a possible way to enhance the degree of CO_2 absorption in the solution could be to extend the duration of the absorption phase, which, however, is not believed to lead to significant improvements since physical absorption is expected to occur only. Studies in the literature [98], [102] show that increasing the operational pressures – by increasing the CO_2 partial pressure – lead to much better absorption performances, thus this path could be followed.

As concerns the desorption phase, in order to achieve the complete regeneration of the solution it may be considered to extend the duration or to increase the N_2 flowrate at this stage; this would allow decreasing the CO_2 partial pressure and enhance the desorption of

the CO_2 molecules. Another option could be to increase the desorption temperature, with the aim of releasing the carbamate species which are stable at high temperatures. Since at the end of the desorption process the CO_2 is still being released, this energy-consuming option does not seem as reasonable as increasing the N_2 flowrate or the duration of the desorption step, though.

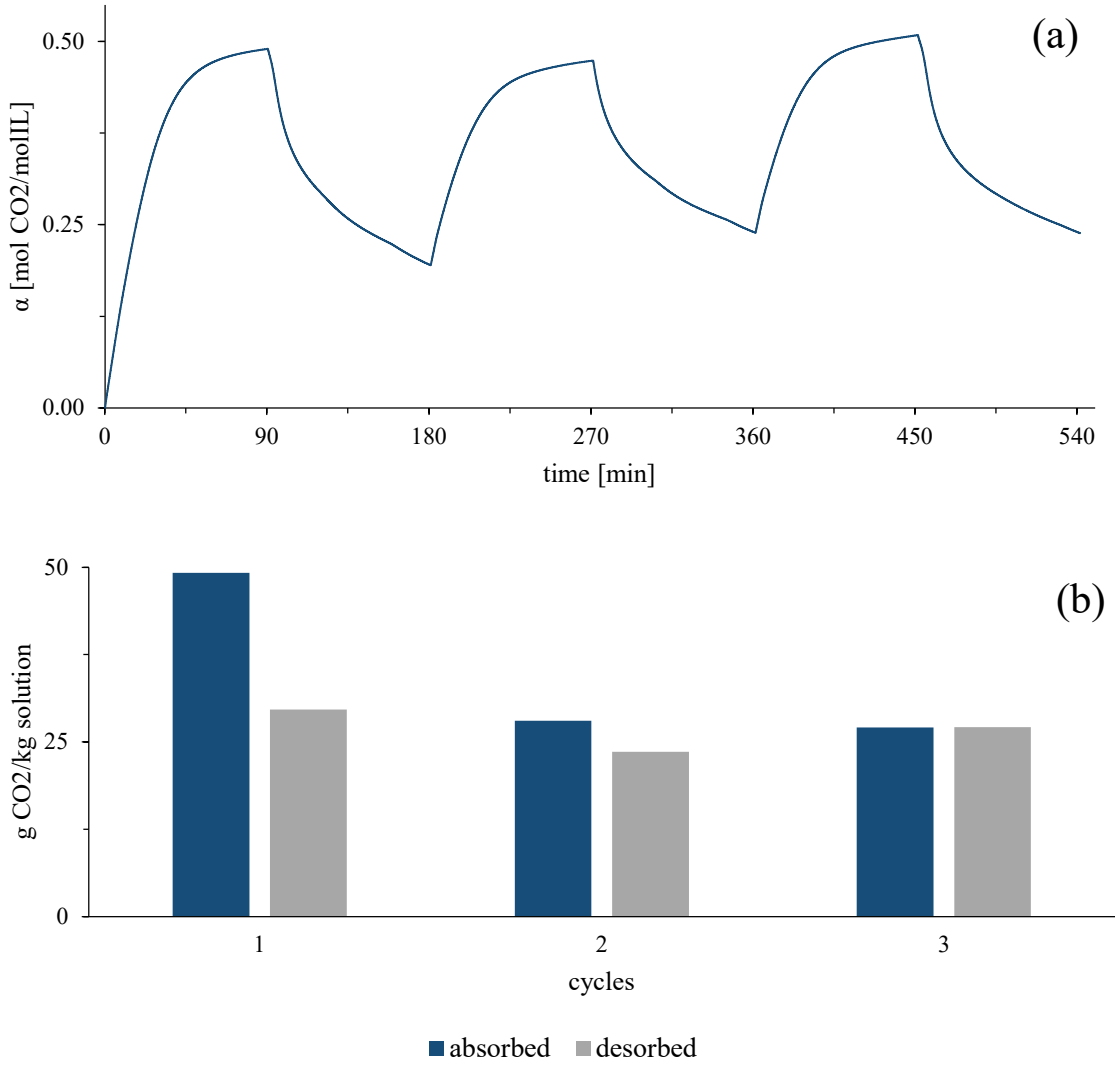

Figure 4.4. (a) Evolution of the CO_2 loading capacity for the 3 cycles performed with the 50%wt [Cho][Pro] in DMSO solution. (b) Amounts of absorbed and desorbed CO_2 per mass of solution employed for each absorption-desorption cycle performed with the 50%wt [Cho][Pro] in DMSO solution.
(Initial absorption temperature: 303 K; CO_2 flowrate: 71 Nl/h; absorption duration: 90 min; initial desorption temperature: 353 K; N_2 flowrate: 71 Nl/h; desorption duration: 90 min; volume of the solution> 0.916 l).

Table 4.2. Moles of CO_2 absorbed and desorbed per cycle with respect to the moles of IL in the solution and the mass of solution employed for the experiment

	1^{st} *cycle*		2^{nd} *cycle*		3^{rd} *cycle*	
	abs	des	abs	des	abs	des
$\boldsymbol{\alpha}$ $[\boldsymbol{mol_{CO_2}/mol_{IL}}]$	0.49	0.30	0.28	0.23	0.27	0.27
$\boldsymbol{m}$ $[\boldsymbol{mol_{CO_2}/kg_{sol}}]$	1.12	0.67	0.64	0.54	0.61	0.62

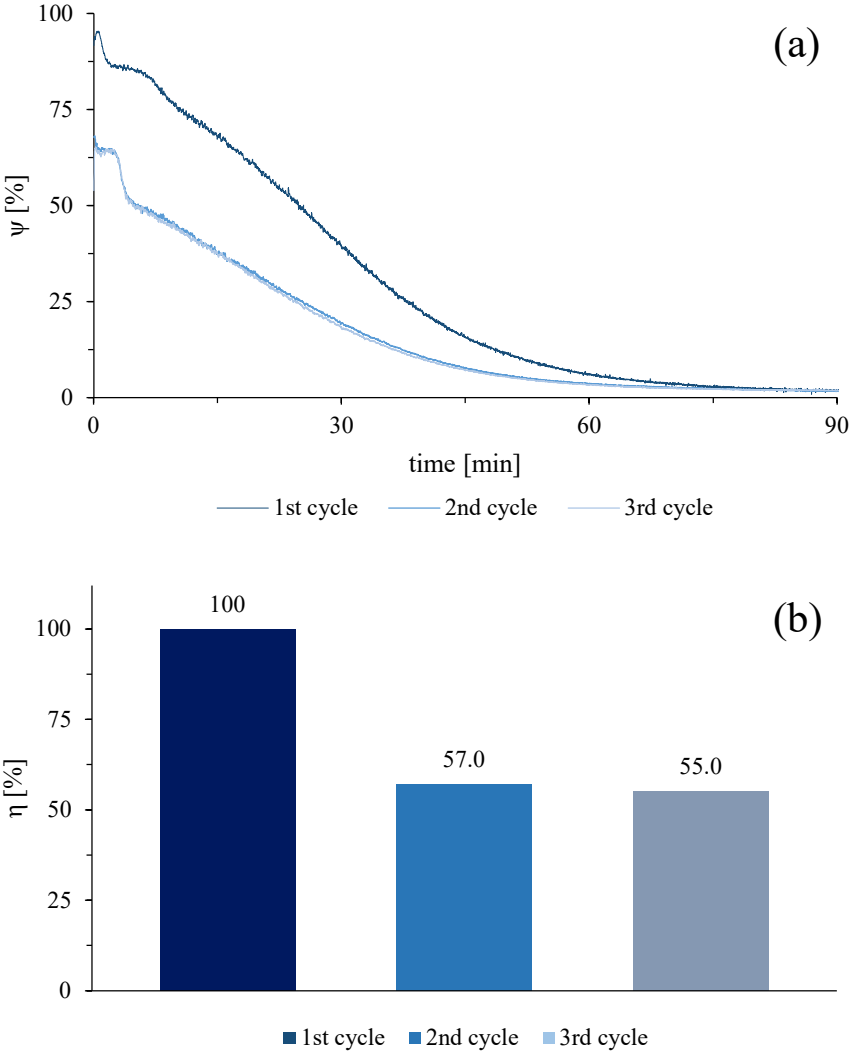

Figure 4.5. (a) Removal rates for the 3 cycles performed with the 50%wt [Cho][Pro] in DMSO solution. (b) Regeneration efficiencies for each absorption cycle carried out. with the 50%wt [Cho][Pro] in DMSO solution.
(Initial absorption temperature: 303 K; CO_2 mass flowrate: 71 Nl/h; volume of the solution: 0.916 l; duration of the test: 90 min).

The considerations made so far do not keep into account the constraints on the maximum percentage of carbon dioxide allowed in the output flow. *Figure 4.5* shows the CO_2 removal rate for the three absorption cycles – expressed as a percentage of CO_2 absorbed in the solution with respect to the one entering it. It should be observed that the curves of the second and third cycle are shifted downwards by approximately 20% if compared to the first cycle, leading to removal rates lower than 50% after $5\ minutes$ from the beginning of the absorption run.

Real applications usually present the continuous configuration, where there is continuous recirculation and the solution regenerated in the stripper is added to the one rich in carbon dioxide. Nevertheless, the low removal rates occurring right from the beginning of the test suggest that practical applications with the 50%wt concentration solution and this operating conditions in the desorption column would require multiple absorption steps in order to achieve satisfactory levels of carbon sequestration from the stream to be purified.

Figure 4.5 reports also the regeneration efficiency of the three subsequent cycles. As already stated above, the quantity of CO_2 absorbed remains almost constant for the second and the third absorption cycles, resulting in similar regeneration efficiencies of about $\sim 55\%$.

4.3.3. Effect of temperature on the absorption process

At the end of the three absorption and desorption cycles discussed above, the solution was completely regenerated by increasing the temperature until $110°C$ for a duration of approximately $120\ minutes$.

The effect of temperature was afterwards investigated and the results obtained are reported in *Figure 4.6.* It can be observed that in the case of [Cho][Pro] in DMSO solutions the influence of the operating absorption temperature is quite significant in terms of capacity loading, with higher amounts of carbon dioxide absorbed with decreasing temperatures. This can be explained by the low exothermicity of the absorption reaction when ILs are involved as carbon capture solvents – as limited rises in temperature occur over the duration of a test run.

In *Figure 4.6 (b)* the CO_2 removal rate curves are plotted both for the absorption runs at increasing absorption temperatures $(30°C, 40°C, 50°C, 60°C)$ and for the further completion of the absorption at $30°C$. As expected, the removal rate decreases with increasing temperatures for the first part of the operation, and then shows an increase for the tests in which the solution was not able to reach the saturation because of the higher temperatures initially involved.

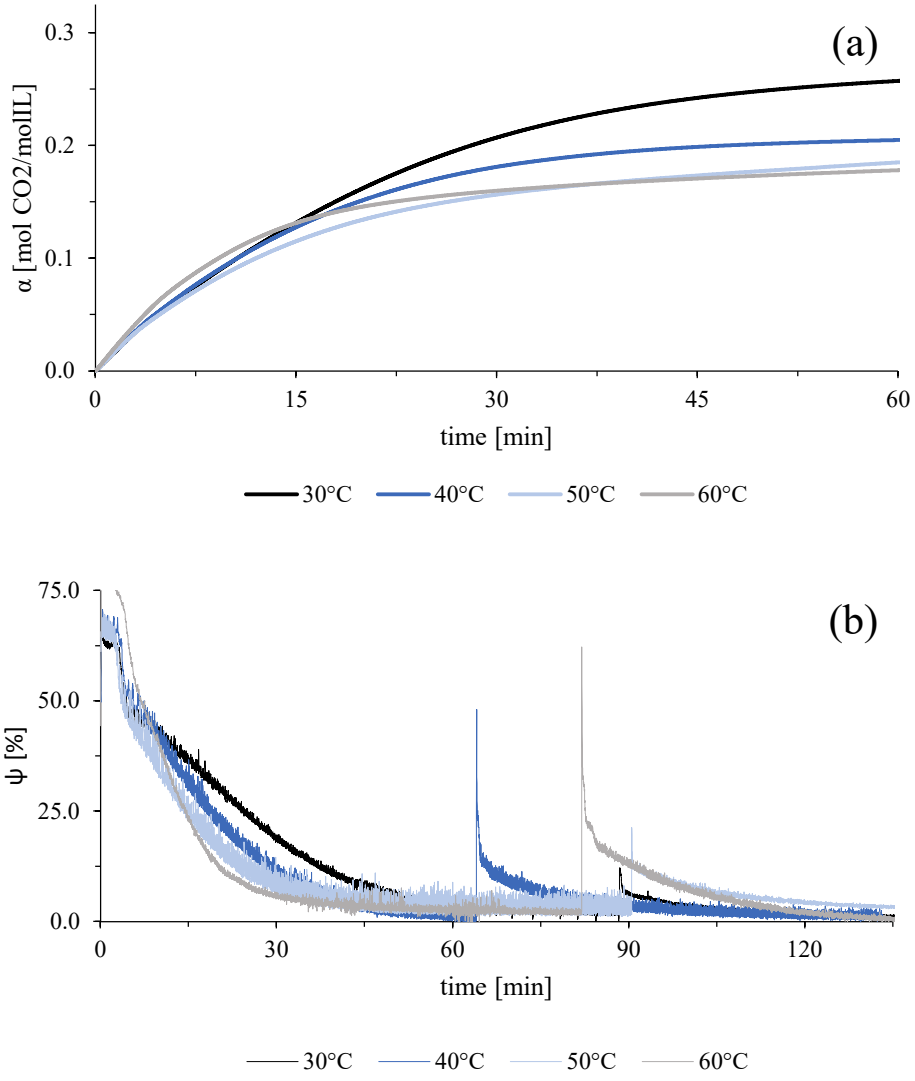

Figure 4.6. (a) CO_2 loading capacity curves for varying initial temperatures absorption runs. (b) CO_2 removal rates for varying initial temperatures absorption runs followed by the completion of absorption at $30°C$.
(Initial absorption temperature: 303 K; 313 K; 323 K; 333 K. Completion of absorption initial temperature: 303 K. CO_2 mass flowrate: 71 Nl/h; volume of the solution: 0.916 l.)

4.3.4. Effect of temperature on the desorption process

Besides the absorption performance, it is of great importance to optimise the regeneration of the solutions involved in carbon capture processes, in order to minimise as much as possible the temperatures involved and thus the external thermal requirements.

The absorption and the completion of absorption tests described in the previous section were followed by a desorption phase in which – starting from an initial value of $70°C$ – the operating temperature was increased up to $110°C$ with a step of $10°C$. The flowrate sent to the reactor consisted of a constant $71\ Nl/h$ nitrogen stream.

Figure 4.7 shows the evolution of the percentage of CO_2 contained within the solution throughout the set of tests performed; it was calculated on the basis of the total amount of CO_2 absorbed at the end of the completion of the absorption phase – where saturation is supposed to be reached. The absorption capacities obtained for each cycle are reported in *Table 4.3*, expressed in molality and in molarity terms.

It can be observed that in all of the four tests the highest percentage of CO_2 released occurs during the initial regeneration phase at the temperature of $70°C$. In this early stage, the desorption is mainly due to the decrease in partial pressure of carbon dioxide which takes place as soon as the nitrogen flow begins. In this phase, therefore, the CO_2 release is due to the desorption of the molecules which were previously physically absorbed and to the decomposition of the carbonic acid species – whose reaction is reversible at room temperature.

Table 4.3. Absorption capacities obtained for varying initial absorption temperatures.

Initial absorption temperature $[°C]$	$\boldsymbol{\alpha}$ $[mol_{CO_2}/mol_{IL}]$	$\boldsymbol{m}$ $[mol_{CO_2}/kg_{solution}]$
30	0.30	0.68
40	0.26	0.58
50	0.26	0.60
60	0.25	0.60

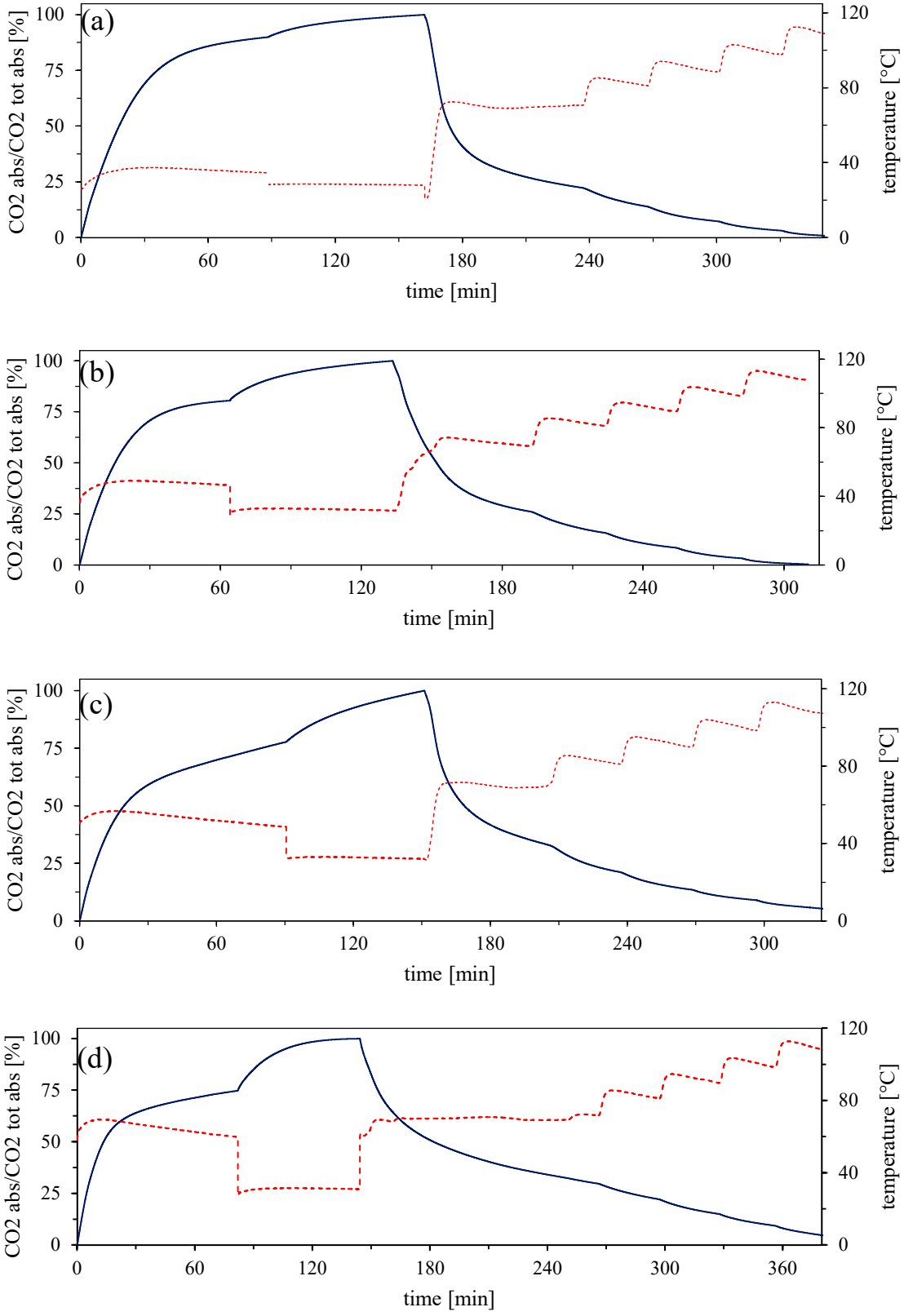

Figure 4.7. $\%CO_2$ absorbed in the 50%wt [Cho][Pro] in DMSO solution for the absorption–completion absorption–desorption runs at progressively increasing temperatures. Initial absorption temperature: (a) 303 K; (b) 313 K; (c) 323 K; (d) 333 K. Initial desorption temperature: 343 K.

When the rate of desorption begins to assume low values, the operating temperature is increased by $10°C$ every $30\ minutes$. This allows the release of the carbamate species – for which the inversion of the formation reaction requires high-temperature values due to their high thermal stability. It can be seen how the progressively increased temperatures leads to a steepening of the curve, which eventually allows the complete regeneration of the solution. It has to be highlighted, though, that when the desorption temperature is raised, the curve does not seem to have reached a plateau yet, therefore the solution is still desorbing carbon dioxide. This suggests that it may be not necessary to reach such high temperatures, but it would be sufficient to increase the duration of the desorption phase.

The experiments performed confirm that the regeneration of IL solutions show good performances at much lower temperatures than those required for the aqueous amine case, for which the desorption starts only when the operating temperature exceeds $100°C$.

With the current operating pressures, the absorption and desorption processes could be optimised by performing the cycles at the operating temperatures of $30°C$ and $90°C$ respectively, which would lead to high regeneration efficiencies on the one side and would lower the energy requirements during the desorption phase on the other one. Both hot and cold sinks – or a proper pinch analysis – should be taken into consideration in this case, due to the necessities to cool the stream to be purified entering the absorption reactor and to heat the rich CO_2 solution during the regeneration phase.

4.4. Comparison of the performances of the 12.5%wt [Cho][Pro] in DMSO and the 50%wt [Cho][Pro] in DMSO solutions

In the following, the carbon capture sequestration performances obtained with the 50%wt [Cho][Pro] in DMSO solution in the experiments performed for this study are compared to the ones achieved in a study on the same test bench which utilised a 12.5%wt concentration solution.

Although the masses of the solutions involved are different in the two cases ($\sim 0.5\ kg$ and $\sim 1\ kg$ for the experiments with the 12.5%wt and the 50%wt concentrations, respectively), the results are comparable since the capacity loadings are normalised on the basis of the

mass of the solution employed or the moles of IL within the solution. *Figure 4.8* shows the evolution of α and m in the two set of test runs. It can be observed that the 50%wt solution presents much higher performances in terms of m – that is, amount of CO_2 absorbed per kg of solution employed. The situation is reversed when the performance is analysed in terms of α, where the amount of moles of CO_2 absorbed in the solution are normalised with respect to moles of IL available.

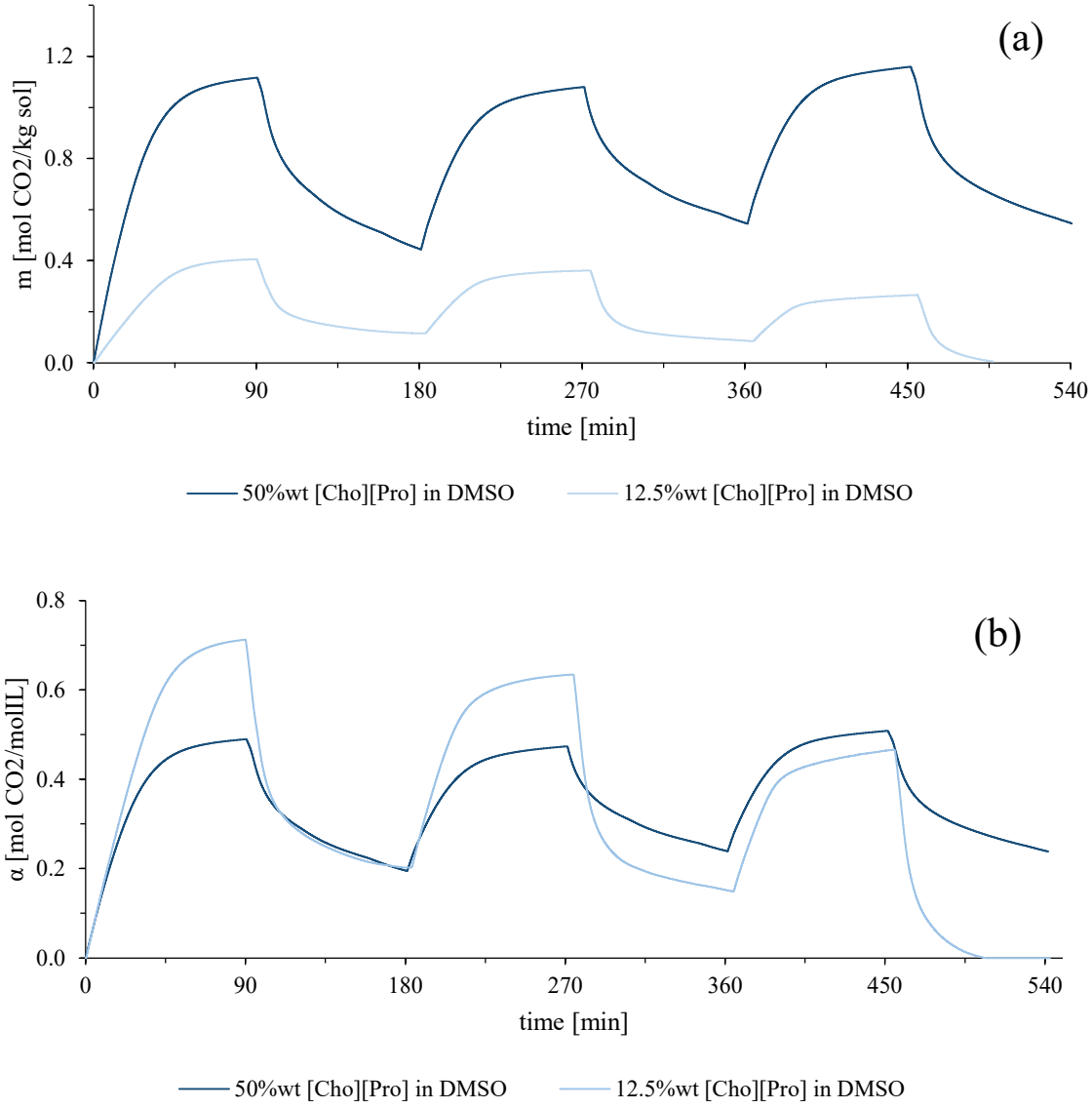

Figure 4.8. Comparison of the capacity load curves obtained from the tests with the 12.5%wt and the 50%wt [Cho][Pro] in DMSO curves. (a) Calculated on the basis of the mass of solution employed for the experiment. (b) Calculated on the basis of the total moles of [Cho][Pro] present within the solution.

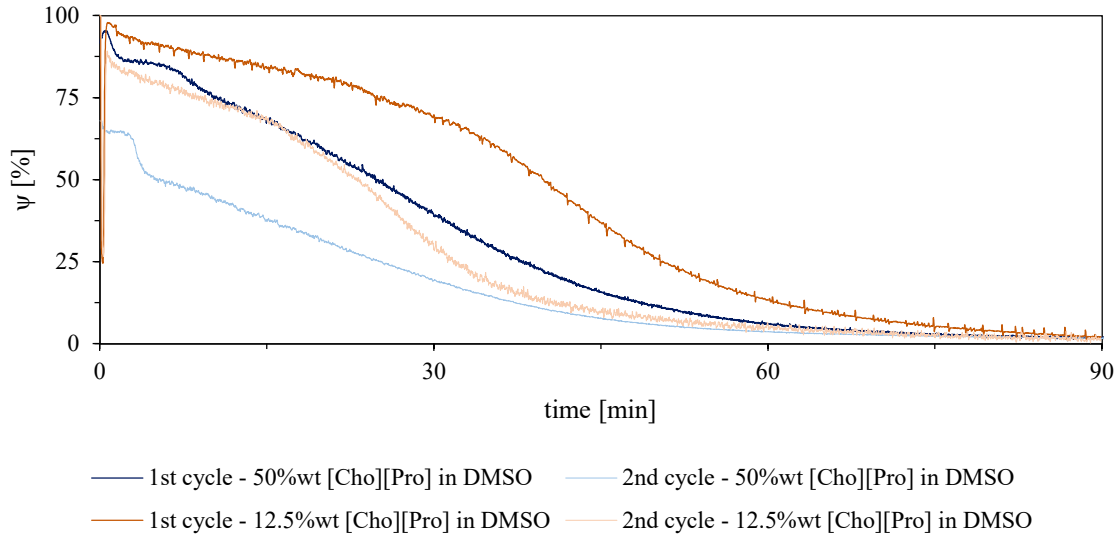

Figure 4.9. Comparison of the removal rates curves for the first and the second cycles performed by means of the 12.5%wt and the 50%wt [Cho][Pro] in DMSO solutions.

The reason for this is that the number of amine functionalities which can react are much higher in the 50%wt solution – because of the increase in both concentration and volume utilised. If this results in higher amounts of CO_2 absorbed on the one hand, on the other one the evolution of α shows that not all the amine moieties are able to react, leading to poor performances in terms of efficiencies of the absorption reaction. The 12.5%wt solution, moreover, presents a larger number of moles absorbed and desorbed per cycle – which translates into higher regeneration efficiencies.

The considerations made above can be again traced back to the difference in viscosity between the two solutions. Possible ways to increase the performances of the 50%wt solution consist in enhancing the diffusion mechanism of the CO_2 molecules within the carbon capture solvent and were discussed previously (see *chapter 4.3.2*).

In addition, it is interesting to look at the removal rates achieved with the two solutions employed. Although it was stated that the overall quantity of carbon dioxide absorbed per kg of solution employed is lower when the 12.5%wt solution is used, *Figure 4.9* highlights that the removal rates are better in this instance. The difference in performances achieved reaches values of 30% in some cases and it is particularly pronounced in the first 30 $minutes$ of the test runs. It can also be noted that the removal rates obtained with the

12.5%wt solution during the second cycle are almost equal to the ones achieved with the fresh 50%wt solution.

In view of the fact that the ratio of the CO_2 flowrate entering the absorption column over the moles of [Cho][Pro] present within the solution is practically the same ($29\ Nl/h$ per mole of IL in case of the 12.5%wt solution and $30\ Nl/h$ per mole of IL in case of the 50%wt solution), the poorer performances of the more concentrated solution may indicate that higher ratios are needed as lager moles of [Cho][Pro] are involved. The increase in amount of IL, therefore, seems to result in the necessity of a longer residence time in the absorption column of the stream to be purified, in order to enhance the mass transfer phenomena and to allow the greatest number of reactions between the CO_2 molecules and the amine functionalities.

In conclusion, the two preliminary experiments on the use of [Cho][Pro] in DMSO solutions as carbon capture solvents showed that the increase in the amount of IL present in the absorbing solution does not lead to higher performances unless the diffusion mechanism is properly optimised. The increase in viscosity which occurs with increasing concentrations, in fact, hinders the reaction mechanism and does not allow the complete reaction between all the amine functionalities and the CO_2 present in the stream. Hence, higher performances were achieved by the 12.5%wt solution, notwithstanding the fact that higher concentrations may be promising if the diffusion phenomena were optimised (e.g., by increasing the operating pressure or lowering the input flowrate).

4.5. Criticalities arose and limits of the test bench

Figure 4.10 shows the changes in capacity loading over the course of the tests performed for the current study. It clearly emerges that the α drastically drops among the first cycle – carried out with the fresh solution – and the subsequent ones. If between the first and the second cycle this can be explained with the non-completion of the regeneration of the solution, the others require different considerations since the solution is supposed to be completely regenerated at the end of the third cycle by increasing the temperature up to $110°C$ for about $120\ minutes$.

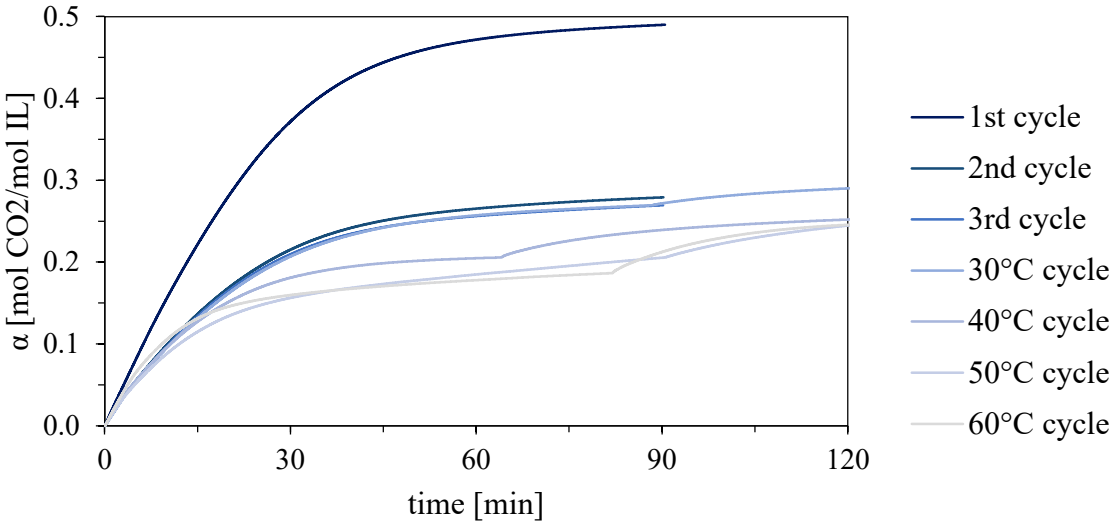

Figure 4.10. Loss in capacity loading with cycles for the 50%wt [Cho][Pro] in DMSO solution.

To this regard, it can be hypothesised that the temperatures involved in the regeneration step are too high and that the lower capacity loading is due to the degradation of the solution. This is supported by the decrease in mass of the solution with respect to the initial value which was measured in the clean-up phase (see *chapter 514.1.2*), which indicates that evaporation losses took place.

Indeed, although the decomposition of the [Cho][Pro] in DMSO solution takes place at $130°C$ and other studies performed the regeneration step at $110°C$ with good results [98], the considerations made above may be a clue that the thermal degradation already starts at lower temperatures if the duration of the desorption phase is prolonged. As good regeneration performances are observed also around $90°C$, future experiments performed on this test bench with [Cho][Pro] solutions should not overcome this value. The completion of the regeneration of the solution could be thus achieved by extending the duration of the desorption phase or by increasing the N_2 flowrate sent to the column.

The limits of the test bench also need to be mentioned. A source of inaccuracy of the results obtained is ascribable to the flowmeters; they are in fact calibrated to nitrogen streams and only the flowmeter which provides the measurements of the input stream is provided with corrective factors for the operations involving CO_2, CO, CH_4, H_2, O_2 and mixtures of them. In order to properly estimate the output flowrates during the absorption

and desorption runs, proper corrective factors were estimated and are reported in APPENDIX II.

Other issues raised by the lack of precision of the heaters in bringing the solution within the reactor at the set temperatures. Once set the desired value required for the operation to be performed, in fact, the system initially exceeds this value in a range of $5°C - 10°C$ and then stabilises to the wanted value.

Despite the criticalities highlighted, the results obtained from these preliminary studies can still be considered in line with the objectives of the current study, which aimed at evaluating the difference in performance – assessed as amount of CO_2 sequestrated form the stream to be purified and molar efficiency of the reactions occurring – with the increase in concentration of [Cho][Pro] in DMSO solutions.

5. Conclusions

The fulfilment of the climate targets set worldwide dictates the transition from a high to a low carbon economy. In this framework, CCS technologies are a powerful tool as long as the CO_2 emissions from the energy sector and the hard-to-abate industries will be at nowadays levels and low-carbon technologies will be available on a commercial scale.

The experiments performed for this study employed a 50%wt solution of [Cho][Pro] in DMSO run on a bench-scale plant. The experimental assessment of the density and viscosity values of the pure IL and the 12.5%wt, 25%wt, and 50%wt solutions allowed to determine empirical equations for future calculations and highlighted the necessity of using [Cho][Pro] together with less viscous solvents – given the two to three orders of magnitude difference in viscosity between pure [Cho][Pro] and the other solutions.

The performance of the solution was then studied in terms of cyclability by operating three consecutive absorption and desorption runs of 90 $minutes$ each, with initial absorption and desorption temperatures of $30°C$ and $80°C$, respectively. The absorption capacity of the fresh solution was 0.49 mol_{CO_2}/mol_{IL} in molarity terms and 1.12 mol_{CO_2}/kg_{sol} in molality terms and then halved at the second and third cycles, leading to regeneration efficiencies of ~55%. Despite the poor absorption efficiencies obtained – which are expected to range between 0.5 mol_{CO_2}/mol_{IL} and 1 mol_{CO_2}/mol_{IL} when ILs are employed – the cyclability of the solution seems to be good. A higher number of cycles (e.g., 20) should be performed to confirm this statement, however.

The effect of the initial temperature was investigated in an interval between $30°C$ and $60°C$, showing a drop in absorption capacity from 0.27 mol_{CO_2}/mol_{IL} to 0.19 mol_{CO_2}/mol_{IL} and thus confirming the significant impact it has, since the absorption reaction is not highly exothermic and the operating temperature does not change remarkably over the operations.

A comparison between the results obtained from a previous study performed with a 12.5%wt [Cho][Pro] in DMSO solution on the same test bench showed that the increase in concentration results in higher absorption capacities in molality terms (1.08 mol_{CO_2}/mol_{IL} with respect to 0.35 mol_{CO_2}/mol_{IL} obtained with the 12.5%wt solution), but lower

in molarity terms ($0.47\ mol_{CO_2}/mol_{IL}$ with respect to the $0.63\ mol_{CO_2}/mol_{IL}$ obtained with the 12.5%wt solution). This indicates that higher concentrations contain a higher number of amine functionalities able to absorb the CO_2 molecules, but the higher viscosities which derive lead to hindered diffusion phenomena and poor molar efficiencies.

Future studies should focus on determining a compromise between these two parameters, in order to guarantee the minimum CO_2 uptake from the stream to be purified and the optimal use of the expensive IL at the same time. Moreover, the effect of the increase in operating pressure during the absorption run should be investigated, since studies in the literature performed with aqueous [Cho][Pro] solutions claim the achievement of better performances. At last, economic analyses should be performed, intending to find the operating conditions which minimise the capital and the operational expenditures.

References

[1] S. Zerveas, E. Kydonakis, P. Moutidis, A. Maragkoudakis, and K. Kotzabasis, "Microalgae strategy in anoxic atmospheres with various CO2 concentrations – Environmental and (astro)biotechnological perspectives," *Environmental and Experimental Botany*, vol. 187, p. 104474, Jul. 2021, doi: 10.1016/J.ENVEXPBOT.2021.104474.

[2] T. S. Ledley, E. T. Sundquist, S. E. Schwartz, D. K. Hall, J. D. Fellows, and T. L. Killeen, "Climate change and greenhouse gases," *Eos, Transactions American Geophysical Union*, vol. 80, no. 39, pp. 453–458, Sep. 1999, doi: 10.1029/99EO00325.

[3] R. K. Pachauri *et al.*, "Climate Change 2014: Synthesis report. Contribution of Working Groups I, II and III to the Fifth Assessment Report of the Intergovernmental Panel on Climate Change," Gian-Kasper Plattner, Geneva Switzerland, 2014. Accessed: Nov. 21, 2021. [Online]. Available: http://www.ipcc.ch.

[4] "Global Monitoring Laboratory - Carbon Cycle Greenhouse Gases." https://gml.noaa.gov/ccgg/trends_n2o/ (accessed Nov. 21, 2021).

[5] D. W. Fahey *et al.*, "REPORT ON UNEXPECTED EMISSIONS OF CFC-11 A Report of the Scientific Assessment Panel of the Montreal Protocol on Substances that Deplete the Ozone Layer Advisory Group Report Coordinator Editorial, Graphics, and Reference Support".

[6] "Global Monitoring Laboratory - Carbon Cycle Greenhouse Gases." https://gml.noaa.gov/ccgg/trends_ch4/ (accessed Nov. 21, 2021).

[7] "Daily CO2." https://www.co2.earth/daily-co2 (accessed Nov. 21, 2021).

[8] H. Ritchie and M. Roser, "CO_2 and Greenhouse Gas Emissions," *Our World in Data*, May 2020, Accessed: Nov. 21, 2021. [Online]. Available: https://ourworldindata.org/co2-and-other-greenhouse-gas-emissions

[9] IEA, "CCUS in Clean Energy Transition," 2020. Accessed: Nov. 21, 2021. [Online]. Available: www.iea.org/t&c/

[10] R. Adib *et al.*, "REN21. Global Status Report," *REN21. Renewable Energy Policy Network*, 2021.

[11] IAEA, “ENERGY, ELECTRICITY AND NUCLEAR POWER ESTIMATES FOR THE PERIOD UP TO 2050,” 2020.

[12] H. C. Lau, S. Ramakrishna, K. Zhang, and A. V. Radhamani, “The role of carbon capture and storage in the energy transition,” *Energy and Fuels*, vol. 35, no. 9, pp. 7364–7386, May 2021, doi: 10.1021/acs.energyfuels.1c00032.

[13] M. Fajardy and N. mac Dowell, “The energy return on investment of BECCS: is BECCS a threat to energy security?,” *Energy & Environmental Science*, vol. 11, no. 6, pp. 1581–1594, Jun. 2018, doi: 10.1039/C7EE03610H.

[14] M. Ramdin, T. W. de Loos, and T. J. H. Vlugt, “State-of-the-art of CO 2 capture with ionic liquids,” *Industrial and Engineering Chemistry Research*, vol. 51, no. 24. pp. 8149–8177, Jun. 20, 2012. doi: 10.1021/ie3003705.

[15] D. Keairns, R. Newby, and V. Shah, “Current and Future Technologies for Power Generation with Post-Combustion Carbon Capture,” Mar. 2012, doi: 10.2172/1489757.

[16] R. E. James III PhD, D. Kearins, M. Turner, M. Woods, N. Kuehn, and A. Zoelle, “Cost and Performance Baseline for Fossil Energy Plants Volume 1: Bituminous Coal and Natural Gas to Electricity,” Sep. 2019, doi: 10.2172/1569246.

[17] K. Gerdes *et al.*, “Cost and Performance of PC and IGCC Plants for a Range of Carbon Dioxide Capture,” May 2011, doi: 10.2172/1515274.

[18] Y. Manoharan *et al.*, “Hydrogen Fuel Cell Vehicles; Current Status and Future Prospect,” *Applied Sciences 2019, Vol. 9, Page 2296*, vol. 9, no. 11, p. 2296, Jun. 2019, doi: 10.3390/APP9112296.

[19] Bui Mai *et al.*, “Carbon capture and storage (CCS): the way forward.,” *Energy & Environmental Science*, vol. 11, no. 5, pp. 1062–1176, 2018.

[20] F. Vega, F. M. Baena-Moreno, L. M. Gallego Fernández, E. Portillo, B. Navarrete, and Z. Zhang, “Current status of CO2 chemical absorption research applied to CCS: Towards full deployment at industrial scale,” *Applied Energy*, vol. 260, Feb. 2020, doi: 10.1016/j.apenergy.2019.114313.

[21] Roger Bottoms Robert, “PATENT OFFICE UNITED STATES,” 1783901, Dec. 02, 1930

[22] A. Krótki *et al.*, “Experimental results of advanced technological modifications for a CO2 capture process using amine scrubbing,” *International Journal of Greenhouse Gas Control*, vol. 96, May 2020, doi: 10.1016/j.ijggc.2020.103014.

[23] Vaidya Prakash D. and Kenig Eugeny Y., “CO2-alkanolamine reaction kinetics: a review of recent studies.,” *Chemical Engineering & Technology: Industrial Chemistry - Plant Equipment - Process Engineering - Biotechnology*, vol. 30, no. 11, pp. 1467–1474, 2007.

[24] J. Huang and T. Rther, “Why are ionic liquids attractive for CO2 absorption? An overview,” *Australian Journal of Chemistry*, vol. 62, no. 4. pp. 298–308, 2009. doi: 10.1071/CH08559.

[25] R. S. Haszeldine, “Carbon Capture and Storage: How Green Can Black Be?” [Online]. Available: https://www.science.org

[26] P. Galindo, A. Schäffer, K. Brechtel, S. Unterberger, and G. Scheffknecht, “Experimental research on the performance of CO 2-loaded solutions of MEA and DEA at regeneration conditions,” *Fuel*, vol. 101, pp. 2–8, Nov. 2012, doi: 10.1016/j.fuel.2011.02.005.

[27] W. Conway *et al.*, “CO2 absorption into aqueous amine blended solutions containing monoethanolamine (MEA), N,N-dimethylethanolamine (DMEA), N,N-diethylethanolamine (DEEA) and 2-amino-2-methyl-1-propanol (AMP) for post-combustion capture processes,” *Chemical Engineering Science*, vol. 126, pp. 446–454, Apr. 2015, doi: 10.1016/j.ces.2014.12.053.

[28] J. I. Huertas, M. D. Gomez, N. Giraldo, and J. Garzón, “CO2 absorbing capacity of MEA,” *Journal of Chemistry*, vol. 2015, 2015, doi: 10.1155/2015/965015.

[29] Freemantle Michael, *An Introduction to Ionic Liquids*. London: RSC Publishing, 2010.

[30] Inman Douglas and Lovering David G., *Ionic Liquids*. New York: Plenum Press, 1981.

[31] L. Glasser, “Lattice and phase transition thermodynamics of ionic liquids,” *Thermochimica Acta*, vol. 421, no. 1–2, pp. 87–93, Nov. 2004, doi: 10.1016/J.TCA.2004.03.015.

[32] P. Walden, “Ueber die Molekulargr¨osse und elektrische Leitf¨ahigkeit einiger geschmolzenen Salze,” *Bulletin de l’Académie Impériale des Sciance de St.-Pétersbourg*, vol. 8, no. 6, pp. 405–422, Mar. 1914, [Online]. Available: http://www.mathnet.ru/eng/agreement

[33] N. v. Plechkova and K. R. Seddon, “Applications of ionic liquids in the chemical industry,” *Chemical Society Reviews*, vol. 37, no. 1. pp. 123–150, 2008. doi: 10.1039/b006677j.

[34] M. Ramdin, T. W. de Loos, and T. J. H. Vlugt, “State-of-the-art of CO 2 capture with ionic liquids,” *Industrial and Engineering Chemistry Research*, vol. 51, no. 24. pp. 8149–8177, Jun. 20, 2012. doi: 10.1021/ie3003705.

[35] M. Hasib-ur-Rahman, M. Siaj, and F. Larachi, “Ionic liquids for CO2 capture-Development and progress,” *Chemical Engineering and Processing: Process Intensification*, vol. 49, no. 4. pp. 313–322, Apr. 2010. doi: 10.1016/j.cep.2010.03.008.

[36] J. L. Anderson and K. D. Clark, “Ionic liquids as tunable materials in (bio)analytical chemistry,” *Analytical and Bioanalytical Chemistry*, vol. 410, no. 19. Springer Verlag, pp. 4565–4566, Jul. 01, 2018. doi: 10.1007/s00216-018-1125-4.

[37] P. Sun and D. W. Armstrong, “Ionic liquids in analytical chemistry,” *Analytica Chimica Acta*, vol. 661, no. 1, pp. 1–16, Feb. 2010, doi: 10.1016/J.ACA.2009.12.007.

[38] K. Sood, Y. Saini, and K. K. Thakur, “Ionic liquids in catalysis: A review,” *Materials Today: Proceedings*, May 2021, doi: 10.1016/J.MATPR.2021.04.225.

[39] A. Cognigni, S. Kampichler, and K. Bica, “Surface-active ionic liquids in catalysis: Impact of structure and concentration on the aerobic oxidation of octanol in water,” *Journal of Colloid and Interface Science*, vol. 492, pp. 136–145, Apr. 2017, doi: 10.1016/J.JCIS.2016.12.063.

[40] T. Kakiuchi, S. Domae, T. Miyadi, K. Kibi, and M. Yamamoto, “The use of the reference electrode equipped with an ionic liquid salt bridge in electrochemistry of ionic liquids: A convenient way to align the formal potentials of redox reactions in ionic liquids based on the standard hydrogen electrode scale,” *Electrochemistry Communications*, vol. 126, p. 107021, May 2021, doi: 10.1016/J.ELECOM.2021.107021.

[41] Y. Zhang *et al.*, “Nanostructure, electrochemistry and potential-dependent lubricity of the catanionic surface-active ionic liquid [P6,6,6,14] [AOT],” *Journal of Colloid and Interface Science*, vol. 608, pp. 2120–2130, Feb. 2022, doi: 10.1016/J.JCIS.2021.10.120.

[42] Y. Deguchi, N. Nakamura, and H. Ohno, “Thermoresponsive ionic liquid/water mixtures for separation and purification technologies,” *Separation and Purification Technology*, vol. 251, p. 117286, Nov. 2020, doi: 10.1016/J.SEPPUR.2020.117286.

[43] S. Zeng, H. Dong, Y. Bai, X. Zhang, and S. Zhang, “New technology of ionic liquid-based NH3/CO2 separation from melamine tail gas,” *Green Chemical Engineering*, vol. 1, no. 1, p. 5, Sep. 2020, doi: 10.1016/J.GCE.2020.10.010.

[44] Z. Dai, R. D. Noble, D. L. Gin, X. Zhang, and L. Deng, “Combination of ionic liquids with membrane technology: A new approach for CO2 separation,” *Journal of Membrane Science*, vol. 497, pp. 1–20, Jan. 2016, doi: 10.1016/J.MEMSCI.2015.08.060.

[45] T. U. Rashid, “Ionic liquids: Innovative fluids for sustainable gas separation from industrial waste stream,” *Journal of Molecular Liquids*, vol. 321, p. 114916, Jan. 2021, doi: 10.1016/J.MOLLIQ.2020.114916.

[46] Zhao Hua, “Innovative applications of ionic liquids as ‘green’ engineering liquids.,” *Chemical Engineering Communications*, vol. 193, no. 12, pp. 1660–1677, 2006.

[47] Z. Wang *et al.*, “From heart drug to propellant fuels: Designing nitroglycerin-ionic liquid composite as green high-energy hypergolic fluids,” *Combustion and Flame*, vol. 233, p. 111597, Nov. 2021, doi: 10.1016/J.COMBUSTFLAME.2021.111597.

[48] Blanchard Lynette A., Hancu D., Beckman E.J., and Brennecke J.F., “Green processing using ionic liquids and CO2,” *Nature*, vol. 399, no. 6731, pp. 28–29, 1999.

[49] S. Lian, C. Song, Q. Liu, E. Duan, H. Ren, and Y. Kitamura, “Recent advances in ionic liquids-based hybrid processes for CO2 capture and utilization,” *Journal of Environmental Sciences (China)*, vol. 99. Chinese Academy of Sciences, pp. 281–295, Jan. 01, 2021. doi: 10.1016/j.jes.2020.06.034.

[50] Y. S. Sistla and A. Khanna, “CO2 absorption studies in amino acid-anion based ionic liquids,” *Chemical Engineering Journal*, vol. 273, pp. 268–276, Aug. 2015, doi: 10.1016/j.cej.2014.09.043.

[51] M. Sivapragasam, M. Moniruzzaman, and M. Goto, “An Overview on the Toxicological Properties of Ionic Liquids toward Microorganisms,” *Biotechnology Journal*, vol. 15, no. 4. Wiley-VCH Verlag, Apr. 01, 2020. doi: 10.1002/biot.201900073.

[52] L. A. Blanchard, Z. Gu, and J. F. Brennecke, “High-pressure phase behavior of ionic liquid/CO2 systems,” *Journal of Physical Chemistry B*, vol. 105, no. 12, pp. 2437–2444, Mar. 2001, doi: 10.1021/jp003309d.

[53] X. Huang, C. J. Margulis, Y. Li, and B. J. Berne, “Why Is the Partial Molar Volume of CO2 So Small When Dissolved in a Room Temperature Ionic Liquid? Structure and Dynamics of CO2 Dissolved in [Bmim+] [PF6-],” *Journal of the American Chemical Society*, vol. 127, no. 50, pp. 17842–17851, Dec. 2005, doi: 10.1021/JA055315Z.

[54] J. Palomar, M. Gonzalez-Miquel, A. Polo, and F. Rodriguez, “Understanding the physical absorption of CO2 in ionic liquids using the COSMO-RS method,” *Industrial and Engineering Chemistry Research*, vol. 50, no. 6, pp. 3452–3463, Mar. 2011, doi: 10.1021/IE101572M/SUPPL_FILE/IE101572M_SI_001.PDF.

[55] C. Cadena, J. L. Anthony, J. K. Shah, T. I. Morrow, J. F. Brennecke, and E. J. Maginn, “Why is CO2 so Soluble in Imidazolium-Based Ionic Liquids?,” *Journal of the American Chemical Society*, vol. 126, no. 16, pp. 5300–5308, Apr. 2004, doi: 10.1021/ja039615x.

[56] S. G. Kazarian, B. J. Briscoe, and T. Welton, “Combining ionic liquids and supercritical fluids: in situ ATR-IR study of CO2 dissolved in two ionic liquids at high pressures,” *Chemical Communications*, no. 20, pp. 2047–2048, Jan. 2000, doi: 10.1039/B005514J.

[57] P. Raveendran and S. L. Wallen, “Exploring CO2-Philicity: Effects of Stepwise Fluorination,” *Journal of Physical Chemistry B*, vol. 107, no. 6, pp. 1473–1477, Feb. 2003, doi: 10.1021/JP027026S.

[58] W. Liu, L. Cheng, Y. Zhang, H. Wang, and M. Yu, “The physical properties of aqueous solution of room-temperature ionic liquids based on imidazolium: Database and evaluation,” *Journal of Molecular Liquids*, vol. 140, no. 1–3, pp. 68–72, Apr. 2008, doi: 10.1016/J.MOLLIQ.2008.01.008.

[59] Y. Chen *et al.*, “Solubility of CO2 in imidazolium-based tetrafluoroborate ionic liquids,” *Thermochimica Acta*, vol. 441, no. 1, pp. 42–44, Feb. 2006, doi: 10.1016/J.TCA.2005.11.023.

[60] S. N. V. K. Aki, B. R. Mellein, E. M. Saurer, and J. F. Brennecke, “High-Pressure Phase Behavior of Carbon Dioxide with Imidazolium-Based Ionic Liquids,” 2004, doi: 10.1021/JP046895.

[61] R. A. Olofson, W. R. Thompson, and J. S. Michelman, “Heterocyclic Nitrogen Ylides,” *Journal of the American Chemical Society*, vol. 86, no. 9, pp. 1865–1866, May 2002, doi: 10.1021/JA01063A051.

[62] S. Chowdhury, R. S. Mohan, and J. L. Scott, “Reactivity of ionic liquids,” *Tetrahedron*, vol. 63, no. 11, pp. 2363–2389, Mar. 2007, doi: 10.1016/J.TET.2006.11.001.

[63] M. J. Muldoon, S. N. V. K. Aki, J. L. Anderson, J. K. Dixon, and J. F. Brennecke, “Improving carbon dioxide solubility in ionic liquids,” *Journal of Physical Chemistry B*, vol. 111, no. 30, pp. 9001–9009, Aug. 2007, doi: 10.1021/jp071897q.

[64] R. E. Baltus, B. H. Culbertson, S. Dai, H. Luo, and D. W. DePaoli, “Low-Pressure Solubility of Carbon Dioxide in Room-Temperature Ionic Liquids Measured with a Quartz Crystal Microbalance,” *Journal of Physical Chemistry B*, vol. 108, no. 2, pp. 721–727, Jan. 2003, doi: 10.1021/JP036051A.

[65] A. Finotello, J. E. Bara, D. Camper, and R. D. Noble, “Room-Temperature Ionic Liquids: Temperature Dependence of Gas Solubility Selectivity,” *Industrial and Engineering Chemistry Research*, vol. 47, no. 10, pp. 3453–3459, May 2007, doi: 10.1021/IE0704142.

[66] G. Hong, J. Jacquemin, M. Deetlefs, C. Hardacre, P. Husson, and M. F. Costa Gomes, “Solubility of carbon dioxide and ethane in three ionic liquids based on the bis{(trifluoromethyl)sulfonyl}imide anion,” *Fluid Phase Equilibria*, vol. 257, no. 1, pp. 27–34, Aug. 2007, doi: 10.1016/J.FLUID.2007.05.002.

[67] J. Jacquemin, P. Husson, V. Majer, and M. F. Costa Gomes, “Influence of the Cation on the Solubility of CO2 and H2 in Ionic Liquids Based on the Bis(trifluoromethylsulfonyl)imide Anion,” *Journal of Solution Chemistry 2007 36:8*, vol. 36, no. 8, pp. 967–979, Jun. 2007, doi: 10.1007/S10953-007-9159-9.

[68] J. L. Anderson, J. N. K. Dixon, E. J. Maginn, and J. F. Brennecke, “Measurement of SO2 solubility in ionic liquids,” *Journal of Physical Chemistry B*, vol. 110, no. 31, pp. 15059–15062, Aug. 2006, doi: 10.1021/JP063547U/SUPPL_FILE/JP063547USI20060628_021546.PDF.

[69] W. Wu, B. Han, H. Gao, Z. Liu, T. Jiang, and J. Huang, “Desulfurization of Flue Gas: SO2 Absorption by an Ionic Liquid,” *Angewandte Chemie International Edition*, vol. 43, no. 18, pp. 2415–2417, Apr. 2004, doi: 10.1002/ANIE.200353437.

[70] J. L. Anthony, E. J. Maginn, and J. F. Brennecke, “Solution Thermodynamics of Imidazolium-Based Ionic Liquids and Water,” *Journal of Physical Chemistry B*, vol. 105, no. 44, pp. 10942–10949, Nov. 2001, doi: 10.1021/JP0112368.

[71] D. M. D’Alessandro, B. Smit, and J. R. Long, “Carbon Dioxide Capture: Prospects for New Materials,” *Angewandte Chemie International Edition*, vol. 49, no. 35, pp. 6058–6082, Aug. 2010, doi: 10.1002/ANIE.201000431.

[72] J. F. Brennecke and B. E. Gurkan, “Ionic liquids for CO2 capture and emission reduction,” *Journal of Physical Chemistry Letters*, vol. 1, no. 24, pp. 3459–3464, Dec. 2010, doi: 10.1021/jz1014828.

[73] S. Zhang, Y. Chen, F. Li, X. Lu, W. Dai, and R. Mori, “Fixation and conversion of CO2 using ionic liquids,” *Catalysis Today*, vol. 115, no. 1–4, pp. 61–69, Jun. 2006, doi: 10.1016/J.CATTOD.2006.02.021.

[74] X. Li *et al.*, “Absorption of CO2 by ionic liquid/polyethylene glycol mixture and the thermodynamic parameters,” *Green Chemistry*, vol. 10, no. 8, pp. 879–884, Aug. 2008, doi: 10.1039/B801948G.

[75] J. H. Davis, “Task-Specific Ionic Liquids,” *http://dx.doi.org/10.1246/cl.2004.1072*, vol. 33, no. 9, pp. 1072–1077, Aug. 2004, doi: 10.1246/CL.2004.1072.

[76] E. D. Bates, R. D. Mayton, I. Ntai, and J. H. Davis, “CO2 capture by a task-specific ionic liquid,” *Journal of the American Chemical Society*, vol. 124, no. 6, pp. 926–927, Feb. 2002, doi: 10.1021/ja017593d.

[77] L. M. Galán Sánchez, G. W. Meindersma, and A. B. de Haan, “Solvent Properties of Functionalized Ionic Liquids for CO2 Absorption,” *Chemical Engineering Research and Design*, vol. 85, no. 1, pp. 31–39, Jan. 2007, doi: 10.1205/CHERD06124.

[78] P. D. Vaidya and E. Y. Kenig, “CO2-Alkanolamine Reaction Kinetics: A Review of Recent Studies,” *Chemical Engineering & Technology*, vol. 30, no. 11, pp. 1467–1474, Nov. 2007, doi: 10.1002/CEAT.200700268.

[79] G. Yu, S. Zhang, G. Zhou, X. Liu, and X. Chen, “Structure, interaction and property of amino-functionalized imidazolium ILs by molecular dynamics simulation and Ab initio calculation,” *AIChE Journal*, vol. 53, no. 12, pp. 3210–3221, Dec. 2007, doi: 10.1002/AIC.11339.

[80] K. E. Gutowski and E. J. Maginn, “Amine-functionalized task-specific ionic liquids: A mechanistic explanation for the dramatic increase in viscosity upon complexation with CO2 from molecular simulation,” *Journal of the American Chemical Society*, vol. 130, no. 44, pp. 14690–14704, Nov. 2008, doi: 10.1021/JA804654B/SUPPL_FILE/JA804654B_SI_001.PDF.

[81] B. E. Gurkan *et al.*, “Equimolar CO2 absorption by anion-functionalized ionic liquids,” *Journal of the American Chemical Society*, vol. 132, no. 7, pp. 2116–2117, Mar. 2010, doi: 10.1021/ja909305t.

[82] D. Chinn, D. Q. Vu, Driver M., and Boudreau L.C., “CO2 removal from gas using ionic liquid adsorbents. ,” 7527775, May 05, 2009

[83] E. J. Maginn, “DESIGN AND EVALUATION OF IONIC LIQUIDS AS NOVEL CO2 ABSORBENTS,” Dec. 2004, doi: 10.2172/836826.

[84] W. Gouveia *et al.*, "Toxicity of ionic liquids prepared from biomaterials," *Chemosphere*, vol. 104, pp. 51–56, Jun. 2014, doi: 10.1016/J.CHEMOSPHERE.2013.10.055.

[85] A. P. Abbott, D. Boothby, G. Capper, D. L. Davies, and R. K. Rasheed, "Deep Eutectic Solvents formed between choline chloride and carboxylic acids: Versatile alternatives to ionic liquids," *Journal of the American Chemical Society*, vol. 126, no. 29, pp. 9142–9147, Jul. 2004, doi: 10.1021/JA048266J/SUPPL_FILE/JA048266JSI20040521_085323.PDF.

[86] L. Morandeira *et al.*, "Testing True Choline Ionic Liquid Biocompatibility from a Biotechnological Standpoint," *ACS Sustainable Chemistry and Engineering*, vol. 5, no. 9, pp. 8302–8309, Sep. 2017, doi: 10.1021/ACSSUSCHEMENG.7B02017/SUPPL_FILE/SC7B02017_SI_001.PDF.

[87] Y. Fukaya, Y. Iizuka, K. Sekikawa, and H. Ohno, "Bio ionic liquids: room temperature ionic liquids composed wholly of biomaterials," *Green Chemistry*, vol. 9, no. 11, pp. 1155–1157, Oct. 2007, doi: 10.1039/B706571J.

[88] J. Hulsbosch, D. E. de Vos, K. Binnemans, and R. Ameloot, "Biobased Ionic Liquids: Solvents for a Green Processing Industry?," *ACS Sustainable Chemistry and Engineering*, vol. 4, no. 6, pp. 2917–2931, Jun. 2016, doi: 10.1021/ACSSUSCHEMENG.6B00553.

[89] L. Gontrani, "Choline-amino acid ionic liquids: past and recent achievements about the structure and properties of these really 'green' chemicals," *Biophysical Reviews*, vol. 10, no. 3. Springer Verlag, pp. 873–880, Jun. 01, 2018. doi: 10.1007/s12551-018-0420-9.

[90] Y. Y. Jiang, G. N. Wang, Z. Zhou, Y. T. Wu, J. Geng, and Z. B. Zhang, "Tetraalkylammonium amino acids as functionalized ionic liquids of low viscosity," *Chemical Communications*, vol. 8, no. 4, pp. 505–507, Jan. 2008, doi: 10.1039/B713648J.

[91] H. Yu, Y. T. Wu, Y. Y. Jiang, Z. Zhou, and Z. B. Zhang, "Low viscosity amino acid ionic liquids with asymmetric tetraalkylammonium cations for fast absorption of CO2," *New Journal of Chemistry*, vol. 33, no. 12, pp. 2385–2390, Dec. 2009, doi: 10.1039/B9NJ00330D.

[92] B. L. Gadilohar and G. S. Shankarling, "Choline based ionic liquids and their applications in organic transformation," *Journal of Molecular Liquids*, vol. 227. Elsevier B.V., pp. 234–261, Feb. 01, 2017. doi: 10.1016/j.molliq.2016.11.136.

[93] J. Pernak *et al.*, “Choline-derivative-based ionic liquids,” *Chemistry - A European Journal*, vol. 13, no. 24, pp. 6817–6827, 2007, doi: 10.1002/chem.200700285.

[94] E. J. García-Suárez, C. Menéndez-Vázquez, and A. B. García, “Chemical stability of choline-based ionic liquids supported on carbon materials,” *Journal of Molecular Liquids*, vol. 169, pp. 37–42, May 2012, doi: 10.1016/J.MOLLIQ.2012.02.022.

[95] B. L. Gadilohar and G. S. Shankarling, “Choline based ionic liquids and their applications in organic transformation,” *Journal of Molecular Liquids*, vol. 227, pp. 234–261, Feb. 2017, doi: 10.1016/J.MOLLIQ.2016.11.136.

[96] S. de Santis *et al.*, “Cholinium-amino acid based ionic liquids: a new method of synthesis and physico-chemical characterization,” *Physical Chemistry Chemical Physics*, vol. 17, no. 32, pp. 20687–20698, Aug. 2015, doi: 10.1039/C5CP01612F.

[97] A. le Donne and E. Bodo, “Cholinium amino acid-based ionic liquids”, doi: 10.1007/s12551-021-00782-0/Published.

[98] S. Yuan, Y. Chen, X. Ji, Z. Yang, and X. Lu, “Experimental study of CO2 absorption in aqueous cholinium-based ionic liquids,” *Fluid Phase Equilibria*, vol. 445, pp. 14–24, Aug. 2017, doi: 10.1016/j.fluid.2017.04.001.

[99] A. Filippov, S. Bhattacharyya, and F. U. Shah, “CO2 absorption and ion mobility in aqueous choline-based ionic liquids,” *Journal of Molecular Liquids*, vol. 276, pp. 748–752, Feb. 2019, doi: 10.1016/j.molliq.2018.12.045.

[100] Y. Chen, B. Li, J. Wu, Z. Yang, X. Lu, and X. Ji, “Kinetics study and performance comparison of CO2 separation using aqueous choline-amino acid solutions,” *Separation and Purification Technology*, vol. 261, Apr. 2021, doi: 10.1016/j.seppur.2020.118284.

[101] N. Noorani and A. Mehrdad, “Experimental and theoretical study of CO2 sorption in biocompatible and biodegradable cholinium-based ionic liquids,” *Separation and Purification Technology*, vol. 254, Jan. 2021, doi: 10.1016/j.seppur.2020.117609.

[102] B. Li, Y. Chen, Z. Yang, X. Ji, and X. Lu, “Thermodynamic study on carbon dioxide absorption in aqueous solutions of choline-based amino acid ionic liquids,” *Separation and Purification Technology*, pp. 128–138, May 2019, doi: 10.1016/j.seppur.2018.01.058.

[103] Pine Stanley H., *Organic Chemistry*, 5th ed. Singapore: McGraw-Hill Book Co. , 1987.

[104] Q. Yang *et al.*, “New Insights into CO2 Absorption Mechanisms with Amino-Acid Ionic Liquids,” *ChemSusChem*, vol. 9, no. 8, pp. 806–812, Apr. 2016, doi: 10.1002/cssc.201501691.

[105] P. S. Kumar, J. A. Hogendoorn, P. H. M. Feron, and G. F. Versteeg, “New absorption liquids for the removal of CO2 from dilute gas streams using membrane contactors,” *Chemical Engineering Science*, vol. 57, no. 9, pp. 1639–1651, May 2002, doi: 10.1016/S0009-2509(02)00041-6.

[106] P. D. Vaidya, P. Konduru, M. Vaidyanathan, and E. Y. Kenig, “Kinetics of carbon dioxide removal by aqueous alkaline amino acid salts,” *Industrial and Engineering Chemistry Research*, vol. 49, no. 21, pp. 11067–11072, Nov. 2010, doi: 10.1021/IE100224F/SUPPL_FILE/IE100224F_SI_002.PDF.

[107] B. E. Gurkan *et al.*, “Equimolar CO2 absorption by anion-functionalized ionic liquids,” *Journal of the American Chemical Society*, vol. 132, no. 7, pp. 2116–2117, Mar. 2010, doi: 10.1021/JA909305T/SUPPL_FILE/JA909305T_SI_001.PDF.

[108] H. J. Song, S. Park, H. Kim, A. Gaur, J. W. Park, and S. J. Lee, “Carbon dioxide absorption characteristics of aqueous amino acid salt solutions,” *International Journal of Greenhouse Gas Control*, vol. 11, pp. 64–72, Nov. 2012, doi: 10.1016/J.IJGGC.2012.07.019.

[109] G. F. Versteeg and W. P. M. van Swaaij, “On the kinetics between CO2 and alkanolamines both in aqueous and non-aqueous solutions—II. Tertiary amines,” *Chemical Engineering Science*, vol. 43, no. 3, pp. 587–591, Jan. 1988, doi: 10.1016/0009-2509(88)87018-0.

[110] A. R. Shaikh, H. Karkhanechi, E. Kamio, T. Yoshioka, and H. Matsuyama, “Quantum Mechanical and Molecular Dynamics Simulations of Dual-Amino-Acid Ionic Liquids for CO2 Capture,” *Journal of Physical Chemistry C*, vol. 120, no. 49, pp. 27734–27745, Dec. 2016, doi: 10.1021/ACS.JPCC.6B07305/SUPPL_FILE/JP6B07305_SI_001.PDF.

[111] A. R. Shaikh, M. Ashraf, T. AlMayef, M. Chawla, A. Poater, and L. Cavallo, “Amino acid ionic liquids as potential candidates for CO2 capture: Combined density functional theory and molecular dynamics simulations,” *Chemical Physics Letters*, vol. 745, p. 137239, Apr. 2020, doi: 10.1016/J.CPLETT.2020.137239.

[112] X. Y. Luo, X. Fan, G. L. Shi, H. R. Li, and C. M. Wang, “Decreasing the Viscosity in CO2 Capture by Amino-Functionalized Ionic Liquids through the Formation of Intramolecular Hydrogen Bond,” *Journal of Physical Chemistry B*, vol. 120, no. 10,

pp. 2807–2813, Mar. 2016, doi: 10.1021/ACS.JPCB.5B10553/SUPPL_FILE/JP5B10553_SI_001.PDF.

[113] X. Zhang, H. Dong, D. Bao, Y. Huang, X. Zhang, and S. Zhang, "Effect of Small Amount of Water on CO2 Bubble Behavior in Ionic Liquid Systems," *Industrial and Engineering Chemistry Research*, vol. 53, no. 1, pp. 428–439, Jan. 2013, doi: 10.1021/IE4020827.

[114] W. Li, S. Wen, L. Shen, Y. Zhang, C. Sun, and S. Li, "Mechanism and Kinetic Study of Carbon Dioxide Absorption into a Methyldiethanolamine/1-Hydroxyethyl-3-methylimidazolium Lysine/Water System," *Energy & Fuels*, vol. 32, no. 10, pp. 10813–10821, Oct. 2018, doi: 10.1021/ACS.ENERGYFUELS.8B02612.

[115] E. Davarpanah, S. Hernández, G. Latini, C. F. Pirri, and S. Bocchini, "Enhanced CO2 Absorption in Organic Solutions of Biobased Ionic Liquids," *Advanced Sustainable Systems*, vol. 4, no. 1, Jan. 2020, doi: 10.1002/adsu.201900067.

[116] G. Latini, M. Signorile, V. Crocellà, S. Bocchini, C. F. Pirri, and S. Bordiga, "Unraveling the CO2 reaction mechanism in bio-based amino-acid ionic liquids by operando ATR-IR spectroscopy," *Catalysis Today*, vol. 336, pp. 148–160, Oct. 2019, doi: 10.1016/j.cattod.2018.12.050.

[117] Martyr A.J. and Plint M.A., *Engine Testing: The Design, Building, Modification and Use of Powertrain Test Facilities*. 2012.

APPENDIX I: Calculation of the experimental errors

According to the theory of errors, given the systematic direct errors which affect a measurement, the indirect ones (i.e., the ones which affect the values calculated with the direct measurements) can be obtained as follow.

Being x, y and z quantities obtained by means of experimental measurements with mean value and errors expressed as $\bar{x} \pm \Delta x, \bar{y} \pm \Delta y$ and $\bar{z} \pm \Delta z$, the indirect error on the value given by the formula $f(x, y, z)$ can be calculated according to the following formula:

$$\Delta f(x, y, z) = \left|\frac{\partial f(x, y, x)}{\partial x}\right| \cdot \Delta x + \left|\frac{\partial f(x, y, z)}{\partial y}\right| \cdot \Delta y + \left|\frac{\partial f(x, y, z)}{\partial z}\right| \cdot \Delta z$$

where the value of the partial derivatives are calculated considering $x = \bar{x}, y = \bar{y}, z = \bar{z}$.

The relative error and the percentage error are the calculated as

$$err_{rel} = \left|\frac{\Delta f(x, y, z)}{f(x, y, z)}\right|$$

$$err_{\%} = err_{rel} \cdot 100$$

In the following, the formulas employed for the calculation of the errors in the current study are briefly reported.

1. Density

- pycnometer volume

$$V = \frac{m_w}{\rho_w} = \frac{m_1 - m_0}{\rho_w}$$

$$\Delta V = \left|\frac{\partial V}{\partial m_w}\right| \cdot \Delta m_w = \frac{\Delta m_w}{\rho_w} = \frac{2 \cdot \Delta m}{\rho_w}$$

$$err_{\%} = \frac{\Delta V}{V} \cdot 100$$

- density

$$\rho_{IL} = \frac{m_{IL}}{V}$$

$$\Delta \rho_{IL} = \left|\frac{\partial \rho}{\partial m_{IL}}\right| \cdot \Delta m_{IL} + \left|\frac{\partial \rho}{\partial V}\right| \cdot \Delta V = \frac{2 \cdot \Delta m}{V} + \frac{m_{IL}}{V^2} \cdot \Delta V$$

$$err_{\%} = \frac{\Delta \rho_{IL}}{\rho_{IL}} \cdot 100$$

2. Viscosity

- kinematic viscosity

$$\nu = CONST_{viscometer} \cdot t_{flow}$$

$$\Delta \nu = \left|\frac{\partial \nu}{\partial t_{flow}}\right| \cdot \Delta t = CONST_{viscometer} \cdot \Delta t$$

$$err_{\%} = \frac{\Delta \nu}{\nu} \cdot 100$$

- dynamic viscosity

$$\mu = \nu \cdot \rho$$

$$\Delta \mu = \left|\frac{\partial \mu}{\partial \nu}\right| \cdot \Delta \nu + \left|\frac{\partial \mu}{\partial \rho}\right| \cdot \Delta \rho = \rho \cdot \Delta \nu + \nu \cdot \Delta \rho$$

$$err_{\%} = \frac{\Delta \mu}{\mu} \cdot 100$$

3. CO_2 absorption

- CO_2 absorbed

$$m_{CO_2,abs} = [m^r_{CO_2} - (V_r - V_{sol}) \cdot d_{CO_2} - [m^r_{N_2} - (V_r - V_{sol}) \cdot d_{N_2}]$$

$$\Delta m_{CO_2,abs} = \left|\frac{\partial m_{CO2,abs}}{\partial m^r_{CO_2}}\right| \cdot \Delta m^r_{CO_2} + \left|\frac{\partial m_{CO_2,abs}}{\partial V_r}\right| \cdot \Delta V_r + \left|\frac{\partial m_{CO_2,abs}}{\partial V_{sol}}\right| \cdot \Delta V_{sol} + \left|\frac{\partial m_{CO2,abs}}{\partial m^r_{N_2}}\right| \cdot \Delta m^r_{N_2} = \Delta m + \left|-d_{CO_2} + d_{N_2}\right| \cdot \Delta V + \left|d_{CO_2} - d_{N_2}\right| \cdot \Delta V + \Delta m$$

$$err_{\%} = \frac{\Delta m_{CO_2,abs}}{m_{CO_2,abs}} \cdot 100$$

- mass of the solution in the vial

$$m_{sol} = \left[m^r_{N_2} - (V_r - V_{sol}) \cdot d_{N_2}\right] - \left[m^r_{empty} - V_r \cdot d_{air}\right]$$

$$\Delta m_{sol} = \left|\frac{\partial m_{sol}}{\partial m^r_{N_2}}\right| \cdot \Delta m^r_{N_2} + \left|\frac{\partial m_{sol}}{\partial V_r}\right| \cdot \Delta V_r + \left|\frac{\partial m_{sol}}{\partial V_{sol}}\right| \cdot \Delta V_{sol} + \left|\frac{\partial m_{sol}}{\partial m^r_{empty}}\right| \cdot \Delta m_{empty} = \Delta m + \left|-d_{N_2} + d_{air}\right| \cdot \Delta V + \left|d_{N_2}\right| \cdot \Delta V + \Delta m$$

$$err_{\%} = \frac{\Delta m_{sol}}{m_{sol}} \cdot 100$$

- molar efficiency

$$ME = \frac{mol_{CO_2,abs}}{mol_{IL}} = \frac{m_{CO_2,abs}/MM_{CO_2}}{m_{IL}/MM_{IL}} = \frac{m_{CO_2,abs}/MM_{CO_2}}{\%IL \cdot m_{sol}/MM_{IL}} = \frac{MM_{IL}}{MM_{CO_2} \cdot \%IL} \cdot \frac{m_{CO_2,abs}}{m_{sol}}$$

$$\Delta ME = \left|\frac{\partial ME}{\partial m_{CO_2,abs}}\right| \cdot \Delta m_{CO_2,abs} + \left|\frac{\partial ME}{\partial m_{sol}}\right| \cdot \Delta m_{so}$$

$$= \left|\frac{MM_{IL}}{MM_{CO_2} \cdot \%IL \cdot m_{sol}}\right| \cdot \Delta m_{CO_2,abs} + \left|-\frac{MM_{IL} \cdot m_{CO_2,abs}}{MM_{CO_2} \cdot \%IL} \cdot \frac{1}{m_{sol}^2}\right|$$

$$\cdot \Delta m_{sol} = ME \cdot \left(\frac{\Delta m_{CO_2,abs}}{m_{CO_2,abs}} + \frac{\Delta m_{sol}}{m_{sol}}\right)$$

$$err_{\%} = \frac{\Delta ME}{ME} \cdot 100$$

- absorption capacity

$$AC = \frac{m_{CO_2,abs}}{m_{sol}} \cdot 100$$

$$\Delta AC = \left|\frac{\partial AC}{\partial m_{CO_2,abs}}\right| \cdot \Delta m_{CO_2,abs} + \left|\frac{\partial AC}{\partial m_{sol}}\right| \cdot \Delta m_{sol}$$

$$= \left|\frac{1}{m_{sol}} \cdot 100\right| \cdot \Delta m_{CO_2,abs} + \left|-\frac{m_{CO_2,abs}}{m_{sol}^2} \cdot 100\right| \cdot \Delta m_{sol}$$

$$= AC \cdot \left(\frac{\Delta m_{CO_2,abs}}{m_{CO_2,abs}} + \frac{\Delta m_{sol}}{m_{sol}}\right)$$

$$err_{\%} = \frac{\Delta AC}{AC} \cdot 100$$

APPENDIX II: Flow rates corrective factors

Since the flowmeters installed in the plant are calibrated to nitrogen streams and only the one which provides the measurements of the input stream is provided with corrective factors for different concentrations of the inlet stream, proper corrective factors were estimated.

Two approaches were considered.

The first one consisted in estimating empirical formulas for the corrective factors for both the inlet (FM1) and outlet (FM4) values provided by the instruments as a function of the values imposed on the software. A logarithmic trend was observed; thus, the following formula was considered:

$$CF = A_1 \cdot \ln(FM) + A_2$$

where CF stands for corrective factor, A_1 and A_2 are the fitting parameters (reported in the table below) and FM is the value of the flowrate provided by the instrument.

Table a. Fitting parameters for the estimation of the corrective factors to be applied to the values provided by all the flowmeters.

		A_1	A_2
absorption	inlet stream – FM1 (CO_2)	-0.02	0.9873
	outlet stream – FM4	-0.049	1.4485
desorption	inlet stream – FM1(N_2)	0.2012	0.1145
	outlet stream – FM4	0.1928	0.1511

The second approach calculated the corrective factors for the CO_2 fraction of the outlet stream only. The values of the inlet flowmeter were considered to be reliable – since the software allows to set its precise composition; for what concerns the outlet flowmeter, the analysis of the absorption and the desorption runs needs to be discussed separately.

In the absorption run, in fact, the outlet flowrate is supposed to consist of the carbon dioxide not absorbed in the absorption column only; hence, a corrective factor was applied

to the overall value provided by the instrument – which is calibrated to nitrogen stream measurements, as said above.

In the desorption run, the outlet flowrate is composed of the nitrogen sent to the column for the regeneration and the carbon dioxide desorbed. In this case, in the data analysis phase, the two components were considered separately and the corrective factor was applied to the CO_2 fraction only. In order to calculate the fraction of carbon dioxide desorbed, the nitrogen fraction was considered to be equal to the inlet one (provided by FM1).

A linear trend was observed in this case, thus the corrective factor was calculated according to the formula

$$CF4 = A_1 \cdot FM4_{CO_2} + A_2$$

where $CF4$ is the corrective factor calculated for the outlet stream, A_1 and A_2 are the fitting parameters reported in the table below, $FM4_{CO_2}$ is the CO_2 flowrate in the outlet stream.

Table b. Fitting parameters for the estimation of the corrective factors to be applied to the CO_2 fraction of the stream values provided by the outlet flowmeter.

	A_1	A_2
outlet stream – FM4	-0.0003	0.7436

The current study followed the second approach, in order to consider the real flowrates sent to the column instead of the ones imposed from the software.